Carbon Fiber Shear Reinforcement for Prestressed Bridge Girders

FINAL REPORT
September 2017

Submitted by:

John Ward
Graduate Research Assistant

Carin L. Roberts-Wollmann, Ph.D., P.E.
Professor

Mitch Magee
Graduate Research Assistant

Thomas E. Cousins, Ph.D., P.E.[1]
Professor

Center for Sustainable Transportation Infrastructure
Virginia Tech Transportation Institute
3500 Transportation Research Plaza
Blacksburg, VA, 24061

External Project Manager:

VTRC Project Manager
Bernard L. Kassner, Ph.D., P.E.
Research Scientist
Virginia Transportation Research Council

In cooperation with

Rutgers, The State University of New Jersey
And
Virginia Department of Transportation

[1] Glenn Department of Civil Engineering, Clemson University

Disclaimer Statement

1. Report No. CAIT-UTC-NC2	2. Government Accession No.	3. Recipient's Catalog No.
4. Title and Subtitle Carbon Fiber Shear Reinforcement for Prestressed Bridge Girders		5. Report Date September 2017
		6. Performing Organization Code Virginia Tech/CAIT
TECHNICAL REPORT STANDARD TITLE PAGE 7. Author(s) John Ward, Mitch Magee, Carin L. Roberts-Wollmann, Ph.D., Thomas E. Cousins, Ph.D.		8. Performing Organization Report No. CAIT-UTC-NC2
9. Performing Organization Name and Address Center for Sustainable Transportation Infrastructure 3500 Transportation Research Plaza Blacksburg, VA 24061		10. Work Unit No.
		11. Contract or Grant No. DTRT13-G-UTC28
12. Sponsoring Agency Name and Address CAIT Rutgers, The State University of New Jersey 100 Brett Road Piscataway, NJ 08854 Virginia Department of Transportation 1401 E. Broad Street Richmond, VA 23219		13. Type of Report and Period Covered Final Report 06/01/14 - 01/31/16
		14. Sponsoring Agency Code

15. Supplementary Notes
U.S. Department of Transportation/OST-R
1200 New Jersey Avenue, SE
Washington, DC 20590-0001

16. Abstract

Corrosion of reinforcing steel reduces life spans of bridges throughout the United States; therefore, using non-corroding carbon fiber reinforced polymer (CFRP) reinforcement is seen as a way to increase service life. The use of CFRP as the flexural reinforcement in bridge girders has been extensively studied. However, CFRP transverse reinforcement has not been investigated as rigorously, and many of those studies have focused on carbon fiber composite cable (CFCC®) stirrups. The use of C-Grid® or NEFMACTM grid as options for transverse reinforcing has not been previously investigated.

This testing program first determined the mechanical properties of C-Grid and NEFMAC grid and their respective development lengths. Five 18-ft long, 19-in deep beams were fabricated to test the C-Grid and NEFMAC, as well as conventional steel and CFCC stirrups. The beams were loaded with a single point load closer to one end of the beam to create a larger shear load for a given moment. Overall beam displacement was measured, and beams were fitted with rosettes and instrumentation to capture initiation of shear cracking.

Test results were compared to theoretical shear capacities calculated using four different methods. The design method which provided the best prediction of shear strength was the AASHTO modified compression field theory, using equations for β and θ. The manufacturer's guaranteed tensile strength should be used for design, as long as that strength is the average strength, as determined by at least five tests, reduced by three standard deviations. Shear cracks were controlled to a similar width as in beams with steel stirrups when at least two layers of grid were in place.

An additional study was undertaken to determine if CFRP grids, either alone or in combination with traditional steel stirrups, could be used to control cracking in the end zones of pretensioned I-beams. Unfortunately, it was determined that, due to its low modulus, the amount of CFRP grid required to control cracking in the end zones was not economically feasible. Nevertheless, this study concluded that C-Grid and NEFMAC grid are both viable shear reinforcement options outside of the end regions. This report presents the initial recommendations for design.

17. Key Words Prestressed concrete, Shear Strength, Carbon Fiber Reinforcement		18. Distribution Statement	
19. Security Classification (of this report) Unclassified	20. Security Classification (of this page) Unclassified	21. No. of Pages 80	22. Price

Form DOT F 1700.7 (8-69)

FINAL CONTRACT REPORT

CARBON FIBER REINFORCED POLYMER GRIDS FOR SHEAR AND END ZONE REINFORCEMENT IN BRIDGE BEAMS

John Ward
Research Assistant
Charles E. Via, Jr. Department of Civil and Environmental Engineering
Virginia Tech

Mitch Magee
Research Assistant
Charles E. Via, Jr. Department of Civil and Environmental Engineering
Virginia Tech

Carin L. Roberts-Wollmann, Ph.D., P.E.
Professor
Charles E. Via, Jr. Department of Civil and Environmental Engineering
Virginia Tech

Thomas E. Cousins, Ph.D., P.E.
Professor
Glenn Department of Civil Engineering
Clemson University

VTRC Project Manager
Bernard L. Kassner, Ph.D., P.E.
Research Scientist
Virginia Transportation Research Council

Virginia Transportation Research Council
(A partnership of the Virginia Department of Transportation
And the University of Virginia since 1948)

Charlottesville, Virginia

September 2017
VTRC 17-RX

ABSTRACT

Corrosion of reinforcing steel reduces life spans of bridges throughout the United States; therefore, using non-corroding carbon fiber reinforced polymer (CFRP) reinforcement is seen as a way to increase service life. The use of CFRP as the flexural reinforcement in bridge girders has been extensively studied. However, CFRP transverse reinforcement has not been investigated as rigorously, and many of those studies have focused on carbon fiber composite cable (CFCC®) stirrups. The use of C-Grid® or NEFMAC™ grid as options for transverse reinforcing has not been previously investigated.

This testing program first determined the mechanical properties of C-Grid and NEFMAC grid and their respective development lengths. Five 18-ft long, 19-in deep beams were fabricated to test the C-Grid and NEFMAC, as well as conventional steel and CFCC stirrups. The beams were loaded with a single point load closer to one end of the beam to create a larger shear load for a given moment. Overall beam displacement was measured, and beams were fitted with rosettes and instrumentation to capture initiation of shear cracking.

Test results were compared to theoretical shear capacities calculated using four different methods. The design method which provided the best prediction of shear strength was the AASHTO modified compression field theory, using equations for β and θ. The manufacturer's guaranteed tensile strength should be used for design, as long as that strength is the average strength, as determined by at least five tests, reduced by three standard deviations. Shear cracks were controlled to a similar width as in beams with steel stirrups when at least two layers of grid were in place.

An additional study was undertaken to determine if CFRP grids, either alone or in combination with traditional steel stirrups, could be used to control cracking in the end zones of pretensioned I-beams. Unfortunately, it was determined that, due to its low modulus, the amount of CFRP grid required to control cracking in the end zones was not economically feasible. Nevertheless, this study concluded that C-Grid and NEFMAC grid are both viable shear reinforcement options outside of the end regions. This report presents the initial recommendations for design.

FINAL CONTRACT REPORT

CARBON FIBER REINFORCED POLYMER GRIDS FOR SHEAR AND END ZONE REINFORCEMENT IN BRIDGE BEAMS

John Ward
Research Assistant
Charles E. Via, Jr. Department of Civil and Environmental Engineering
Virginia Tech

Mitch Magee
Research Assistant
Charles E. Via, Jr. Department of Civil and Environmental Engineering
Virginia Tech

Carin L. Roberts-Wollmann, Ph.D., P.E.
Professor
Charles E. Via, Jr. Department of Civil and Environmental Engineering
Virginia Tech

Thomas E. Cousins, Ph.D., P.E.
Professor
Glenn Department of Civil Engineering
Clemson University

INTRODUCTION

Virginia is experiencing significant corrosion problems in prestressed bridge girders in the coastal areas such as Hampton Roads and Newport News. The chlorides in the sea water are causing the steel stirrups and prestressing strands in these bridges to corrode at an accelerated rate. The premature aging of this infrastructure will lead to expensive repairs and retrofits, so new alternatives must be found to extend the design life of new bridges.

Carbon Fiber Reinforced Polymers

Carbon fiber reinforced polymer (CFRP) is a material that has quickly gained footing as a replacement for steel reinforcing. CFRP does not corrode and has higher tensile strength but typically slightly lower modulus of elasticity compared traditional steel reinforcing and prestressing. However, one of the major concerns with CFRP products is the brittle nature of the material. The use of CFRP as shear reinforcing is of great interest to the Virginia Department of Transportation (VDOT), due to the increased design life and mitigation of corrosion in coastal areas.

Tokyo Rope in Japan produces a carbon fiber composite cable (CFCC®) which is a type of CFRP that is used in place of steel prestressing strand. CFCC can be formed into stirrup shapes to use as transverse reinforcing in concrete beams. A typical single-legged CFCC stirrup is shown in Figure 1. While the performance of the material is somewhat similar to steel, CFCC is not a perfect solution as stirrups for two reasons. One is the high cost of CFCC. Another is that the stirrups are custom made for every design, and the stirrups are shaped immediately after application of the polymer, before the polymer fully cures. Since the polymer is a thermoset material, no additional modification of the stirrup geometry can be made once the material has cured. Any fabrication error means these products will not fit into the formwork properly. This will lead to beam fabrication delays and added construction expense, because replacement stirrups must be replaced by the manufacturer, which can require additional lead time from order until delivery.

These disadvantages led VDOT to express interest in alternative CFRP options that do not need to be custom built for each bridge. Having a material on hand that could be modified or cut to size would allow the contractor to fabricate the beams faster and cheaper, particularly when additional reinforcement is needed.

Figure 1. Typical CFCC Stirrup

Alternative CFRP Materials

Although several CFRP materials were considered for use in the project, ultimately only two grid products were selected for further study, due to their ability to be field cut and adapted to use in multiple configurations as transverse reinforcing in a concrete beam. The first grid selected for testing was C-Grid®, which is a CFRP product that is made in the United States. C-Grid comes on large rolls, as shown in Figure 2(a) and can easily be cut to size. The second product chosen was NEFMAC™ grid, which is a heavier, stiffer product than C-Grid. Produced in Japan, NEFMAC grid comes in sheets of roughly 9 ft by 6 ft that can be cut to size or spliced as needed (Figure 2(b)).

PURPOSE AND SCOPE

The first objective of the project was to determine basic material properties of the C-Grid and NEFMAC grid such as tensile strength, modulus of elasticity and development length. The

2

second objective was to investigate the behavior and shear strength of concrete beams containing C-Grid and NEFMAC grid transverse reinforcement in comparison with conventional steel stirrups, and CFCC stirrups.
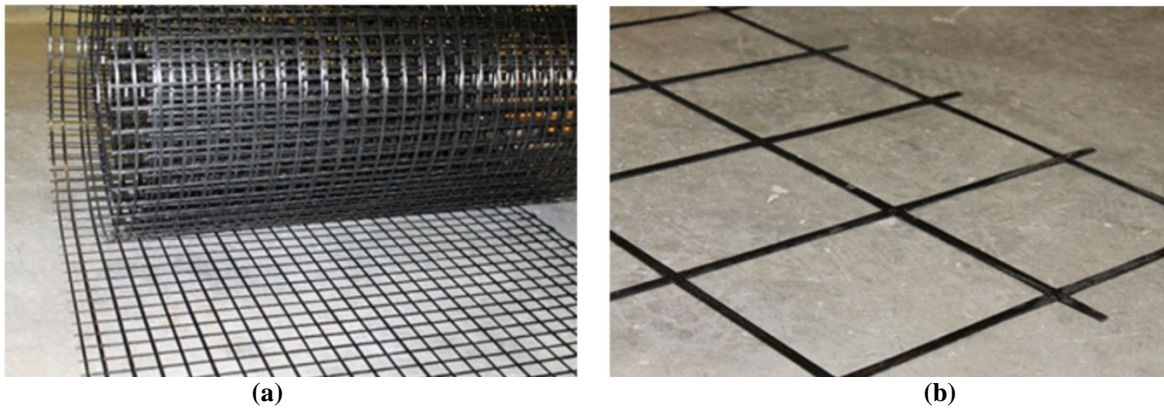

(a)   (b)
Figure 2. (a) C-Grid® and (b) NEFMAC^{TM} Grid

The third objective of the project was to determine the suitability of using shear design methods given by the American Concrete Institute (ACI 2014, 2006, and 2004) and the American Association of State Highway and Transportation Officials (AASHTO, 2014) to determine the shear strength of a beam reinforced with a CFRP grid. Comparisons of the predicted strengths with test results could then be used to develop example design calculations.

The final objective was to determine the feasibility of using CFRP grids in the end zones of pretensioned bridge beams to relieve congestion in this area yet still control anchorage zone cracking.

To achieve the aforementioned objectives, individual tows of the C-Grid were tested in tension to determine the ultimate strength, ultimate strain, and modulus of elasticity. Test results were compared to the data presented by the manufacturer. Development length tests of both C-Grid and NEFMAC grid were conducted with embedment lengths of 4 to 8 in into the concrete. The results from these tests were used to establish recommendations for development length in future designs as well as to design the beams used for shear testing.

Five beams were fabricated, each 19 in deep and 18 ft long. Of the tested beams, one had conventional steel shear reinforcing, one had CFCC, two had C-Grid, and one had NEFMAC grid shear reinforcing. Half of each beam had the AASHTO minimum shear reinforcement ratio, while the other half had a typical shear reinforcement ratio. The two beams with C-Grid had layers in two different arrangements.

Background

CFRP Stress-Strain Behavior

CFRP has been used as reinforcing and prestressing in concrete. One of the major benefits of CFRP is that its modulus of elasticity is only somewhat smaller than typical prestressing and reinforcing steel. However, CFRP is a brittle material compared to steel. A

CFRP prestressing rope can show about 1.7% elongation before failure (Grace et al., 2013), compared to 4 or 5% elongation for typical prestressing steel after yielding at about 1% (Nilson, 1987). In Figure 3, the stress-strain behavior of steel prestressing strand is compared to CFCC.
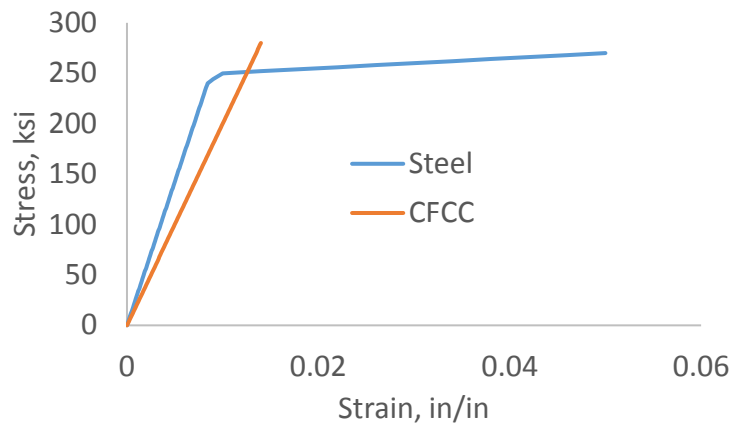

Figure 3. Stress Strain Behavior of Prestressing Materials

CFRP as Flexural Reinforcing

CFRP has already been used as prestressing strand in some bridges in the United States (Grace et al., 2012). The CFRP prestressing rope currently used is very similar in shape to seven-wire strand, and the most common manufacturer is Tokyo Rope. Figure 4 is a picture of the typical seven-strand CFCC cable from Tokyo Rope. Grace has completed a considerable amount of research in using CFRP prestressing strand, and has provided recommendations for the flexural design of prestressed concrete using CFRP strand. Grace also constructed a full scale double T-beam, and tested the beam under multiple loadings (Grace, 2000), as well as box-beams (Grace et al., 2006) and decked Bulb T-beams (Grace et al., 2013). This promising research, combined with the state of disrepair of our current infrastructure, has led some DOTs to consider the use of CFRP in prestressed concrete due to the anticipated longer design life (Grace et al., 2012).

Figure 4. Seven-Strand CFCC

CFRP as Shear Reinforcing

While the use of CFRP as flexural reinforcing has been studied and used in bridges in the United States (Grace et al., 2012), the use of CFRP as shear reinforcing in reinforced and

prestressed concrete beams has not been studied extensively. Shear capacity in prestressed sections comes from the resistance provided by the prestressing strand, concrete, and transverse reinforcement. CFRP prestressing strands could add shear capacity to a beam in which they are draped or harped. However, the deviation force applied laterally to drape or harp the strand can cause premature failures, so most CFPR prestressing tendons are straight. Methods for shear design using CFRP are presented in the Methods section of this report.

CFRP Stirrups

One option for CFRP shear reinforcement is solid bars similar to mild steel reinforcing. These stirrups can be made from the same strand material as the prestressing cable or can be solid more like a traditional reinforcing bars with ridges to help mechanical bond. The CFRP stirrups used in this study were the CFCC stirrups produced by Tokyo Rope.

An issue with using CFRP bars is that bending them in a tight radius decreases their strength. A bend radius similar to that allowed for a No. 3 steel reinforcing bar can reduce the strength of CFRP bars by 60% (Morphy et al., 1997). The same study recommended not exceeding 50% of the parallel CFRP strength when designing CFRP stirrups to account for loss of strength due to bending (Morphy et al., 1997). This strength reduction greatly impacts the cost, as the stirrups must therefore be larger or spaced more closely together. Thus, CFRP bars can be less cost competitive than steel bars. According to Andrew Zickler at VDOT, the cost of a CFRP stirrup was approximately nine times that of a typical steel stirrup (personal communication, June 23, 2014).

NEFMAC Grid

NEFMAC grid (see Figure 2(b)) is a CFRP product that is a replacement for welded wire mesh. This product is manufactured in locations outside the United States, but has been used in multiple structural applications in the US and Canada. One such application was the reinforcing in a bridge deck in New Hampshire (Steffen et al., 2001). Placing the NEFMAC grid was found to be faster than placing conventional steel reinforcing as the grid was shipped in large sheets that needed fewer connections tying in place. Also, fewer people were needed to handle the light weight sheets and they were easier to set in place compared to conventional steel reinforcement. NEFMAC grid comes in different spacing configurations and tow sizes depending on the application. However, one problem was that the NEFMAC grid floated when concrete was placed and would not stay in the proper location. The solution was to tie the grid to PVC spacers to keep the grid from moving and floating to the surface.

C-Grid

C-Grid (see Figure 2(a)) is a product similar to NEFMAC grid, but it is manufactured by Chomarat North America, which is one of the only CFRP concrete reinforcing manufacturers in the United States. C-Grid was originally designed for use in precast wall panels, but has also been used in the top flanges of precast double T-beams. C-Grid enables thinner flanges in double T-beams due to the smaller amount of cover needed compared to steel. However, C-grid

has not been used as shear reinforcing in large scale members because its tension capacity is on the order of 5 kip/ft width of material, which is much weaker than typical steel stirrups.

Nevertheless, both the C-Grid and NEFMAC grids show great potential for a shear reinforcing solution. These materials can be fabricated in different strengths and can easily be cut and put in place in the field, using zip ties to hold the material in position during concrete placement. However, the appropriate shear design methods for CFRP grids have not been verified, nor has the development length.

CFRP to Control End-Zone Cracking

The anchorage zone is the region in prestressed concrete members in which the force from the prestressing steel gradually transfers to the concrete through the bond between concrete and steel. Compressive stresses form through this transfer and spread through the member in a curved pattern until a linear stress distribution occurs. These curved compressive stresses create tensile stresses that can cause cracking in the member. A typical crack pattern for anchorage zones of precast Bulb-T (PCBT) beams is shown in Figure 5.
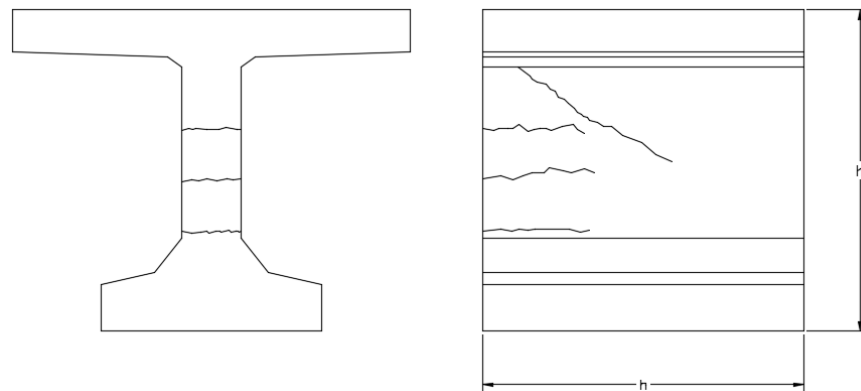

Figure 5. Typical Anchorage Zone Crack Pattern for PCBT

Anchorage zone cracking causes concern because the cracks may allow corrosive agents to reach the reinforcing. Although repairs can be made to these cracks, repairs are expensive and time consuming. In order for VDOT to implement CFRP reinforcing in girders, the proper amount of end zone CFRP reinforcement to control cracking must be determined.

METHODS AND MATERIALS

This section presents the test methods used in this study to determine the tensile properties of the C-Grid, the development length of the C-Grid and NEFMAC grid, and the shear strength of beams reinforced with steel, CFCC stirrups, C-Grid and NEFMAC grid. Also presented are the shear design methods used for comparisons to test results, and the anchorage zone parametric study methods.

6

C-Grid Tensile Strength and Elastic Modulus Tests

Test Specimens

Tensile property testing was performed following the recommended procedures of the manufacturer, Chomarat (2011). Test specimens consisted of single tow specimens with an epoxy grip at each end, which prevented crushing of the fibers in the grips of the testing apparatus. Test specimens were cut from C50 1.6 x 1.8 grid and C50 2.36 x 2.36 grid. C50 refers to the amount of fibers in each tow, which determines the strength of the tow. The second two numbers refer to the spacing of the tows in each direction in inches. There were five specimens of each grid in each tow direction, for a total of 20 specimens. Both directions of tow were used to ensure all C50 grid was the same strength, no matter the direction of the tows. Plywood molds were made for the end grips; wax paper lined the molds to allow for easy removal after the the Scotch-Weld DP 420 epoxy had cured for 24 hours. Test specimens are shown in Figure 6 and the dimensions of the specimens are shown in Figure 7.
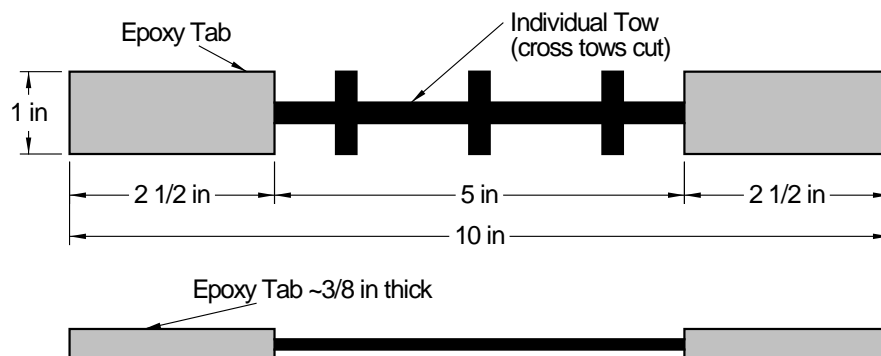

Figure 6. Tensile Strength Specimens

Figure 7. C-Grid Tensile Specimen Dimensions

Test Set-Up

The cross-sectional area was measured before placing each specimen into the MTS testing machine and attaching an extensometer. The elongation speed of the crossheads was 0.079 in/min, per Chomarat North America's testing protocol (2011). Specimens were loaded in tension to failure, while continuously recording the load and elongation data. All failures were

in the length of tow between the grips, as opposed to in the grips, and were quite brittle. A typical failure is shown in Figure 8.
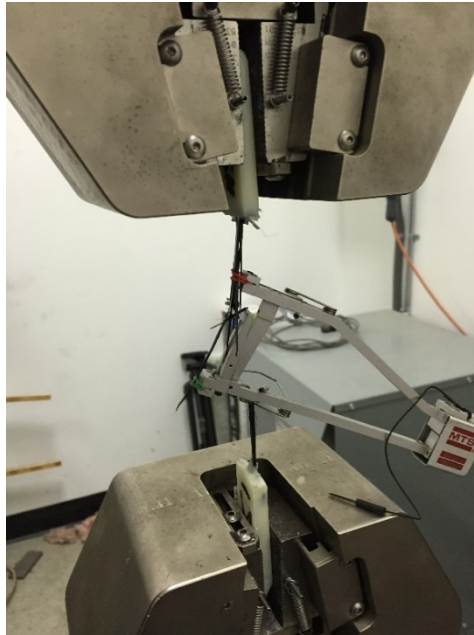

Figure 8. Typical Failure of Tensile Specimen

Instrumentation

Each specimen was tested using an MTS Insight testing machine, which contained a pre-calibrated load cell to record the load on the specimen. Each specimen also used an MTS 634.25 extensometer to measure the strain under axial load. Because the cross-section of the specimens was not perfectly rectangular, but was thicker in the center and thinner at the edges, the extensometer would not stay attached using the built-in clips. Instead, orthodontic rubber bands were much better for affixing the extensometer to the specimens. Data was recorded continuously until failure by a dedicated computer attached to the MTS Insight.

Development Length Tests

Test Specimens

As mentioned previously, there has been minimal research into the development length of C-Grid and NEFMAC grid; this development length was an important factor in the overall design of the beams for shear testing. Research by Ding et al. (2011) showed that the development length for C100 grid was 8 in. Based upon this previous testing, the development length of the C50 1.6 x 1.8 grid was expected to be smaller due to closer spacing and lower strength compared to the C100 grid. Therefore, the tested embedment length varied from 4 in to 8 in, in 1 in increments. There were two specimens of each test length, for a total of ten specimens. Only the C50 1.6 x 1.8 was tested because this was the size to be used in the shear tests.

Figure 9 presents a test specimen, which consisted of two concrete blocks that were 12 in wide and 11 in tall, while the length of the blocks varied with the tested embedment length. The ends of two layers of grid were embedded in each block, with the layers spaced 8 in apart. All specimens had 2 in of clear cover on all sides of the C-grid. Specimen naming followed the convention of *i-j*, where *i* represented the number inches of embedment, and *j* indicated the sample number for that embedment length. Diagrams of C-Grid embedment for each length can be found in Ward (2016).
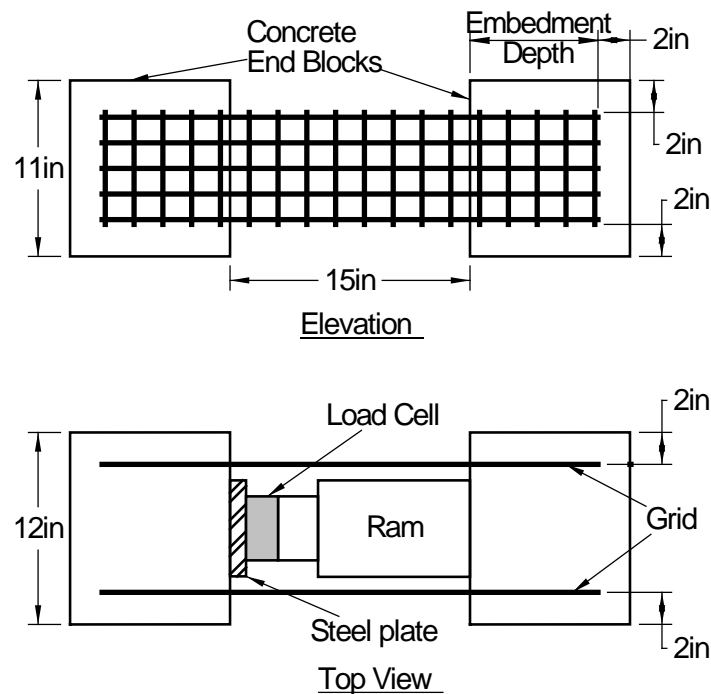

Figure 9. Elevation View of Development Length Specimen for C-Grid

Similar embedment length specimens were fabricated for the NEFMAC grid with the C6 8 in by 10 in spacing. In this case, the test embedment lengths were set at 4 in, 6 in, and 8 in, for a total of six specimens, with each specimen containing two grid sections that were 8 in apart. Each end of both grids had one transverse tow embedded 2½ in into the concrete, as measured from the inside edge of the blocks. The depth of embedment of the specimen was defined by the length of the longitudinal tow after the transverse tow. Figure 10 shows the typical specimen diagram. Note the length of the block was always 2 in more than the tested embedment depth. Identification of the NEFMAC samples followed the same convention as that of the C-Grid specimens.

The specimens were cast in wooden formwork. To reduce the possibility of damaging the specimens prior to testing, the base of the formwork was used as the base of the test set-up. Typical formwork is presented in Figure 11. The C-Grid and NEFMAC specimens were cast on two different occasions, using concrete with the mix design given in Table 1, which was the same mixture used for the beams tested for shear strength.
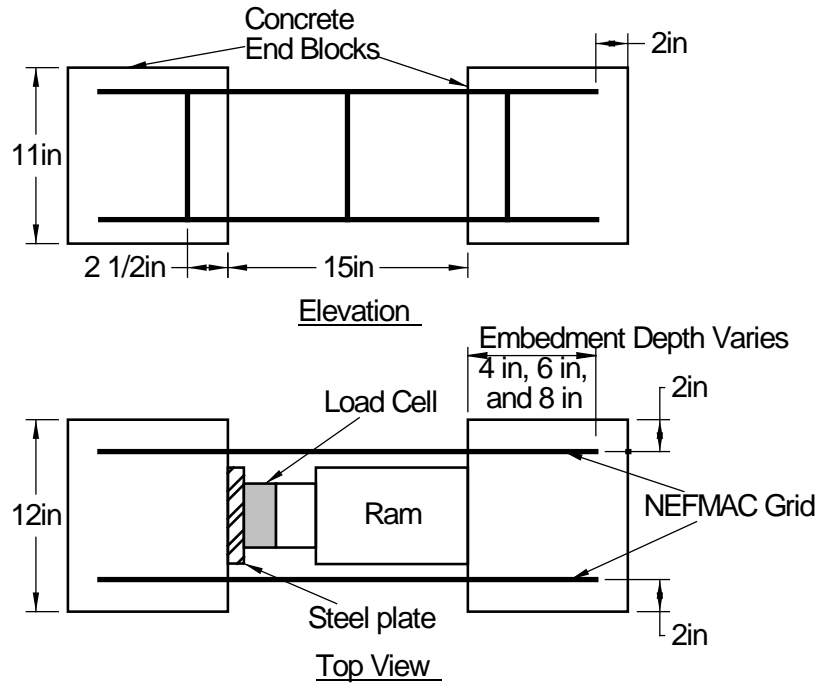
9

Figure 10. Typical Development Length Specimen for NEFMAC

The slump and 28-day compressive strength of the concrete ordered from a local ready mix plant were specified to be 6½ in and 7000 psi, respectively. The concrete was also specified with a maximum aggregate size of ½ in to allow the concrete to easily flow through the C-Grid material. A local ready-mix concrete plant delivered fresh concrete to the lab for each of the two development length specimen placements and three beam specimen placements.   The slump for each batch was measured before placing the concrete in the forms. Twelve 4 in by 8 in cylinders for concrete material testing were cast for each batch. Compressive tests following ASTM C39 protocol were performed at approximately 7 and 14 days after placement to determine strength gain of the mix design. Additional compression testing, splitting tensile testing following ASTM C496, and elastic modulus testing following ASTM C469 also took place before and after testing.
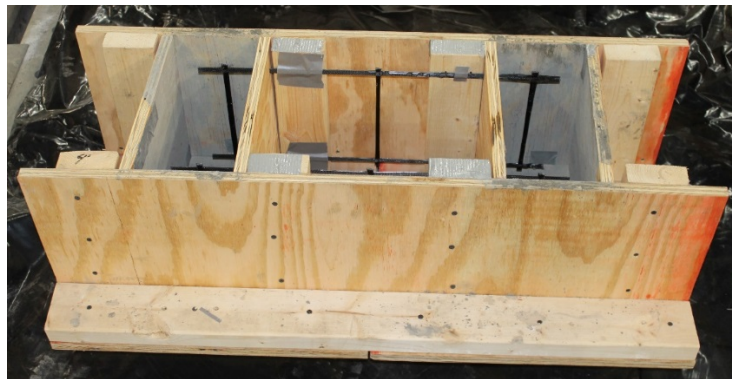

Figure 11. Typical Formwork for Development Length Testing with NEFMAC

Table 1. Concrete Mix Design

Constituent	Amount per cubic yard
No. 8 Stone	1576 lbs
Natural Sand	1530 lbs
Type I/II Cement	652 lbs
Water	159 lbs
Microsilica	53 lbs
Air Entraining Admixture	1.4 oz
Retarder	24.7 oz
Water Reducing Admixture	28.2 oz
w/c ratio	0.37

Test Methods

Figure 12 shows the test set-up for the C-Grid and Figure 13 for the NEFMAC. The formwork was removed from the sides after placing the specimen on the roller table. As shown in Figure 12, the base of the formwork was separated into two halves so that friction of the concrete block against the plywood had no effect on the test results. A hydraulic jack was positioned between the two end blocks and in between the two sections of grid. As the piston extended, the end blocks pulled the grids in tension. There was a load cell in between one block and the jack, but there was some difficulty aligning the jack in the middle of the blocks. Extensometers were placed on the two sides of the specimen to measure the amount of elongation of both sections of grid.

Loading on the blocks was increased slowly until the grid material ruptured. If slip had occurred before rupture, this would indicate that the embedment depth was shorter than the development length. None of the tested blocks failed due to slip. In almost every test, one of the two grids ruptured first. After a few tests, a collar frame was installed around the specimen to help control the movement of the blocks upon the violent fracture of the grid. A typical failure of a development specimen inside of the collar is shown in Figure 14.

Figure 12. Typical C-Grid Test Set Up

Figure 13. Typical NEFMAC Test Set Up

Figure 14. Typical Failure of a Development Length Specimen

Beam Tests

Beam Design

Five 18-ft long beam specimens were fabricated for shear capacity testing: one beam was a control with steel stirrups, one contained CFCC stirrups, two beams used various amounts of C-Grid, and the fifth specimen had NEFMAC grid shear reinforcement. With the exception of the second beam containing C-Grid reinforcing, the beams were initially designed so that one end of the beam contained the minimum transverse reinforcing ratio and the other end contained a typical transverse reinforcement ratio. The second C-Grid specimen was designed using two layers of grid throughout the beam. However, one end used two layers separated by 1 in to allow concrete to consolidate between the layers. For the other end of the beam, the two C-Grid layers were zip tied together approximately every 12 in. This testing was used to determine if placing two layers directly together influenced the shear capacity of the beam. One test was performed at each end of each beam, for a total of ten tests.

Beam cross-sections were small scale versions of bulb-tee beams typically used in highway bridge construction. A spreadsheet was developed to calculate the gross section properties and to iterate the design to arrive at the final dimensions. The top and bottom flanges were made deep enough to ensure development of the C-Grid and the NEFMAC grid while the

12

web was made thin enough that failure of the beam was controlled by shear instead of flexure. Figure 15 shows the cross-section of the beam with major dimensions
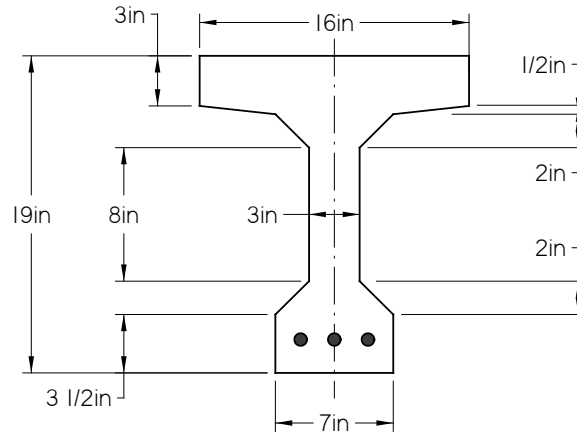

Figure 15. Beam Cross-Section

Using the AASHTO LRFD (2014) method for flexure and both the AASHTO and ACI 318 (2014) codes for shear, the investigators determined the anticipated load for shear failure and the amount of longitudinal reinforcing needed to resist longitudinal flexural failure prior to a shear failure. The typical transverse reinforcement ratio taken from NCHRP report 733 (Cousins, Roberts-Wollmann, Brown, 2013), which was based on a review of many bridge beam designs. Minimum transverse reinforcement specimens were designed based on the AASHTO minimum transverse reinforcement given in Equation 1.

$$A_{v,min} = \frac{\sqrt{f'_c} b_v s}{f_y}$$

Eq. 1

Specimens are presented in Table 2 along with their anticipated shear strength for each of the transverse reinforcing ratios in the specimen. Note that "V_n by AASHTO" in the table is the general procedure, or modified compression field theory method for calculating shear strength, which will be discussed later in the subsection, *Methods for Shear Design with CFRP*. The final column is the expected load in the actuator at failure based on the span length, the shear span and the shear strength.

Figure 16 shows the typical dimensions for the steel and CFCC stirrups. The tail length for the steel stirrups was based on ACI 318 recommendations. CFCC stirrup tail length was based on recommendations from ACI 440.1, which is 12 bar diameters.

Due to a calculation error, Specimens 1 and 2 used three No. 5 bars for the bottom tension reinforcement. This was not enough tension reinforcement to prevent a flexural failure from occurring prior to a shear failure with the point load at 4 ft from the nearest support. Therefore the load points of Specimens 1-Typical Steel and 2-Min C-Grid were modified to ensure a shear failure before flexural failure, as shown in Table 2. After the error was found, Specimens 3, 4 and 5 were designed with three No. 7 bars as the bottom tension steel reinforcement.

Table 2. Beam Specimens

Specimen	Shear Reinforcing	Bar/Tow Area, in²	Bar/Tow Strength, kips	Spacing, in	No. of Layers	V_n by AASHTO, kips	Shear Span, ft	Predicted Failure Load, kips
1	Typ Steel	0.11	6.60	6.0	1	28.4	2.5	36
	Min Steel	0.11	6.60	12.0	1	17.0	4.0	26
2	Typ C-Grid	0.0029	0.83[1]	1.6	3	31.0	4.0	46
	Min C-Grid	0.0029	0.83[1]	1.6	1	18.3	3.5	26
3	Typ CFCC	0.09	4.05[2]	4.0	1	29.2	4.0	44
	Min CFCC	0.09	4.05[2]	9.0	1	19.7	4.0	30
4	C-Grid Zip Tied	0.0029	0.83[1]	1.6	2	29.5	4.0	44
	C-Grid Spaced	0.0029	0.83[1]	1.6	2	29.5	4.0	44
5	Typ NEFMAC	0.027	4.69[1]	10.0	2	28.5	4.0	43
	Min NEFMAC	0.027	4.69[1]	10.0	1	20.5	4.0	31

[1]**According to manufacturer's reported data of mean minus three standard deviations**
[2]**According to ACI 440.4R, maximum stress is at a strain of 0.002**

Beam Construction

After constructing the base and then one side of the formwork, the longitudinal reinforcing was installed using 1¾-in chairs to place the center of the longitudinal reinforcing at 2 in from the bottom of the beam. The transverse reinforcing was tied to the bottom longitudinal reinforcing and then the second side of the formwork was attached to the base. Next, the transverse reinforcement was tied to the top bar, which was held in place by pencil rod anchored across and through the top of the form. Figure 17 shows completed formwork with C-Grid and NEFMAC transverse reinforcement in place.
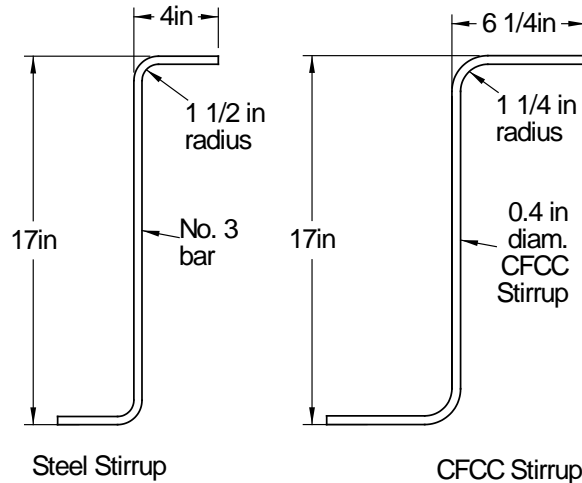

Figure 16. Stirrup Design for Beams

<table>
<tr><td align="center">(a)</td><td align="center">(b)</td></tr>
</table>

Figure 17. Completed Beam Formwork with (a) C-Grid and (b) NEFMAC Grid

As mentioned previously, the concrete cast for the shear test specimens was the same as the concrete used for the development length testing (see Table 1).   The concrete was placed into the forms using a pencil vibrator to consolidate the concrete and magnesium floats to provide a smooth finish on top of the beams. The concrete cured for 7 days with wet burlap and plastic over the top surface. After form removal, the beams cured under ambient conditions for an additional 21 days before testing.

There was a problem with consolidation in the bottom flange of Beam 2 on the end with a typical amount of C-Grid shear reinforcement. Upon closer inspection, it was determined that one of the two outer layers of the C-Grid had buckled into the middle layer, thus blocking the flow of concrete directly into the area of the shear testing. Figure 18 shows the extent of the honeycombing that occurred in the specimen. As a result, this end of the beam was not tested; therefore, there were only nine shear tests instead of the proposed ten. Also, the spacing between layers of C-Grid was increased in Beam 4 in order to ensure adequate space for consolidation of the concrete.

Figure 18. Honeycombing in Three Layers of C-Grid

Test Set-Up

Testing was conducted in the Thomas M. Murray Structures and Materials Laboratory on a self-reacting beam system with two W 21x73 beams clamped to the main reaction beams. Although the specimens were 18 ft long, the two support beams were spaced 12 ft apart, making the tested span length for each shear specimen 12 ft. This allowed for two tests per specimen.

15

The supports for the test specimens were a greased pin at one end and roller at the other to create a simply supported condition. A rubber pad was placed between the bottom of the beam and the top of each support to reduce stress concentrations on the concrete. Figure 19 shows the test set-up schematic for one beam, with the first test on the top and the second test for each beam on the bottom. As indicated in the figure, the point of load application was typically placed at 4 ft from one of the support beams to help ensure failure was controlled by shear. However, for reasons mentioned earlier, the shear span was decreased to 2.5 ft for the typical steel stirrup specimen test and to 3.5 ft for the one layer of C-Grid test. The loading apparatus was a single 150-ton Enerpac hydraulic ram held in place by columns and channels. The load from the hydraulic ram was transferred to the top of the beam via a set of steel plates with a neoprene bearing pad.   The complete testing frame set-up is shown in Figure 20. The test specimens were loaded monotonically to failure, with intermittent pauses to assess cracking patterns during testing.

Beam Instrumentation

Three wire potentiometers were used to measure the deflection of the beam: one near the support at each end of the beam and the third under the load application point. This arrangement enabled the true deflection of the concrete beam specimens to be determined by accounting for any deflection at the steel support beams.

Each beam was also fitted with a rosette on each side of the web, at the midpoint of the shear span (typically 2 ft from the support), for the purposes of determining the principal stresses in the web. The first test used a 0, 45, 90 degree approach, but subsequent tests used a 90, +45, -45 degree rosette made up of Trans-Tek 0350-0000 LVDTS (linear variable differential transformers). The LVDTS were held onto the beam with steel channel brackets adhered to the beam. Also, two additional LVDTs measured the deformation along the height of the web. Since it was not possible to place bonded electrical resistance gages on the small CFRP tows, the vertical LVDTs were used to get an average strain in the grid within the web height. The LVDTs were positioned directly over transverse reinforcement in the beams using CFCC and steel stirrups. The typical LVDT arrangement for the first four beams is shown in Figure 21(a).
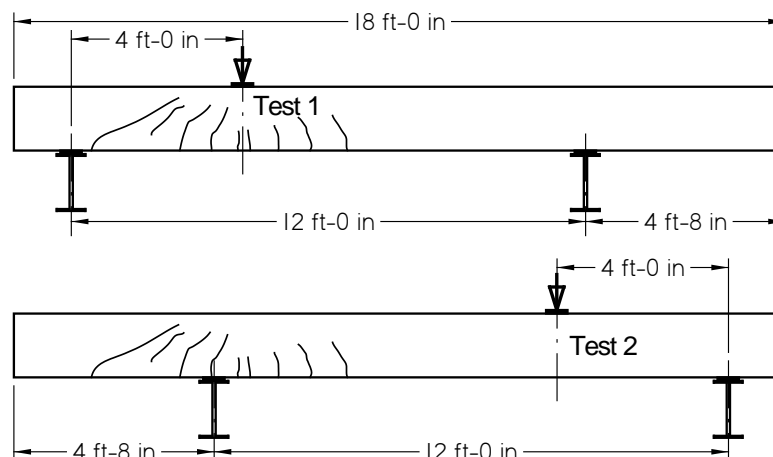

Figure 19. Test Set-up Schematic

Figure 20. Overview of Test Set-up

Figure 21(b) shows the other side of the web with Bridge Diagnostic Inc. strain transducers (BDIs) instead of LVDTs for the rosette and average vertical strain measurements. The positions of the BDI gages mirrored the LVDTs positions to compare values between the two instrumentation types. The BDIs attached to the beam via metal feet that were glued to the beam using adhesive. There were two additional BDI gages aligned vertically on the web, one near the top and adjacent to the load, and the other at the bottom and closer to the support. These two gages, named B1 and B2, were aligned over transverse reinforcement in the beams using CFCC and steel stirrups, with B1 always closer to the applied load and B2 closer to the support. The full instrumentation plan for the beam is shown in Figure 22.   The Beam 5 had a slightly different layout, which is presented in the Results section.

Data from the tests were gathered via a System 5000 computer system made by Vishay. All instrumentation was calibrated before testing, including the load cell, which was calibrated using a Forney concrete compression testing machine.
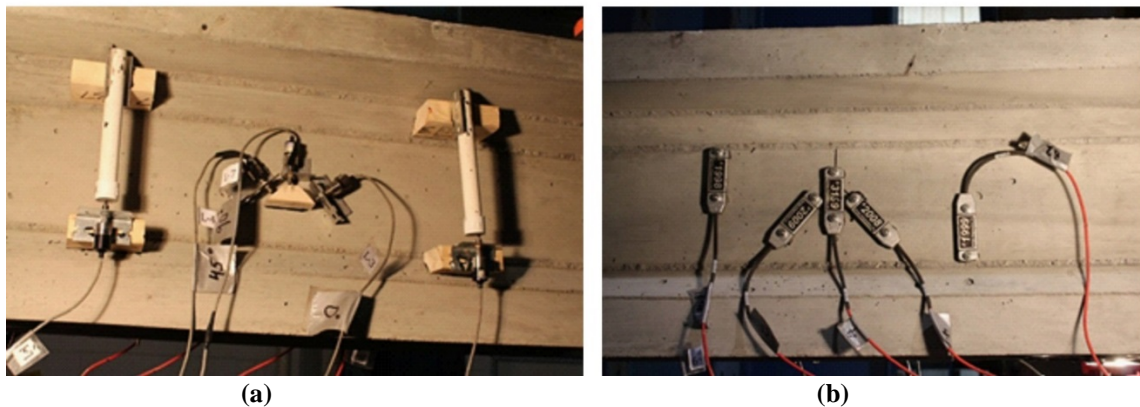

(a)   (b)

Figure 21. (a) Typical LVDT and (b) BDI Gage Rosette and Vertical Strain Set-up for Testing
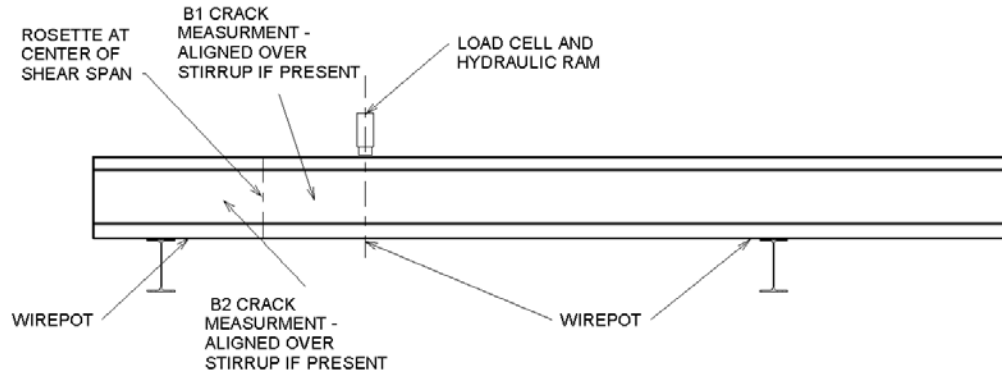
Figure 22. Full Instrumentation for Shear Testing

Methods for Shear Design with CFRP

All test results were compared to four shear design methods. This section presents the four investigated methods.

AASHTO LRFD Shear Design Method

The AASHTO LRFD Bridge Design Specifications (AASHTO, 2014) shear design method was evaluated, although these specifications are intended for bridge members with steel reinforcing bars and prestressing strands. While the specifications present several methods for shear design, this report only presents the most commonly used method, which is the general procedure for shear design using equations to calculate the crack angle and concrete contribution (as opposed to the iterative method using tables presented in Appendix B of Chapter 5 of the specifications). This general method with equations provides a straightforward approach for calculating the shear resistance of prestressed and reinforced concrete sections, taking into account three distinct contributions: resistance of the concrete, resistance from transverse reinforcement, and the resistance from the vertical component of the prestressing force of draped or harped tendons.

The general procedure for shear design in the AASHTO specifications is based upon the Modified Compression Field Theory, which was first developed by Collins et al. (1996). This method predicts the angle, θ, at which shear cracks will develop and calculates a factor, β, to account for the concrete strength. The concrete contribution to shear strength is due to the tensile stress in the concrete before cracking and the aggregate interlock after cracking. To develop appropriate aggregate interlock, the transverse and longitudinal reinforcement restrain the cracks so that they stay narrow enough to allow the engagement of the aggregate.

Therefore, the concrete shear resistance term is a function of the concrete compressive strength, the area of concrete resisting the shear forces (typically the thinnest portion of the web), and β, which is based on the strain in the tension reinforcing. Thus, β is dependent upon the ratio of tension reinforcing and the load that the beam resists, and is defined as:

18

$$\beta = \frac{4.8}{(1+750\varepsilon_s)}$$ <div align="right">Eq. 2</div>

where ε_s is the strain in the tension reinforcement of the beam under maximum loading, and can be calculated as:

$$\varepsilon_s = \frac{\frac{M_u}{d_v} + 0.5N_u + [V_u - V_p] - A_{ps}f_{po}}{E_s A_s + E_p A_{ps}}$$ <div align="right">Eq. 3</div>

where:
 M_u = factored moment of the beam, in-kip
 N_u = factored axial force in the section, kips
 V_u = factored shear force, kips
 V_p = vertical component of prestressing force, kips
 E_s = modulus of elasticity of reinforcing steel, ksi
 A_s = area of tension reinforcing steel, in^2
 E_p = modulus of elasticity of the prestressing steel, ksi
 A_{ps} = area of the prestressing steel, in^2
 f_{po} = stress in the prestressing steel, typically taken as $0.7f_{pu}$, ksi
 f_{pu} = ultimate stress of the prestressing steel, ksi

Note that Equation 3 divides the force in the tension steel by the stiffness of the longitudinal reinforcing in order to determine the strain.

Given β, the concrete shear resistance is calculated as:

$$V_c = 0.0316\beta\sqrt{f'_c}b_v d_v$$ <div align="right">Eq. 4</div>

where:
 f'_c = 28-day compressive strength of the concrete, ksi
 b_v = effective web width, in
 d_v = effective depth, in

The shear resistance from the transverse reinforcement is calculated as:

$$V_s = \frac{A_v f_y d_v (cot\theta + cot\alpha)sin\alpha}{s}$$ <div align="right">Eq. 5</div>

where:
 s = spacing of the transverse ties (or tows if a grid material is used), in
 A_v = area of transverse reinforcement within each spacing, in^2
 f_y = yield stress of transverse reinforcement, ksi
 α = angle of the transverse reinforcement from the horizontal
 θ = angle of diagonal compressive stresses at the section, which is calculated as:

$$\theta = 29 + 3500\varepsilon_s \qquad\qquad \text{Eq. 6}$$

According to Equation 6, θ is dependent upon the strain in the longitudinal tension steel. Again, the smaller the strain in the tension steel, the smaller the value of θ. That strain in the tension steel is dependent upon the longitudinal reinforcing ratio and the loading to which the section is subjected.

If the transverse reinforcing is placed at 90 degrees to the longitudinal axis of the section, then Equation 5 simplifies to:

$$V_s = \frac{A_v f_y d_v \cot\theta}{s} \qquad\qquad \text{Eq. 7}$$

When using CFRP, f_y should be replaced with f_{fu}, which is the design tensile strength of the tow or bar, as these products do not yield. According to ACI 440.1R, f_{fu} is the guaranteed tensile strength reduced by an environmental degradation factor. AASHTO limits the magnitude of the f_y term to no more than the lesser of 0.0035 times the modulus of elasticity or 75 ksi, provided that specified minimum yield strength is greater than 60 ksi (AASHTO, 2014, Section 5.8.2.8).

As previously mentioned, the strength of a prestressed section includes the shear resistance from the prestressing, V_p. This force is the vertical component of the prestressing force due to harped or draped tendons in kips. Using this additional resistance component can help reduce the amount of shear reinforcement needed, especially in beams with a large amount of prestressing. Because the tests in this report did not use prestressed reinforcement, this term is not applicable.

Again, the terms β and θ in the equations for the V_c and V_s term depend on the amount of longitudinal reinforcement in the section and the loading the section undergoes. A higher loading on the beam will result in a higher ε_s for all longitudinal reinforcement ratios. Also, if the section has a larger longitudinal reinforcement area or modulus of elasticity, then ε_s will be smaller.

A smaller ε_s will give a larger β term, meaning the concrete resistance to shear will increase due to increased aggregate interlock. The smaller strain also will make θ smaller, which increases the shear resistance provided by the transverse reinforcement because the crack will cross and engage more stirrups. Therefore, increasing the flexural reinforcement of the beam under the same loading and with the same transverse reinforcement can increase the shear capacity of the beam.

ACI 318-14 Shear Design Method

The ACI 318 Building Code (ACI, 2014) provides methods to calculate shear capacity of both reinforced and prestressed beams when using steel reinforcement. Because the beams in this report were not prestressed, the ACI method for shear capacity presented is for reinforced

sections only.   ACI determines the shear resistance provided by two components of the section. The first component is the shear resistance of the concrete, V_c. The concrete contribution is based on formulas that were empirically derived by fitting curves to previously tested data sets, and is given as:

$$V_c = 2\lambda\sqrt{f'_c}b_w d$$

Eq. 8

where:
   f'_c = specified 28 day compressive strength of concrete, psi
   λ = modification factor for the reduced tensile and shear strength of lightweight concrete (1.0 is used if normal weight concrete used)
   d = depth of the section from the extreme compression fiber to center of tension reinforcement, in
   b_w = minimum web width, in

The second component of shear resistance is V_s, the contribution of the reinforcing and is based upon spacing and yield strength of that reinforcing:

$$V_s = \frac{A_v f_{yt} d}{s}$$

Eq. 9

where:
   s = center-to-center spacing of the transverse reinforcement, in
   A_v = area of transverse reinforcement within the spacing, in^2
   f_{yt} = specified yield strength of the transverse reinforcement, psi

When using CFRP, f_{yt} should be f_{fu}, the design tensile strength of the tow or bar, as these products do not yield. As mentioned in the previous section, according to ACI 440.1R, f_{fu} is the guaranteed tensile strength reduced by an environmental degradation factor. ACI 318 places a limit of 80 ksi on the yield strength to be used in shear calculations. Although ACI 318 does not specifically address FRP reinforcement, this limit was applied in this study. The contribution of the reinforcing and concrete are summed together to find the nominal shear resistance of the section.

ACI 440.4R-04 Shear Design Method

ACI 440.4R-04 (ACI, 2004) presents a method for the shear design of prestressed FRP concrete sections. The shear design method in this document mirrors the standard shear design method from ACI 318. The two equations are presented as Equations 10 and 11, which are equations 5-2 and 5-3, respectively, in the 440.4R document. One interesting note is that, unlike AASHTO specifications for steel, this document does not allow for an additional shear resistance from the prestressing strands, because CFRP tendons are rarely harped.

$$V_c = 2\sqrt{f'_c}b_w d$$

Eq. 10

$$V_{frp} = \frac{A_v f_{fb} d}{s}$$

Eq. 11

where most terms are as previously defined except:

V_{frp} = contribution from the transverse FRP reinforcing to the shear resistance

f_{fb} = strength of the bent portion of the FRP bar, psi

Note that the concrete resistance equation uses the same terms as ACI 318-14, with the exception of the lightweight concrete modification factor. The transverse reinforcing equation for V_{frp} is also the same except that f_{fb} is based on the minimum design strength of the bend in the FRP stirrup, which is the weakest area of the stirrup according to past studies (Morphy et al., 1997). The equation takes into account the bend radius and diameter of the bar to ensure a safe, conservative design when using FRP stirrups. The necessary equations for calculating f_{fb} are:

$$f_{fb} = \text{Lesser of: } \phi_{bend} f_{fu} \text{ or } 0.002 E_f \qquad \text{Eq. 12}$$

$$\phi_{bend} = \left(0.11 + 0.05 \frac{r}{d_b}\right) \text{ and } 0.25 \leq \phi_{bend} \leq 1.0 \qquad \text{Eq. 13}$$

where:

f_{fu} = design tensile strength of the FRP, psi,

E_f = design modulus of elasticity of the FRP, psi,

ϕ_{bend} = strength reduction factor that depends on the radius of the bend

r = bend radius, in

d_b = diameter of the FRP bar, in

The above limits were established to ensure that the bar will not rupture at the bend. Note that all FRP stirrups should be closed with a 90 degree bend; this bend should have an r versus d_b ratio of 3.0 or greater and have a minimum tail length of $12d_b$.

ACI 440.1R-06 Shear Design Method

While ACI 440.4R-04 deals with prestressed FRP applications, ACI 440.1R-06 (ACI, 2006) provides guidelines for the design and construction of reinforced concrete sections using FRP reinforcement that is not prestressed. Like the other two ACI methods, this shear capacity method uses the concrete and transverse reinforcement shear resistance equations, but the concrete equation is much different. The premise of the equation is that there is no shear transmitted across the open shear crack. Instead, the shear force is transmitted by the uncracked concrete above the neutral axis, as suggested by Tureyen and Frosch (2003). The 440.1R document defines the concrete contribution with Equation 14. All these terms except for c, which is discussed below, were defined previously in the ACI 318 shear design section.

$$V_c = 5\sqrt{f'_c} b_w c \qquad \text{Eq. 14}$$

The term c is defined as the distance, in inches, from the compression face to the neutral axis. The neutral axis is calculated using the cracked transformed section. The cracked transformed section helps to provide a better estimate of shear strength by taking into account the axial stiffness of the longitudinal tension reinforcement. That stiffness is the product of the area and modulus of elasticity. If the stiffness of the longitudinal reinforcement is larger, then c will

also be larger. As a result, there will be a larger section of concrete in compression to carry the shear, and thus, increased shear resistance from the concrete. In a way, this approach is similar to the AASHTO method in that increasing the longitudinal tension reinforcing increases the shear capacity of the concrete.

ACI 440.1R calculates the concrete contribution based upon a cracked section analysis to find the depth to the neutral axis, c, which is straight forward for rectangular sections. However, because the beams in this study had wide flanges, the web width, b_w, was not the proper dimension for calculating the shear capacity of the concrete because the flange provided such a large portion of uncracked concrete to carry the shear. Therefore, the concrete's shear resistance was determined by adapting the shear funnel approach, described in Tureyen, Wolf, and Frosh (2006). The authors recommend an area determined by extending lines at a 45° from the edges of the web up into the flanges. This area is illustrated by the shaded region in Figure 23. The area of this shaded region, or shear funnel, replaces the $b_w c$ term in Equation 14.
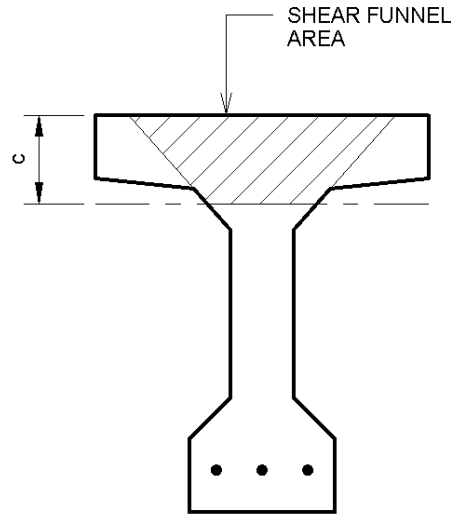

Figure 23. Shear Funnel Diagram for Beam Specimens

The reinforcing shear resistance is very similar to the previously discussed ACI methods. The FRP resistance equation is shown below as Equation 15. The terms d and s were previously defined in the ACI 318 section.

$$V_f = \frac{A_{fv} f_{fv} d}{s}$$

Eq. 15

where:

A_{fv} = area of transverse FRP reinforcement within the spacing, in^2
f_{fv} = design tensile strength of the FRP shear reinforcement (psi), but limited to

$$f_{fv} = \min \begin{cases} f_{fb} = (0.05\frac{r_b}{d_b} + 0.03)f_{fu} \\ f_{fu} \\ 0.004E_f \end{cases}$$

Eq. 16

Parametric Study on Anchorage Zone Design with CFRP Grids

A concern for the long term durability of prestressed beams is the cracking that occurs in the end zones during detensioning. Two parametric studies were conducted to determine the amount of CFRP grid reinforcing required to control end zone cracking. The design approach proposed by Crispino (2007) was used. The allowable stresses in the CFRP required to control cracking to acceptable levels was determined based on cracking observed in the shear tests. The first study developed anchorage zone designs with CFRP grid as the sole transverse reinforcement. The second study considered a combination of steel stirrups and CFRP grids as a way to reduce current beam-end reinforcement congestion for beams that are not in areas highly susceptible to corrosion. Three different PCBT beams were investigated, each with three different combinations of beam spacing, span length, and number of prestressing strands. This resulted in nine anchorage zone designs for each of the two parametric studies. Table 3 lists these beams.

Table 3. Parametric Study Beam Selection

Trial Name	Beam Type	Bean Spacing, ft	Span Length, ft	No. of 0.5-in diameter strands
PCBT-45A	PCBT-45	6	40	16
PCBT-45B	PCBT-45	7.5	65	20
PCBT-45C	PCBT-45	9	60	16
PCBT-61A	PCBT-61	6	90	22
PCBT-61B	PCBT-61	7.5	80	26
PCBT-61C	PCBT-61	9	80	26
PCBT-77A	PCBT-77	6	75	20
PCBT-77B	PCBT-77	7.5	100	26
PCBT-77C	PCBT-77	9	90	24

Assumptions

There were many assumptions about material properties for the beam design. Based on AASHTO, steel stirrups are allowed a working stress of 20 ksi. However, based on recommendations provided by Crispino (2007), the steel stirrups in this project were limited to 18 ksi for normal weight concrete in order to better control cracking. To achieve a similar level of cracking when using the CFRP grids, the working stress for the C-grid and NEFMAC reinforcement was limited based on the crack measurements obtained from the shear testing performed in this study. The methods used to make the determination are described in the Results section of this report.

The unit weight of normal weight concrete was assumed to be 150 lb/ft^3. The design compressive strength of concrete at release was 5,500 psi. Using these two assumptions, the

modulus of elasticity of the concrete at transfer was computed using AASHTO LFRD equation 5.4.2.4-1, shown in Equation 17.

$$E_{ci} = 33w^{1.5}\sqrt{f_{ci}}$$

Eq. 17

where:
  E_{ci} = Concrete modulus of elasticity at transfer, ksi
  w = Unit weight of concrete, lb/ft^3
  f_{ci} = Compressive strength of concrete at release, psi

The ultimate strength of the prestressing steel was taken as 270 ksi, and 75 percent of this strength, 202.5 ksi, was the assumed initial stress at transfer. Harping points for draped strands were located at 40 and 60 percent of the beam length. The rows of prestressing strands were filled in from the bottom-up for straight strands, and top-down for harped strands. The top row of harped strands was at a height of 2 in below the top at the end of the beam. All strands were spaced 2 in apart, center-to-center. Lastly, there were no debonded strands in this study.

Strut-and-Tie Model

The strut-and-tie model used for the design of prestressed anchorage zones in this report was developed for PCBT sections by Crispino (2007). This strut-and-tie model is shown in Figure 24. Note that P_1 and P_2 in the figure are the prestressing forces produced by the straight and harped strands, respectively. Crispino found that the required stirrup area within $h/4$ and between $h/4$ and $3h/4$ (measured from the beam end) are very similar, where h is the overall height of the beam. Based on other models, Crispino placed the compressive strut at $3h/4$ from the beam end and also set the two tension ties in Figure 24, $T1$ and $T2$, equal to each other. By doing so, $T1$ and $T2$ can be calculated using Equation 18.
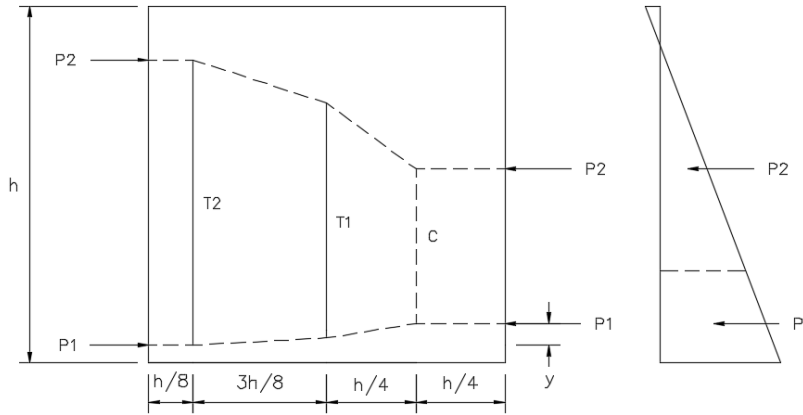

Figure 24. Strut-and-Tie Model

$$T1 = T2 = \frac{8P_1 y}{7h}$$

Eq. 18

where:
  P_1 = Force in straight strand group, kip

25

y = difference in height between resultant force and applied prestress force, in
h = girder height, in

Parametric Study Design Procedure

For this project, a spreadsheet was created to easily solve the strut-and-tie model discussed above. The spreadsheet used the PCBT girder geometry, material properties of the concrete and prestressing steel, and the strand pattern to calculate the transformed section properties at a distance h from the beam and at the harping point. Also, the spreadsheet computed the tensile and compressive stresses at the top and bottom of these locations. The location of the resultant force was determined through integration of the stress on the area of concrete from bottom-to-top. Once the location of the resultant force was determined, *T1* and *T2* could be calculated using Equation 18. With these results, the stirrup area required within h/4 and between h/4 and 3h/4 could be determined, based on the assumed working stresses for the material used. As previously noted, the second parametric study combined CFRP grid with a pre-determined amount of steel stirrups. That amount of steel was based on ease of construction and reducing the amount of congestion. Detailed examples of this procedure after finding the resultant force location are provided in the following Results section. Also, see Magee (2016) for the process of completing the strut-and-tie model and calculating the resultant force location.

RESULTS

C-Grid Tensile Properties

Tensile tests were conducted to determine tow strength and modulus of elasticity of the C-Grid and the results were compared to values reported by the manufacturer. Each specimen's width and thickness were measured and then each specimen was loaded in tension until failure. Results are shown in Table 4. The mean tensile strength for the tows was 1337 lbs. For the ACI definition of guaranteed tensile strength, f*$_{fu}$, the mean must be reduced by three standard deviations, giving a guaranteed tensile strength of 968 lbs, which is about 17% more than the manufacturer reported strength of 830 lbs per tow.

The elastic modulus found in testing was 8,830 ksi, which was much smaller than the manufacturer reported value of 34,000 ksi, due to the discrepancy in measuring the area of the individual tows. The area of the tows in this project was determined by measuring the width and thickness with a set of calipers at the center of each specimen. However, the tows are thicker at the center and very thin at the edges. Therefore, the recorded areas from this project averaged 0.011 in^2, which was much larger than the reported area of 0.00286 in^2 by Chomarat. Using the manufacturer's reported area, the average elastic modulus was recalculated to be 32,600 ksi, which was much closer to the value given for the C50 materials. Because the measured strength of each tow was similar to that reported by Choromat, and the modulus was similar using their cross-sectional area, it was concluded that Choromat's area was more accurate that the simple length times width calculation used to determine the areas shown in Table 4.

26

Table 4. C-Grid Tensile Test Results

Sample	Max Load, lbs	Max Strain in/in	Area, in²	Max Stress, ksi	Elastic Modulus, ksi
NS1	1210	0.014	0.010	117	8690
NS2	1391	0.017	0.013	104	6330
NS3	1434	0.015	0.012	122	8390
NS4	1323	0.016	0.011	119	7670
NS5	1384	0.015	0.010	133	8870
EW1	1299	0.015	0.011	118	8130
EW2	1600	0.017	0.010	157	9250
EW3	1499	0.016	0.010	148	9220
EW4	1453	0.016	0.010	145	9390
EW5	171	0.013	0.011	111	8890
NS6	1319	0.013	0.009	142	10900
NS7	1407	0.014	0.009	165	11800
NS8	1379	0.014	0.009	147	10900
NS9	1324	0.013	0.009	156	12000
NS10	1360	0.014	0.010	137	9750
EW6	1151	0.012	0.013	88	7650
EW7	1042	0.017	0.012	86	5060
EW8	1280	0.014	0.013	101	7230
EW9	1351	0.014	0.011	119	8510
EW10	1371	0.014	0.012	113	8060
Average	1337	0.014	0.011	126	8830
Std. Dev.	123.0	0.001	0.001	22	1670
Average – 3*Std. Dev.	968	0.010	-	60	3820

NEFMAC Tensile Properties

Several attempts were made to perform tension tests on NEFMAC grid, but failures always occurred in the grips. Therefore, the manufacturer's reported design properties are used and are as shown in Table 5. The strength and modulus are the tested average minus three standard deviations.

Table 5. Material Properties for NEFMAC C6

Tow Area	0.027 in²
Guaranteed Tensile Strength	4.69 kips
Tensile Stress	173 ksi
Modulus of Elasticity	14500 ksi

Development Length Tests

Concrete Material Property Tests

The concrete used for the development length tests was purchased from the local ready-mix concrete plant and delivered to the lab. The C-Grid and NEFMAC grid test specimens were cast on different days, and the 28-day properties are presented in Table 6.

Table 6. Concrete Properties for Development Length Tests

Grid	Compressive Strength, psi	Tensile Strength, psi
C-Grid	5540	500
NEFMAC	7490	565

C-Grid

There were a total of ten development length tests. However, there was a slight issue during the test of the first specimen, Specimen 8-1. In this test, the jack was too close to the bottom of the blocks, causing a bending force in the grids instead of a pure axial force. The bending became apparent as the end of the blocks began to lift and only the bottom tows of the grids failed. Therefore, Specimen 8-1 was discounted from the analysis of the rest of the specimens due to this error.

The jack misalignment was corrected for the remainder of the specimens. Nevertheless, in all tests, only one side of the grid ruptured, indicating that there was still some unintended eccentricity in the force application due to the difficulty in exactly centering the jack between the two grids and the fact that the concrete face and grids were not perfectly square.

The load versus displacement data on each side of the specimens was examined using graphs similar that shown in Figure 25. Note that the graph indicates when the grids started to slip within the concrete by a change in slope of one or both of the lines before the grid reached ultimate failure. Furthermore, all of the plots showed that one side of the specimen was more heavily loaded than the other. Because the load came from a single source (that is, the jack) and there were no strain gages on the tows, the fraction of the total load carried by each tow was determined using the slope of the ascending branch of the load versus displacement plot for each side of each specimen. Table 7 presents LVDT readings at two loading points, 1000 lb and 10,000 lb, as well as the slope of the line between these points. No slip had occurred in any of the specimens up to 10,000 lb. Therefore, all changes in LVDT readings were due to a change in strain of the grids. Thus, the side with the larger slope was resisting a higher percentage of the load. Based on the ratios of the slopes, the load in each grid was calculated; the larger load is presented in the table. Because there were five tows in each grid, this larger load was divided by five to arrive at the load per tow, which is listed in the final column of Table 7.

That last column in Table 7 shows that the load per tow at rupture was always greater than the manufacturer's reported strength of 830 lbs per tow, which includes the reduction of three standard deviations from the average. All failure loads also exceeded the tested average strength minus three standard deviations, which was 968 lbs per tow. However, the average strength from the tensile testing presented in this report was 1370 lbs per tow, and many of the reported values fall below this. The lower apparent tensile strengths may be due to eccentricities in the vertical direction and the horizontal direction, as well as variations in strength.

To better determine if the embedment length influenced the failure loads, Figure 26 presents a plot of the load per tow versus the embedment depth, where the load was that for the more heavily loaded tows in a given specimen. The figure clearly shows that there was essentially no change in the failure load with increasing embedment depth. Therefore, the C-Grid was fully developed with a 4-in embedment depth.
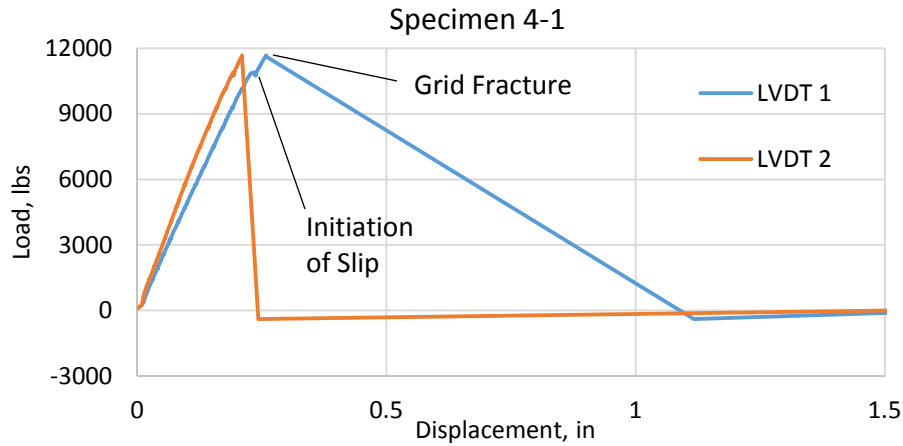
Figure 25. Typical Load versus Displacement Plot for C-Grid

Table 7. C-Grid Development Length Testing Results

| Test	Max Load, lb	Slip?	LVDT 1, in		LVDT 2, in		Slope, lbs/in		Larger Load, lb	
			1000 lb	10,000 lb	1000 lb	10,000 lb	LVDT 1	LVDT 2	per side	per tow
4-1	11676	No	0.0231	0.2070	0.0174	0.1737	48,940	57,580	6310	1260
4-2	12783	No	0.0176	0.1691	0.0210	0.2086	59,410	47,970	7070	1410
5-1	11208	No	0.0226	0.1898	0.0260	0.2095	53,830	49,050	5900	1180
5-2	10186	No	0.0129	0.1726	0.0238	0.2208	56,360	45,690	5630	1130
6-1	11883	No	0.0243	0.2278	0.0213	0.1690	44,230	60,930	6890	1380
6-2	10692	No	0.0163	0.2433	0.0199	0.2231	39,650	44,290	5640	1130
7-1	11117	No	0.0353	0.2127	0.0130	0.1949	50,730	49,480	5630	1130
7-2	12676	No	0.0155	0.2009	0.0167	0.1834	48,540	53,990	6680	1330
8-1	6110	No	0.0146	0.1022	0.0233	0.1293	57,080	47,170	-	-
8-2	10213	No	0.0185	0.2258	0.0117	0.1533	43,420	63,560	6070	1210
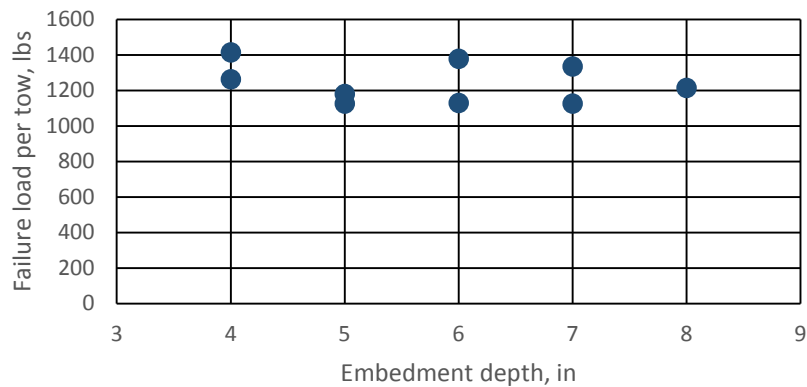
Figure 26. Failure Load versus Embedment Depth for C-Grid

NEFMAC Grid

There were six development tests with the NEFMAC grid; the results are presented in Table 8. Unfortunately, a portion of the formwork for Specimen 4-1 became misaligned during concrete placement. This misalignment resulted in the jack applying a bending force in addition to an axial force to the concrete blocks. The unanticipated load subsequently resulted in a failure load slightly smaller than the expected rupture load of the NEFMAC grid.

There were no casting issues for the five remaining development test specimens, which were only loaded axially. NEFMAC Specimens 4-1 and 8-1, only ruptured on one side of the specimen, likely due to the jack not being perfectly centered. Even though only one side ruptured, there was no apparent slippage of the grid out of the concrete, as evidenced by the constant slope in the load versus displacement plot up to the point of rupture in Figure 27. Specimen 6-1 in this figure is fairly typical. There were difficulties with the LVDTs for Specimen 6-2, so only the full failure load is reported in Table 8. The plots for all of the specimens are in Magee (2016).

Table 8. NEFMAC Development Length Testing Results

| Test	Max Load, lb	Slip?	LVDT 1		LVDT 2		Slope, lbs/in		Larger Load, lb	
			1000 lb	15,000 lb	1000 lb	15,000 lb	LVDT 1	LVDT 2	per side	per tow
4-1	15081	No	0.0122	0.165	0.0154	0.189	91,620	80,640	8020	4010
4-2	17875	No	0.0066	0.163	0.0136	0.209	71,650	71,650	9930	4960
6-1	20279	No	0.0170	0.195	0.0140	0.153	100,720	100,720	11,390	5690
6-2	18098	No	-	-	-	-	-	-	-	-
8-1	16073	No	0.0114	0.167	0.0101	0.161	92,780	92,780	8160	4080
8-2	17651	No	0.0143	0.176	0.0140	0.157	97,900	97,900	9370	4684
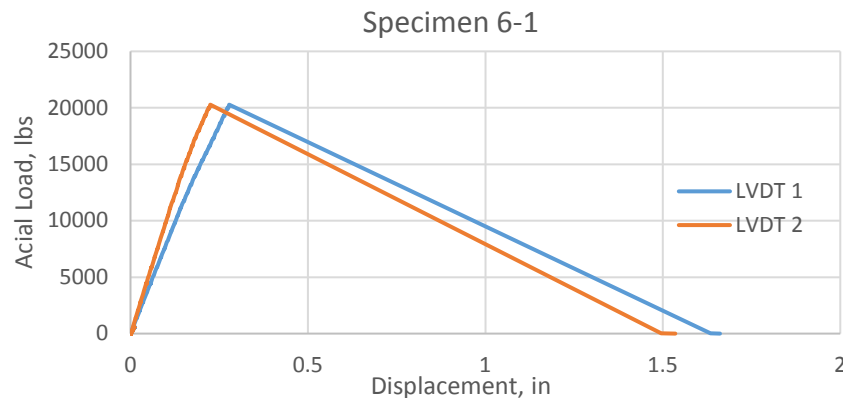
Figure 27. Typical Load versus Displacement Plot for NEFMAC Grid

The NEFMAC data was analyzed in the same fashion as the C-Grid to account for the unequal loading. As shown in Table 8, the breaking load per tow varied from 4010 lbs to 5690 lbs. The NEFMAC manufacturer reported each tow in the grid to have a guaranteed tensile strength of 4690 lbs, which is the tested mean minus three standard deviations. Some of the test results fell below the expected failure load, but this could be due to eccentricity in the vertical, as well as the horizontal direction.

To better assess whether embedment length influenced the breaking load, consider Figure 28, which presents a plot of load per tow versus embedment depth. Again, the load per tow was that of the more heavily loaded side of the specimen. As seen with the C-Grid, there is essentially no change in the failure load with increasing embedment depth. Therefore, the NEFMAC grid was fully developed with a 4-in embedment depth.
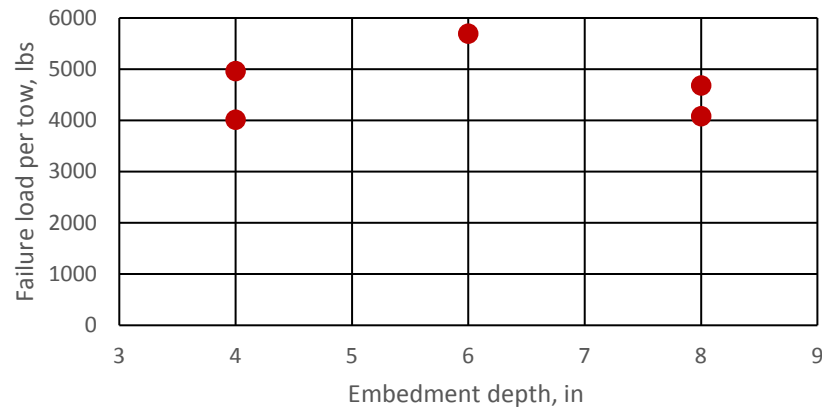

Figure 28. Failure Load versus Embedment Depth for NEFMAC Grid

Beam Test Results

Concrete Material Testing for Beam Specimens

The average concrete properties for shear beam testing are shown in Table 9. Placement 1 was for Specimens 1 and 2, Placement 2 was for Specimens 3 and 4, and Placement 3 was for Specimen 5. Full concrete test data are available in Ward (2016) and Magee (2016).

Table 9. Beam Test Concrete Properties

Property	Placement 1	Placement 2	Placement 3
Compressive Strength, ksi	7.99	7.35	6.34
Splitting Tensile Strength, ksi	0.690	0.605	0.435
Modulus of Elasticity, ksi	5020	4620	4540

Steel Longitudinal Reinforcing Material Tests

In addition to the concrete material properties, the properties of the steel reinforcing bars used in the construction of the beams were also determined. The test procedure followed that outlined in ASTM A370 (2014). Only No. 5 bar was tested, even though the beams also contained No. 3 and No. 7 bars. All bars were ordered from the same supplier, and it was assumed that all bars had similar material properties. There were three separate 18-in sections of bar tested in the SATEC universal testing machine.   The average modulus of elasticity for the reinforcing bar was 29,900 ksi, while the yield and ultimate stresses were 59 ksi and 90 ksi, respectively.

Rosette Data

Recall that rosettes were installed on both sides of Beams 1 through 4 to gather strain data that would allow the principal stresses and angles to be calculated. However, analysis of the strain data provided very little useful information due to scatter; the principal angle inconsistently bounced back and forth from positive to negative angles. Therefore, no data from the LVDTs on 45 degree angles is presented herein.

Specimen 1 Minimum Steel Reinforcement

One half of Specimen 1 contained No. 3 steel stirrups spaced at 12 in on center, which was the minimum reinforcement ratio allowed by AASHTO, as previously described in this report. The cross-section of Specimen 1 is shown in Figure 29. The load applied to the beam was increased in 5-kip increments up to 20 kips, and then in 2-kip increments until completion of testing. Flexural cracking first occurred at 10 kips; the first shear crack, which formed at 15 kips, was initially 0.004 in wide. The testing ended at 32 kips, due to yielding of the tension reinforcement. However, the predicted shear capacity was 26 kips of applied load (17 kips of shear). The load versus deflection plot for this specimen is shown in Figure 30. Note the plateau in the curve indicating that the beam had reached its flexural capacity.
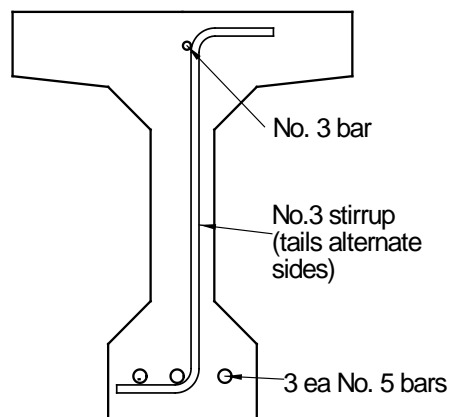

Figure 29. Cross-section of Specimen 1 Steel Reinforcement

For this test, the investigators only measured one crack using a crack microscope initially, but then determined that using a crack card was a simpler and safer method. The researcher team did not measure crack widths after 24 kips of applied load (16 kips of shear), due to concerns about safety. Crack width measurements are shown in Figure 31, along with the best fit linear equation for crack widening versus the shear load.

Because LVDTs can accommodate a larger range of displacement than the BDI gages, the LVDTs can capture post-cracking movement better. Figure 32 shows the displacement measurements by gages B1, B2, and the 90° LVDT in the rosette set-up. This plot indicates that cracking occurred at about 10 kips of shear load, which corresponds to the first visible crack appearing at 10.5 kips of shear load. Also, the displacement measurements from gages LVDT 90 and B1 match very well with the measurement using the crack card at 15 kips.
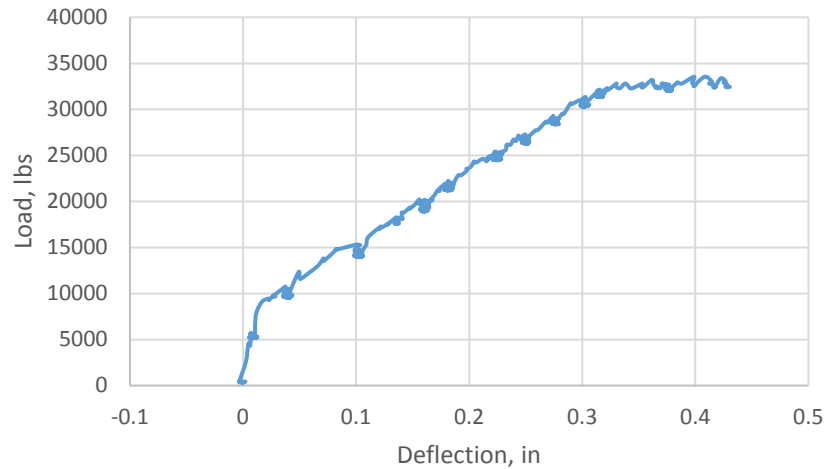
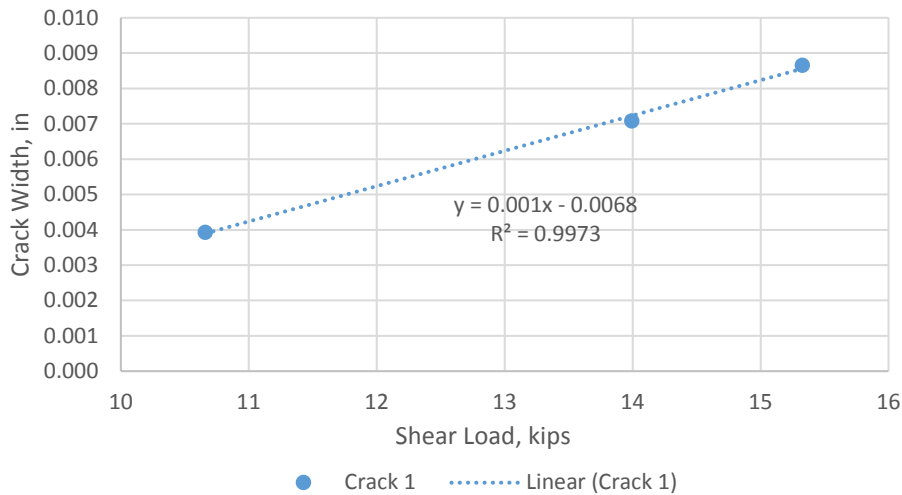32

Figure 30. Load-Deflection Specimen 1 Minimum Steel

Figure 31. Measured Crack Width during Testing for Specimen 1 with Minimum Steel Reinforcement

Specimen 1 with Typical Steel Reinforcement

The end of the specimen with typical steel reinforcement had No. 3 stirrups at 6 in on center. The cross-section is the same as shown in Figure 29. Due to the flexural yielding of the tension reinforcement in the test with the minimum shear reinforcement, the loading point for this test was modified to 2.5 ft from the support to place a higher shear load for a given moment in the beam, thus causing a shear failure to occur before flexural yielding.

The load was applied in 5-kip increments up to 20 kips and then in 2-kip increments until removing instrumentation from the beam at 44 kips because the beam became inelastic in flexure, as shown by the plateau at the end of the plot in Figure 33. From that point, the beam was loaded to 54 kips, when the beam failed in flexure due to crushing of the top flange, as shown in Figure 34. The predicted shear capacity was 36 kips of applied load (28.4 kips of shear).
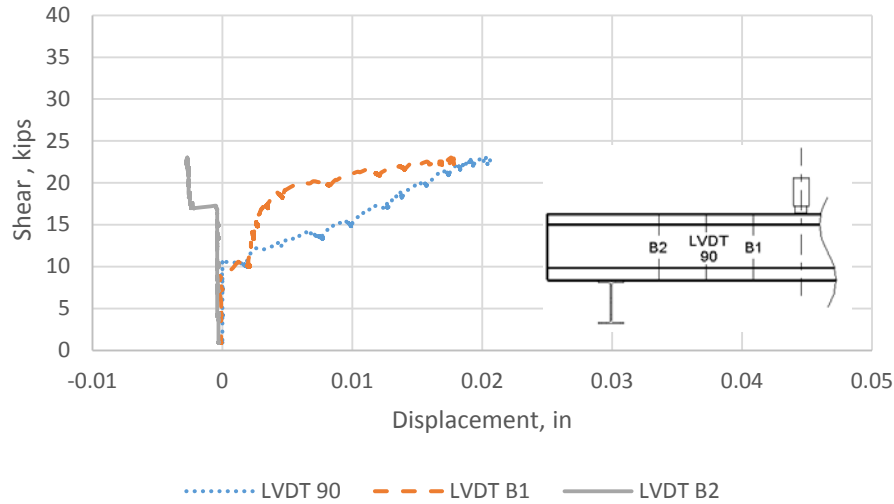
33

Figure 32. Vertical LVDT Displacement of Specimen 1 with Minimum Steel Reinforcement
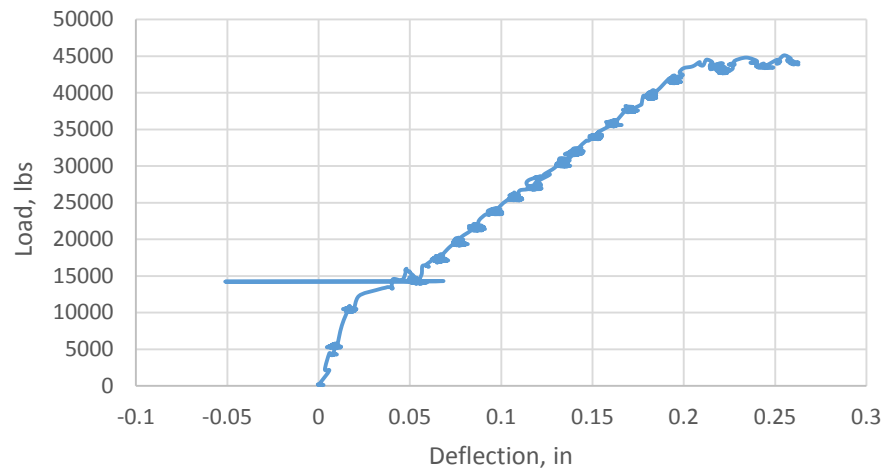

Figure 33. Load versus Deflection Plot for Specimen 1 with Typical Steel Reinforcement

The widths of two shear cracks were measured: the first crack to appear during testing and the crack that took a direct path from the support to the load point. These two cracks appeared at approximately 13.5 kips and 22.8 kips of shear load, respectively, and followed a very linear propagation rate throughout testing. Figure 35 shows the increase in the width of each crack using a best fit line.

The vertical LVDT displacement measurements are shown in Figure 36 for this specimen. LVDT B1 indicated that the first crack initiated at about 13 kips of shear load, which corresponds almost exactly with the shear crack first visually observed at about 13.5 kips.

34

Figure 34.   Top Flange Compression Failure of Specimen 1 Typical Steel Reinforcement
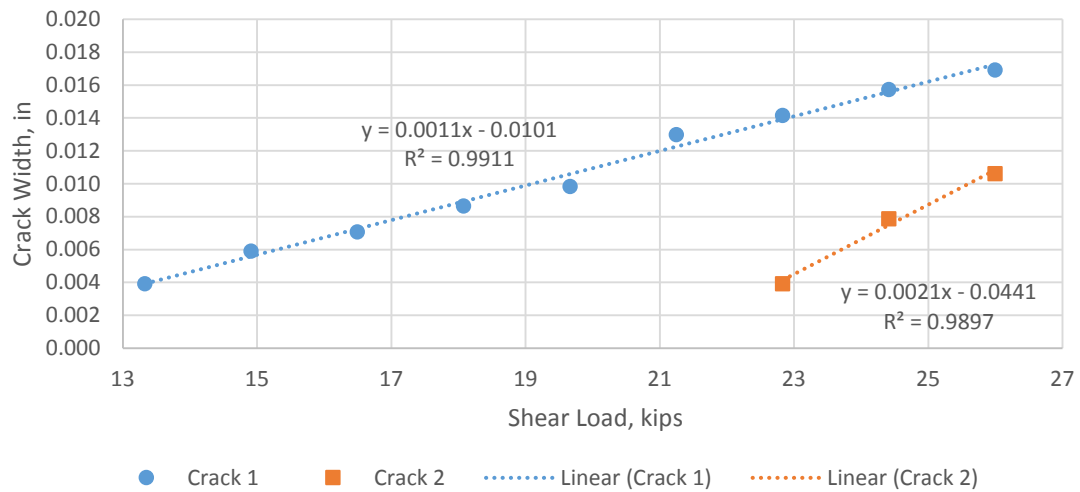

Figure 35. Measured Crack Width during Testing for Specimen 1 with Typical Steel Reinforcement
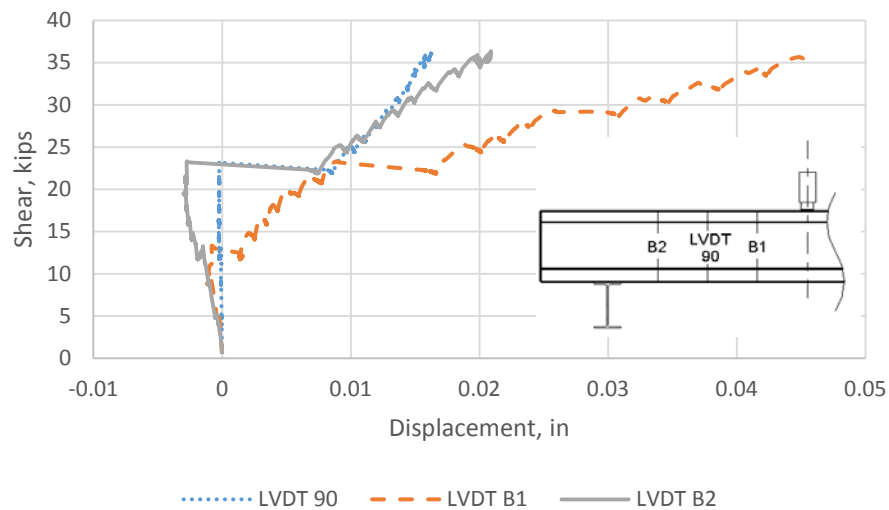

Figure 36. Vertical LVDT Displacements of Specimen 1 Typical Steel Reinforcement

Specimen 2 with Minimum C-Grid Reinforcement

The minimum C-Grid reinforcement placed in one half of Specimen 2 comprised one layer of C50 1.6 x 1.8 grid, where 1.6 designation indicated that the vertical legs of the grid acting as stirrups were 1.6 in apart. The cross-section of the specimen is shown in Figure 37. Again, because the specimen was under-reinforced for flexure, the investigators applied the load at 3.5 ft from the support, instead of the as-planned 4 ft.
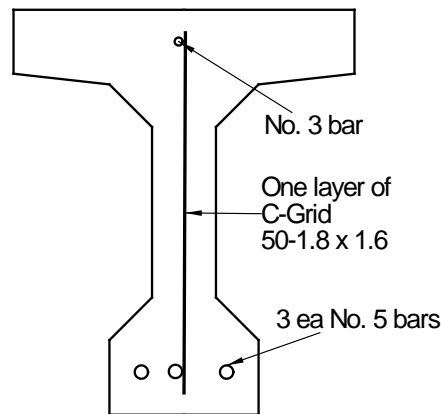
Figure 37. Cross-Section of Specimen 2 with Minimum C-Grid Reinforcement

The load was applied in 5-kip increments up to 15 kips, and then 3-kip increments after. Flexural yielding occurred at about 35 kips, which was after the expected shear failure of 26 kips of applied load (18.3 kips of shear). Figure 38 clearly shows the yield plateau of the section.
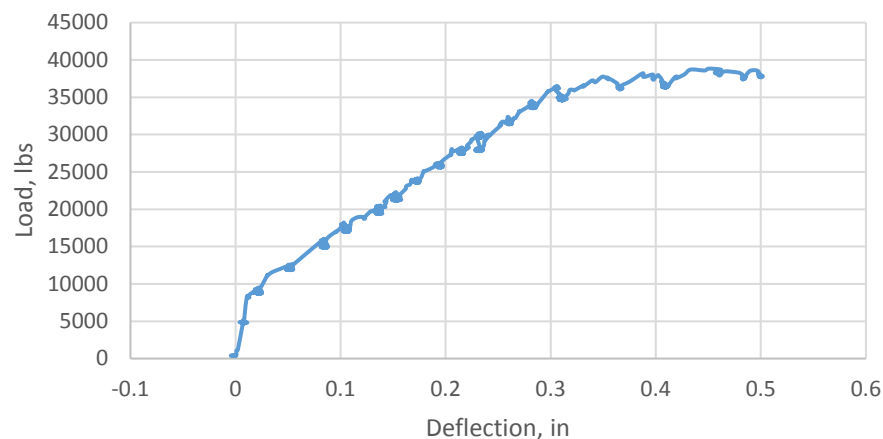
Figure 38. Load-Deflection Specimen 2 Minimum C-Grid Reinforcement

After the longitudinal reinforcement in the beam had yielded, the instrumentation was removed. The load was then increased to the yielding point and then increased to failure. The beam failed in shear at 40 kips of applied load, approximately 50% more load than predicted. There was an audible crack at 40 kips, after which, the applied load remained steady at 35 kips. Because the beam seemed to be stable, the load was increased to 38 kips, at which point the

36

beam lost all load carrying ability. The failure crack is shown in Figure 39. Upon closer inspection of the shear crack, both the vertical and horizontal tows had visibly ruptured across the crack.

Figure 39. Shear Failure of Specimen 2 with Minimum C-Grid Reinforcement

Again, two cracks in this beam were monitored: the first shear crack that appeared and the crack extending from the support to the loading point. Cracks were only measured up to 22 kips of applied load due to safety concerns about excessive load. The crack width measurements relative to the shear load, along with the associated best fit lines, are presented in Figure 40.

Figure 40. Crack Propagation Specimen 2 with Minimum C-Grid Reinforcement

Vertical LVDT displacement measurements are presented in Figure 41. Cracking first occurred around 10 kips in shear, based on the jump in the data for LVDT B1. As seen in Figure 40, the first visual crack did not occur until 12 kips. However, visual crack width measurements were made at the end of each increment of loading, so the visual measurements were probably not as exact as those using the LVDTs. However, LVDT B1 measurement at 15 kips was about 0.015 in, which is much higher than the 0.008-in crack width determined with the crack card at the same shear. This discrepancy was probably due to multiple cracks opening along the length of gage B1; the sum of these crack openings would be greater than the single crack measured with the crack card.
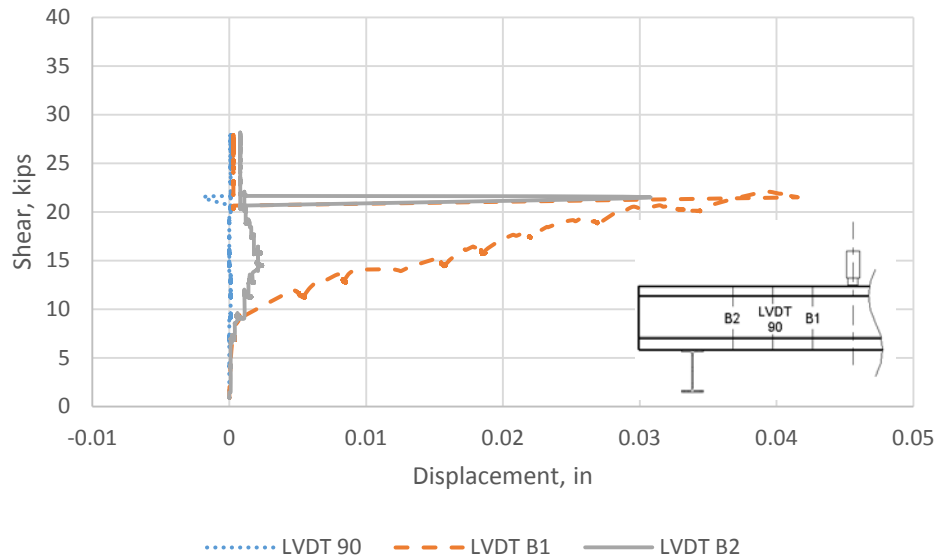
37

Figure 41. Vertical LVDT Displacement Measurements of Specimen 2 with Minimum C-Grid Reinforcement

Specimen 2 Typical C-Grid Reinforcement

The typical C-Grid reinforcement specimen was reinforced with three layers of C-Grid C50 1.6 x 1.8 placed in the beam. The cross-section of the beam is shown in Figure 42.
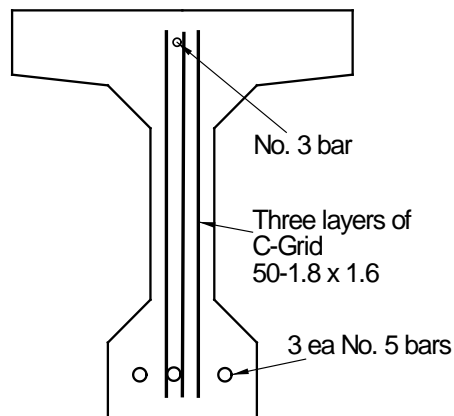
Figure 42. Cross-Section of Specimen 2 with Typical C-Grid Reinforcement

As noted in the *Methods* section, the concrete did not consolidate properly in the bottom flange of the beam due to the tight spacing of the C-Grid. Therefore, the project team did not test this beam. Nevertheless, the experience proved to be valuable in understanding that C-Grid needs to have adequate lateral support in the formwork, especially when multiple layers are used close together. Such support would have prevented the honeycombing from occurring, which was previously shown in Figure 18.

Specimen 3 with Minimum CFCC Reinforcement

   The CFCC stirrups were placed in the section in the same manner as the steel stirrups, but due to their longer tail lengths (as shown in Figure 16), the stirrups had to be turned approximately 60 degrees in order to fit into the bottom flange of the formwork. The typical cross-section of Specimen 3 is shown in Figure 43. The stirrups were placed 9 in on center. Due to the large size of the No. 7 bars, two of the flexural reinforcement bars were bundled on one side of the beam to allow spacing for the stirrup.

   Load on the beam was increased in 5-kip increments up to 15 kips and then in 3-kip increments until about 48 kips, at which point the test was terminated without failure, due to the desire to preserve the integrity of the other half of the specimen designed with a typical reinforcement ratio. The expected shear failure was at 30 kips of applied load (19.7 kips of shear). The load-deflection plot for this specimen is shown in Figure 44.
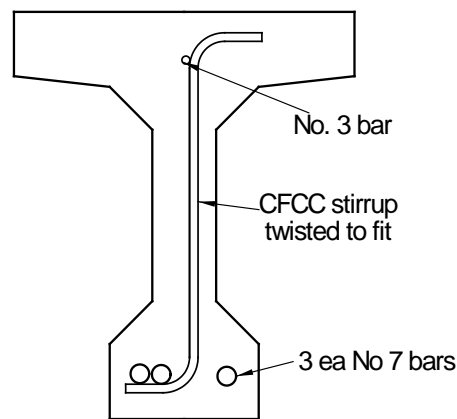
Figure 43. Cross-Section of Specimen 3 with Minimum CFCC Reinforcement

   Cracks were measured at two locations on the beam. Crack 1 was the first shear/flexure crack that opened in the web of the beam at 21 kips of applied load (14 kips of shear). Crack 2 was a major shear crack that opened along the web of the section at 15.3 kips of shear. These cracks relative to applied shear, along with best fit lines for propagation are shown in Figure 45.

   Figure 46 shows vertical LVDT displacement measurements relative to shear for comparison with visual crack width measurements. The large jump in displacement recorded by LVDT 90 indicated the initial shear cracking occurred at 13 kips of shear. The other LVDTs indicated a more gradual displacement, which did not occur in the other tests. The cracking from LVDT 90 corresponds well with the initial crack measurement occurring at 14 kips of shear.
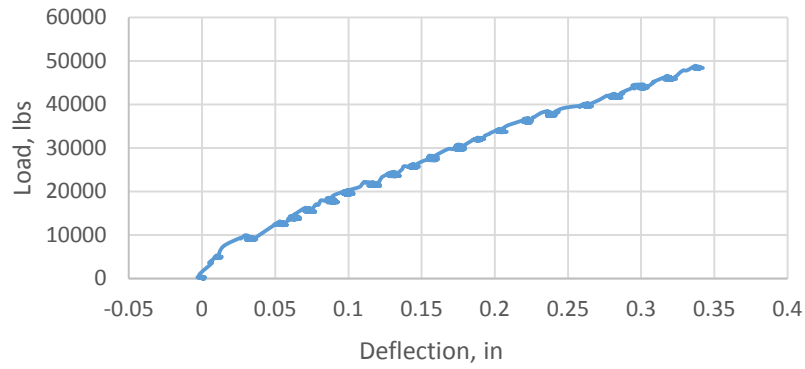
Figure 44. Load-Deflection Specimen 3 with Minimum CFCC Reinforcement

$y = 0.0009x - 0.0067$
$R^2 = 0.9557$
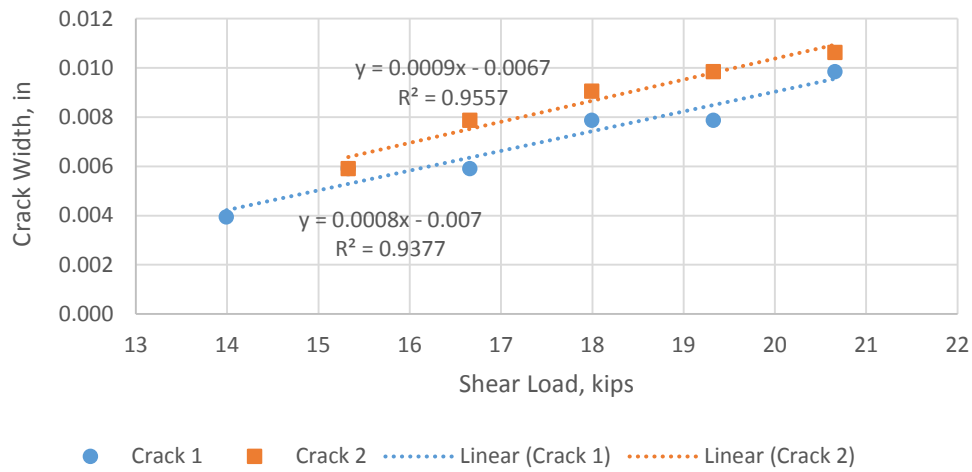
$y = 0.0008x - 0.007$
$R^2 = 0.9377$

Figure 45. Crack Propagation Specimen 3 with Minimum CFCC Reinforcement
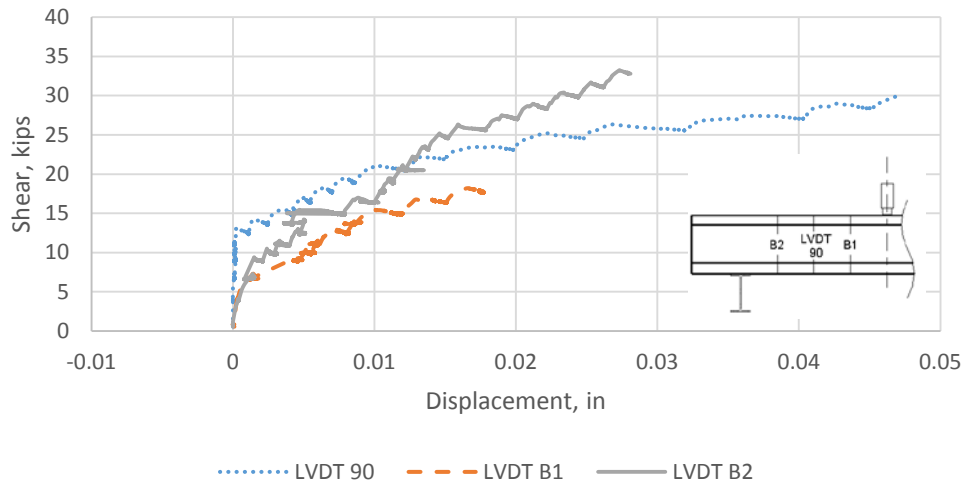

Figure 46. Vertical LVDT Displacements of Specimen 3 with Minimum CFCC Reinforcement

Specimen 3 with Typical CFCC Reinforcement

The typical reinforcement side of Specimen 3 was the same as shown in Figure 43 with the stirrups spaced at 4 in on center. This specimen was loaded to 15 kips in 5-kip increments and then in 3-kip increments up to 51 kips. The load versus deflection plot is in Figure 47. Due to some popping noises coming from the beam at 51 kips, the testing was stopped and the beam was unloaded to remove all instrumentation except for the wire potentiometers before loading the specimen to ultimate failure. The wire potentiometers were left in place because the two previous tests did not fail catastrophically; thus, there was minimal crushing hazard to the instrumentation.
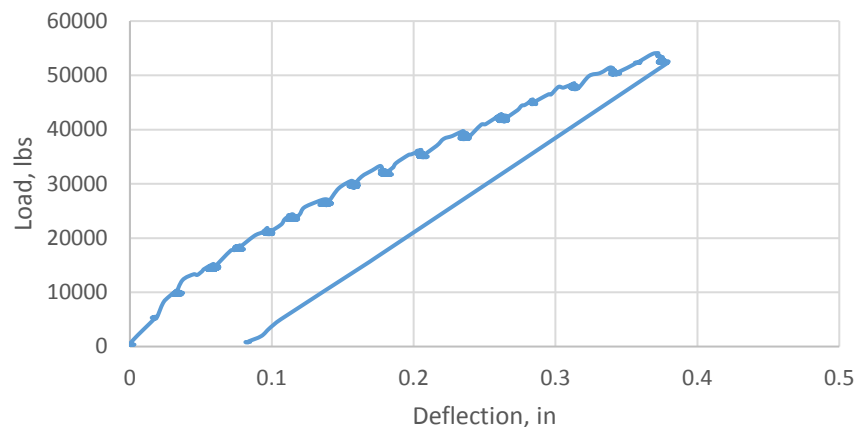
Figure 47. First Test, Load versus Deflection Plot for Specimen 3 with Typical CFCC Reinforcement

For the ultimate load test, load was applied up to the previously recorded 51-kip load and then slowly increased by 2-kip increments. The ultimate load was 63 kips at which point the longitudinal reinforcement yielded, as shown by the plateau of the load-deflection curve in Figure 48.

The failure of this specimen appeared to be a combination of shear failure and bond failure at ultimate load, due to the concrete splitting at the bottom of the beam, as shown in Figure 49. Also, the shear crack formed between two CFCC stirrups. After testing had ended, some of the concrete was removed to check whether CFCC stirrups ruptured, which had not. The large splitting failure along the longitudinal bars was thought to be caused by the tails of the CFCC stirrups. Due to the required length of the tail, the stirrups were angled to fit in the beam with all tails in one direction. This resulted in a plane of weakness which could have exacerbated the longitudinal cracking in the bottom bulb.

Crack widths measured at three locations on the beam are presented in Figure 50, along with a linear fit for widening as the loading progressed. Note that the cracks are numbered in order of their appearance in the web.
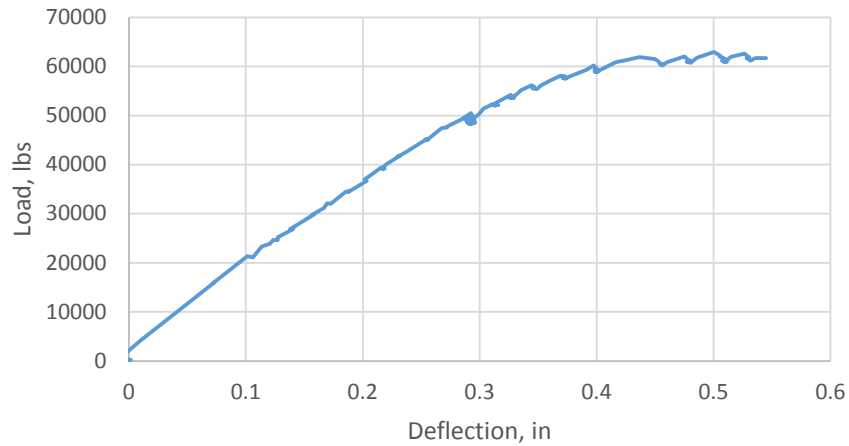
41

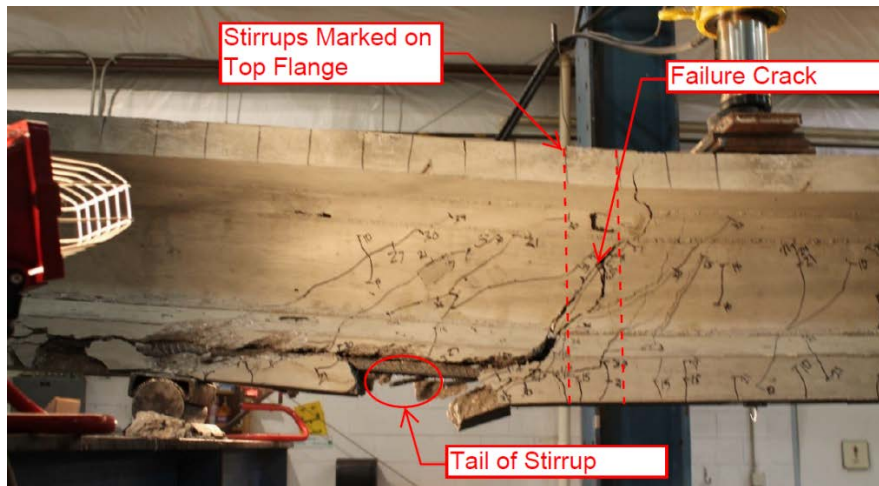**Figure 48. Second Test, Load versus Deflection Plot for Specimen 3 with Typical CFCC Reinforcement**

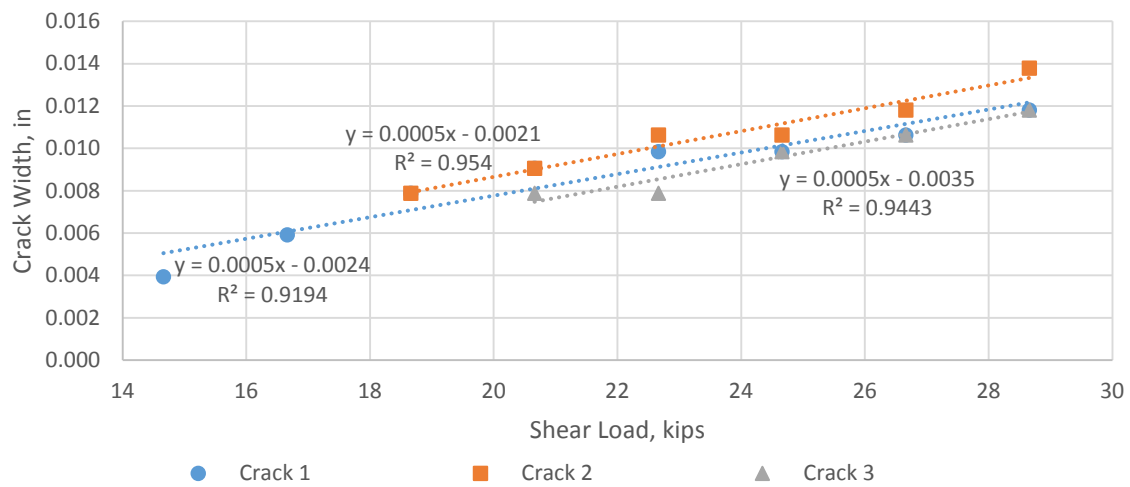**Figure 49. Failure of Specimen with 3 Typical CFCC Reinforcement**

Figure 50. Crack Propagation for Specimen 3 with Typical CFCC Reinforcement

42

As shown in Figure 51, vertical LVDT displacement measurements correlate well with the crack width measurements taken of Specimen 3 with typical CFCC reinforcement. According to the LVDTs, the crack occurred at about 13 kips of shear, which corresponds with the initial crack first measured visually at 14.7 kips of shear (see Figure 50). At 20 kips, the LVDT measurements averaged about 0.0075 in, while the measurements using the crack card averaged 0.0085 in. The similar results show a strong correlation between the instrumentation and the manual crack measurements and increase the confidence in the accuracy of the crack width measurements for this specimen.
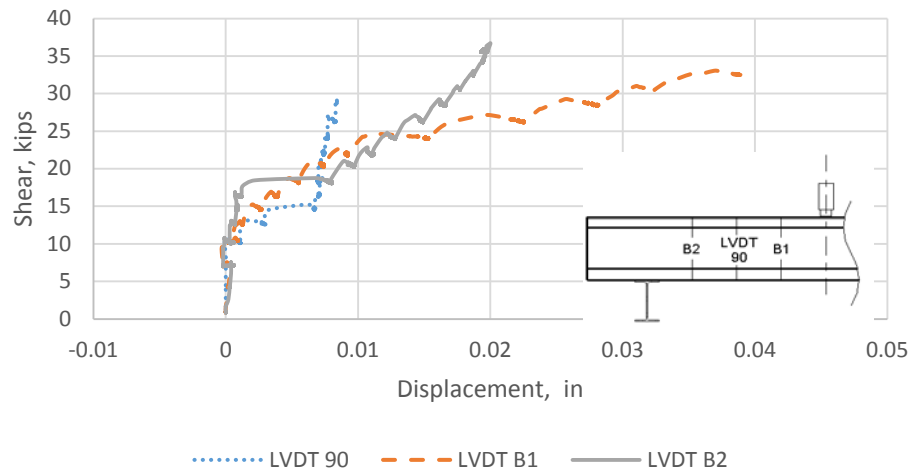
Figure 51. Vertical LVDT Displacement Measurements of Specimen 3 with Typical CFCC Reinforcement

Specimen 4 with Two Layers of C-Grid Zip Tied Together

The fourth beam specimen was a C-Grid reinforced beam designed to investigate whether putting layers together without room for concrete would change the strength and performance of the beam. This specimen had two layers of the C50 1.6 x 1.8 grid that were tied together at 12 in on center with small zip ties available at a local hardware store. The layers were then placed into the beam as shown in Figure 52, and tied in place. One thing noticed about the zip tied layers was the increased stiffness made the reinforcement easier to move and tie in place.

The load was applied to the beam in 5-kip increments until 15 kips, and then in 3-kip increments for the remainder of testing. The beam failed in shear at 53 kips of applied load (35.3 kips of shear). Two popping noises were heard emanating from the beam, and immediately thereafter, the beam failed with a loud crack. The anticipated shear failure of the beam was 44 kips of applied load (29.5 kips of shear). The load-deflection plot for the test is in Figure 53, and the shear failure is shown in Figure 54.

There were three locations for crack width measurements for this beam. Figure 55 shows both the measured widths and the best fit line for the increase in width. Note that the crack numbers given in the figure correspond with the appearance of the cracks as testing progressed. One interesting thing to notice is that Crack 1 started to get smaller after 20 kips of shear because another crack opened beside this crack, causing a reduction in the width of the Crack 1. Due to

Crack 1 closing back up, the linear fit was not useful and was not used in any averages for crack growth.

Figure 52. Cross-Section of Specimen 4 with Two Layers of C-Grid Zip Tied Together
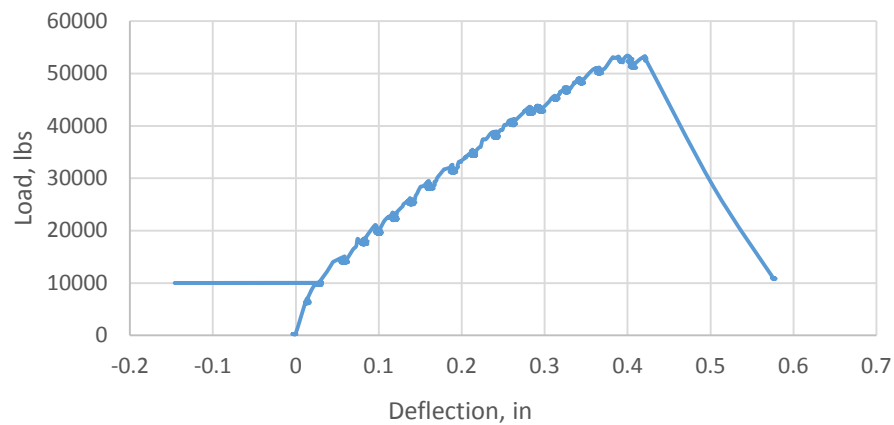
Figure 53. Load versus Deflection Plot of Specimen 4 with Two Layers of C-Grid Zip Tied Together

Figure 54. Shear Failure of Specimen 4 with Two Layers of C-Grid Zip Tied Together

Figure 55. Crack Propagation for Specimen 4 with Two Layers of C-Grid Zip Tied Together
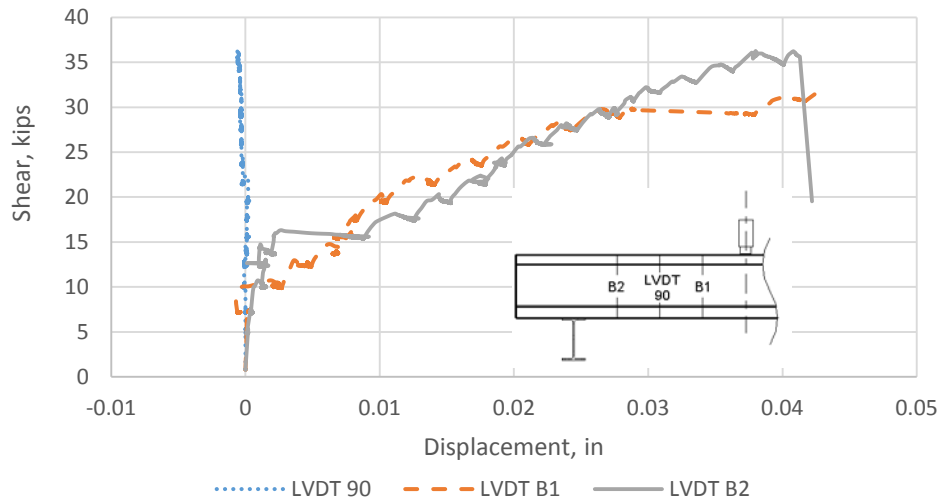
Figure 56. Vertical LVDT Displacement Measurements of Specimen 4 with Two Layers of C-Grid Zip Tied Together

Specimen 4 with Two Layers of C-Grid Spaced Apart

This specimen was used to determine if using multiple layers of C-Grid with a spacing between layers made a difference in the capacity of the beam. A No. 5 bar was used as the top bar to give a larger spacing between grids and help ensure that proper consolidation of the concrete would could be achieved. The cross-section of the specimen is shown in Figure 57.

Loading for this specimen was in 5-kip increments up to 15 kips and then in 3-kip increments until the end of testing. The shear failure in this test was very similar to the specimen with two layers of C-Grid zip tied together. The applied load at failure was 56 kips, which was higher than the anticipated failure load of 45 kips. Figure 58 gives the load versus deflection plot, while Figure 59 shows the shear failure of the specimen. Upon inspection of the failure, nearly all the tows of C-Grid crossing the crack had fractured.
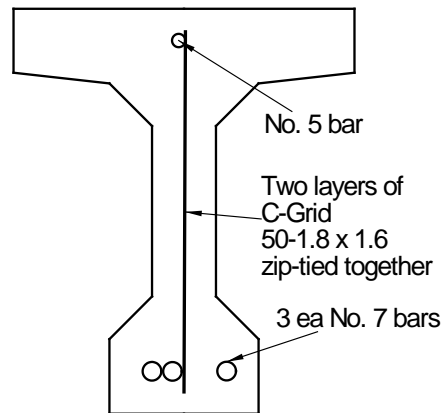
45
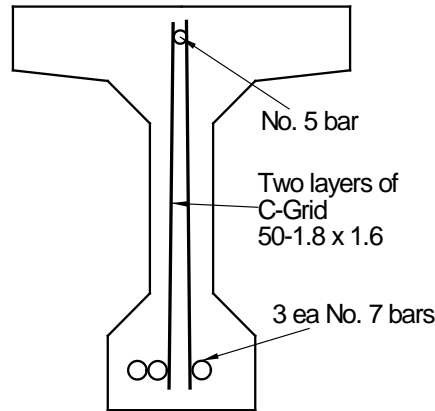
Figure 57. Cross-Section of Specimen 4 with Two Layers of C-Grid Spaced Apart
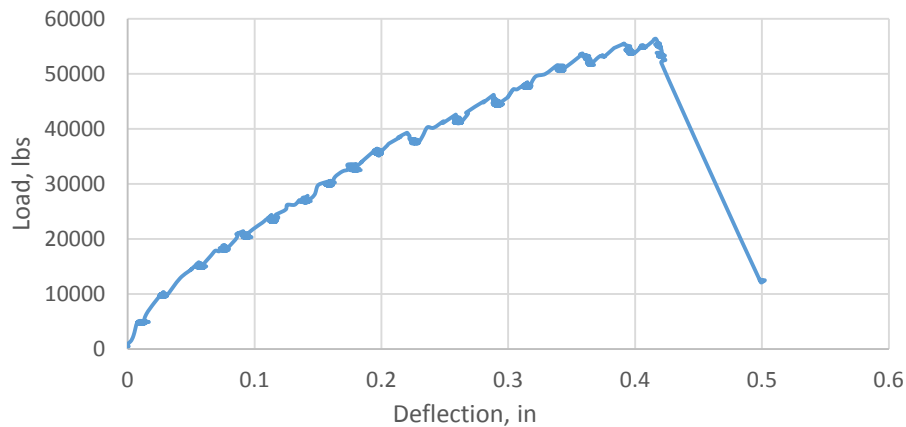
Figure 58. Load versus Deflection Plot for Specimen 4 with Two Layers of C-Grid Spaced Apart

The width of the first three shear cracks that opened in the web were measured. Crack 3 became narrower after 27 kips of shear load, due to another crack opening beside it. Therefore, the linear best fit line used to estimate the increase in width did not work well on Crack 3, and thus was not used in averages discussed later. On the other hand, Crack 1 did have a large increase in size once higher loads were reached, as presented in Figure 60.

The displacement measurements of the vertical LVDTs are presented in Figure 61. From the measurement of LVDT B2, the first shear crack opened up at about 11 kips, which correlates well with Figure 56. The visually measured crack width at 25 kips of shear was about 0.011 in, which was similar to the LVDT displacement of 0.01 in at the same load.
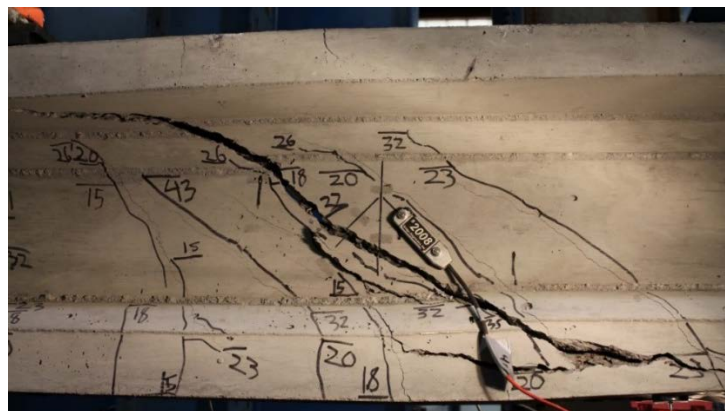
46

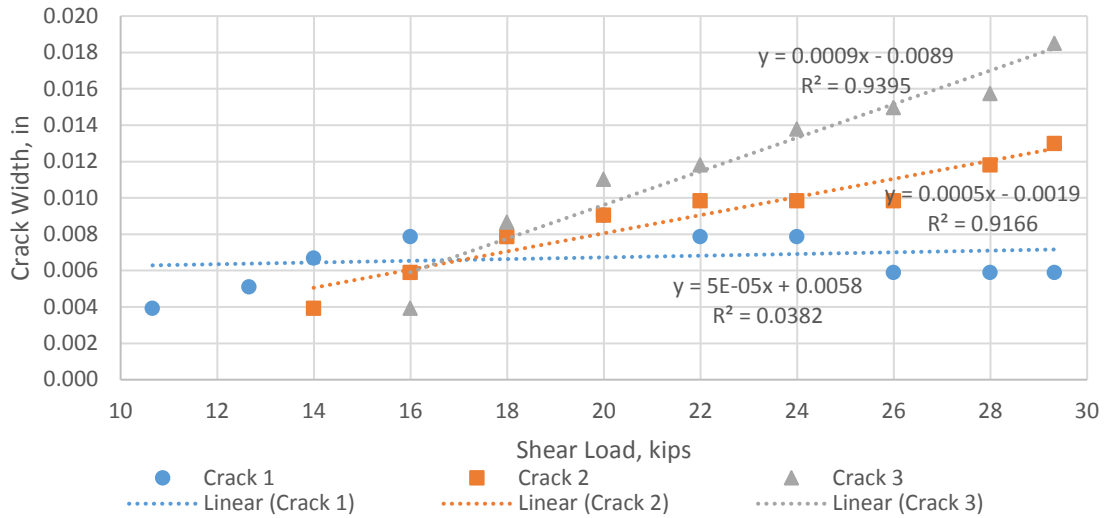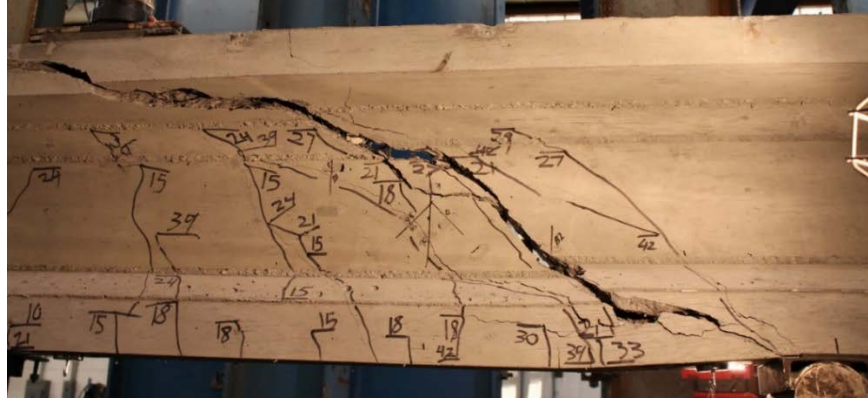**Figure 59. Shear Failure of Specimen 4 with Two Layers of C-Grid Spaced Apart**
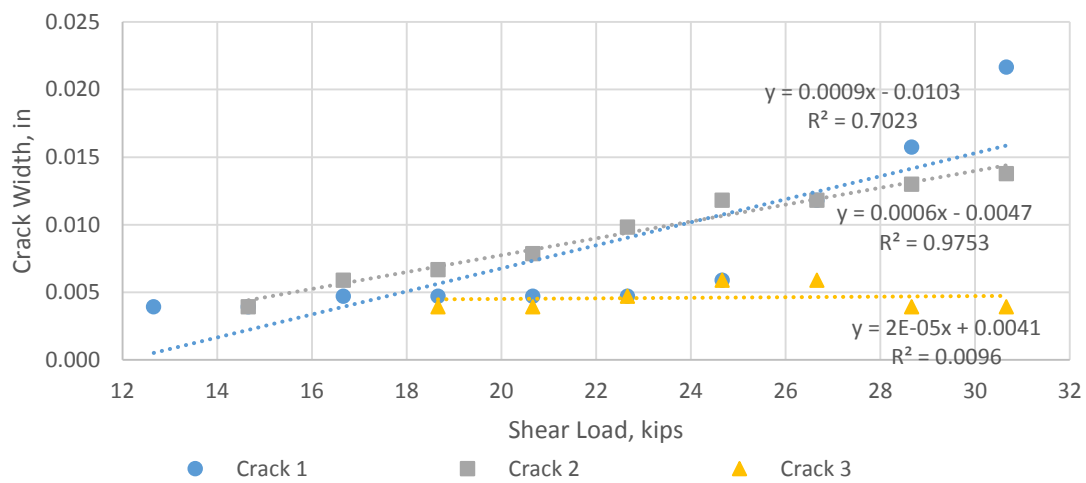
Figure 60. Crack Propagation for Specimen 4 with Two Layers of C-Grid Spaced Apart
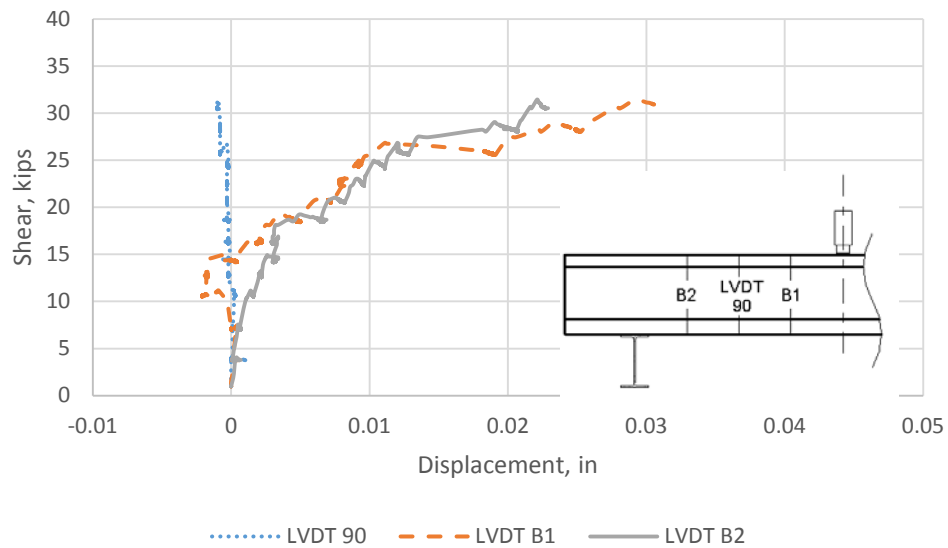
Figure 61. Vertical LVDT Displacement Measurements of Specimen 4 with Two Layers C-Grid Spaced Apart

47

Specimen 5 with Minimum NEFMAC Reinforcement

The specimen with minimum NEFMAC grid reinforcement was composed of one layer of C6 10 x 8 grid, where the "10" in the grid designation indicates that the spacing of the vertical legs of the grid acting as stirrups was 10 in. The cross-section of the specimen is shown in Figure 62. The load was applied at 4 ft from the support on a 12 ft span. Using the AASHTO LRFD method, the predicted loading for shear failure for this test was 30 kips.
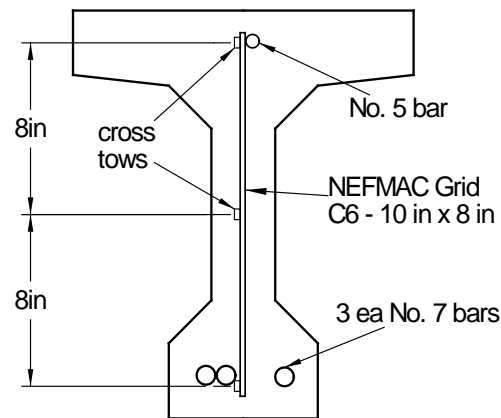
Figure 62. Cross-Section of Specimen 5 Minimum NEFMAC Reinforcement

The applied load was increased in 3-kip increments until reaching the predicted failure load of 31 kips, at which point the investigators terminated the testing to minimize damage to the other half of the beam containing a typical reinforcement ratio. The vertical deflection of the beam at the load point can be seen in Figure 63.
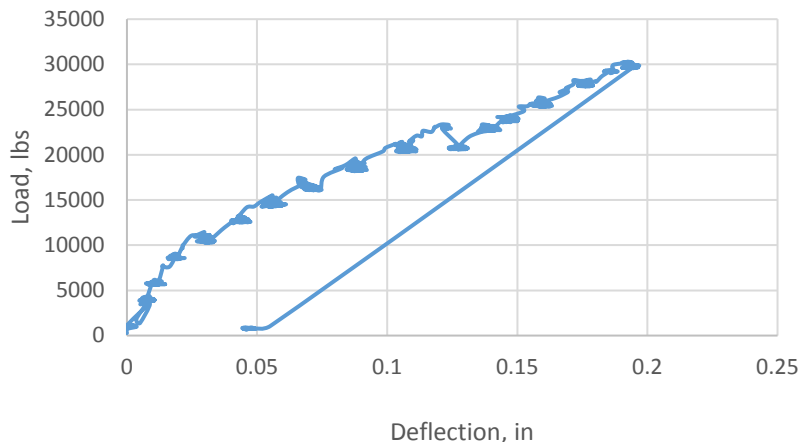
Figure 63. Load versus Deflection at Load-Point for Specimen 5 with Minimum NEFMAC Reinforcement

After testing the half with typical reinforcement, the minimum reinforcement end of the specimen was re-loaded and tested to failure. After reaching 5 kips, load was increased in 2-kip increments until a shear failure occurred at 50 kips of applied load. This failure load was approximately 67% more than predicted. Figure 64(a) shows the failure crack. Upon closer inspection of the shear crack, there was no visible rupture of the vertical tows; however, tows were frayed. This fraying may have weakened the grid, as seen in the photo in Figure 64(b).

48

(a)   **(b)**

Figure 64. (a) Unloaded Shear Failure of Specimen 5 with Minimum NEFMAC Reinforcement, and (b) Frayed NEFMAC grid within the Shear Failure Crack

Crack widths of the first two shear cracks to open on this beam were measured. The first crack appeared at a shear loading of about 11 kips, and the second crack appeared at 16 kips. Figure 65 indicates that once the second crack formed, the first crack got smaller because the second crack was the point of shear failure. Thus, the second crack opened up very wide and allowed the first crack to close. The expected shear failure load was 20.5 kips. Therefore, the crack widths measurements were stopped after a shear load of 17.5 kips, due to safety concerns. The crack measurements along with best fit lines are in Figure 65.
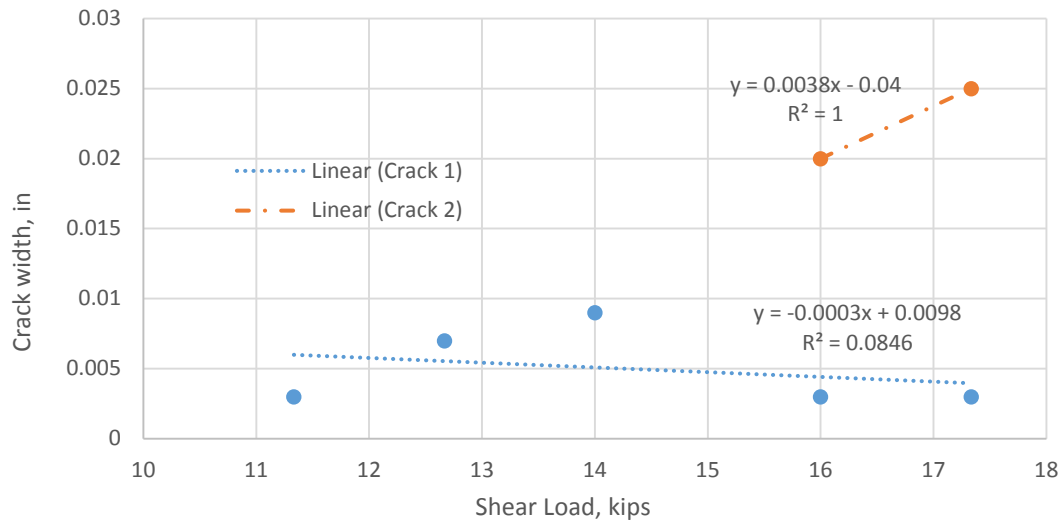
Figure 65. Crack Width Measurements for Specimen 5 with Minimum NEFMAC Reinforcement

LVDTs were oriented along the vertical tows within the shear failure region. Figure 66 shows the crack propagation relative to the LVDTs. The data from the LVDT are in Figure 67, which shows that initial cracking occurred around a shear load of 11 kips. However, the larger displacements occurred around 16 kips, which corresponded to the second shear crack opening. The LVDT readings indicated larger crack openings than the visual measurements, which again was due to the LVDTs taking into account all of the cracking along the entire web depth, while the visual readings for were two specific cracks within the web.

49
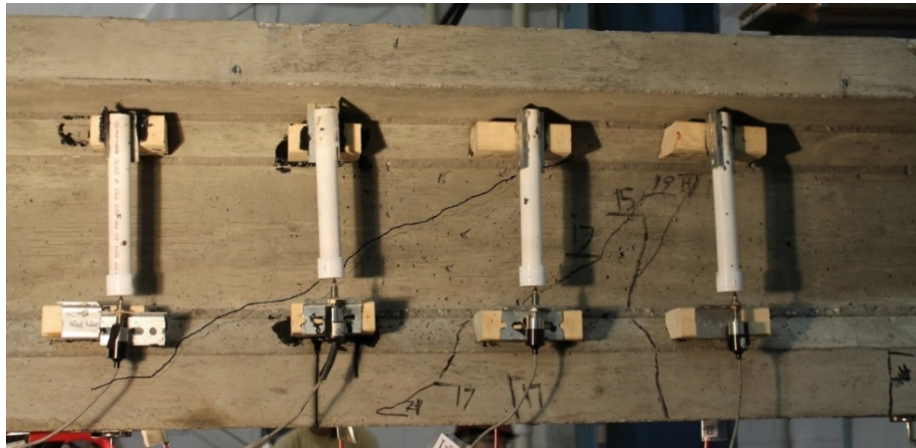
Figure 66. Crack Propagation through LVDTs for Specimen 5 with Minimum NEFMAC Reinforcement
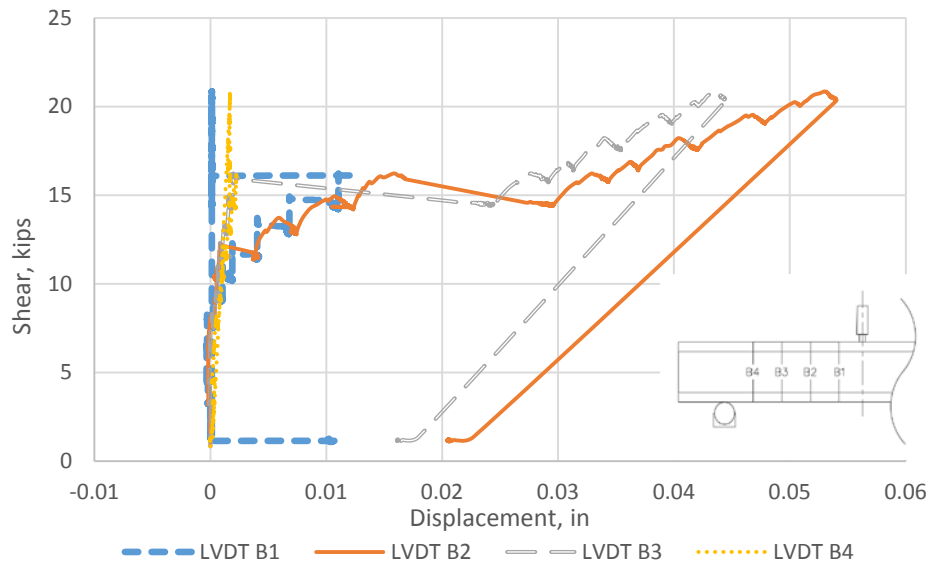
Figure 67. LVDT Displacement Measurements for Specimen 5 with Minimum NEFMAC Reinforcement

Specimen 5 with Typical NEFMAC Reinforcement

The typical NEFMAC grid reinforcement comprised two layers of C6 10 x 8 grid that were placed to approximately midspan of the beam. The 10 in spacing was the spacing of the vertical legs of the grid that acted as stirrups. The cross-section of the specimen is shown in Figure 68. The load was applied at 4 ft from the support on a 12 ft span. Based on the AASHTO LRFD method, the predicted loading for shear failure for this test was 43 kips (28.5 kips of shear).

The load was applied in 2 kip to 3 kip increments until the beam reached its ultimate failure load. Shear failure occurred at 54 kips, which was approximately 29% more load than predicted. The deflection of the beam at the load point versus the applied load is plotted in Figure 69. Figure 70 shows the failure crack, while Figure 71 gives a detailed view of the failed reinforcement, where both the vertical and horizontal tows had ruptured.

50
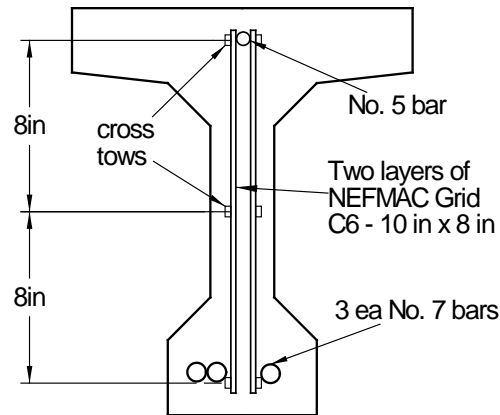
Figure 68. Cross-Section of Specimen 5 Typical NEFMAC Reinforcement
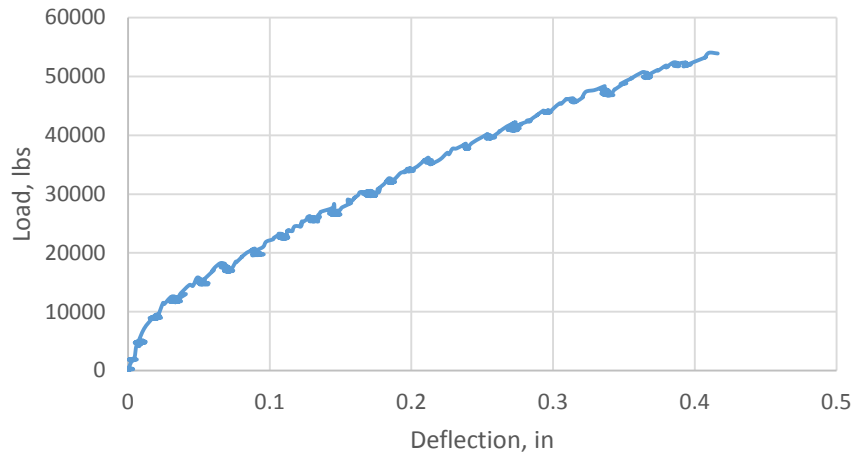
Figure 69. Load versus Deflection at Load Point for Specimen 5 with Typical NEFMAC Reinforcement

As testing progressed, the width of the first two shear cracks to form on this beam were measured, but only up to a shear load of 20 kips, due to safety concerns. The first crack appeared at a shear load of 11 kips, and the second crack appeared at 19 kips. The crack width measurements with their associated best fit lines are shown in Figure 72.

Vertical LVDTs were located along the vertical tows within the shear failure region. Figure 73 shows the crack propagation relative to those LVDTs. The displacement measurements are provided in Figure 74, which indicates that initial cracking occurred around a shear load of 12 kips. That cracking load corresponds precisely with the first visual record of shear crack formation (see Figure 72). Similar to the test on the beam with minimum NEFMAC reinforcement, the LVDT readings for the typical NEFMAC reinforcement test indicate larger crack openings than the visual readings. Again, the LVDT took into account all of the cracks along the depth of the web, while the visual readings were for two specific cracks.
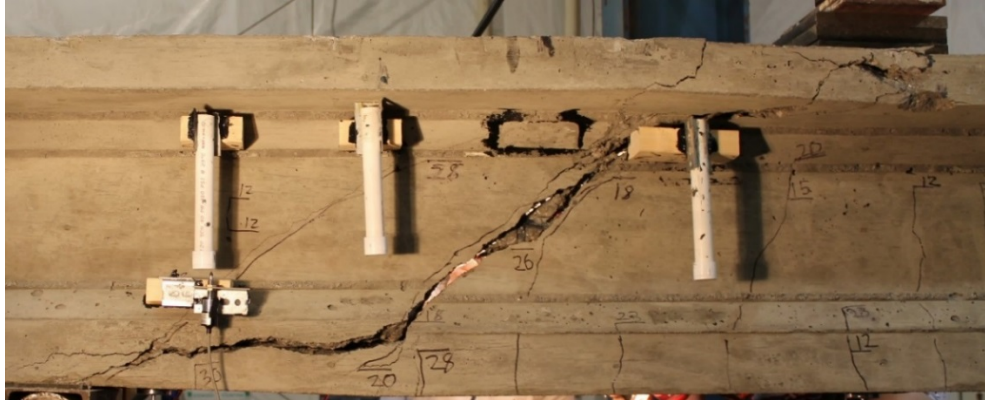
Figure 70. Shear Failure of Specimen 5 with Typical NEFMAC Reinforcement
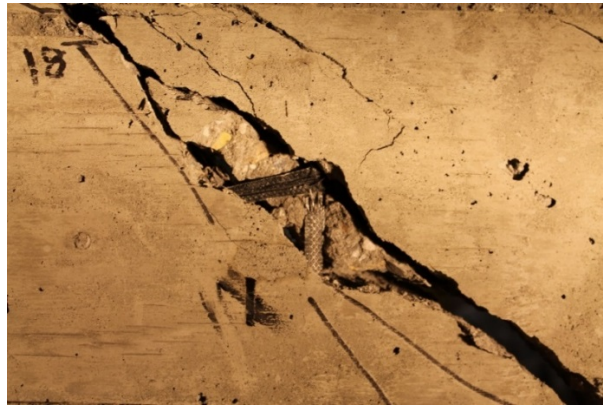
Figure 71. Rupture of Vertical and Horizontal NEFMAC Tows
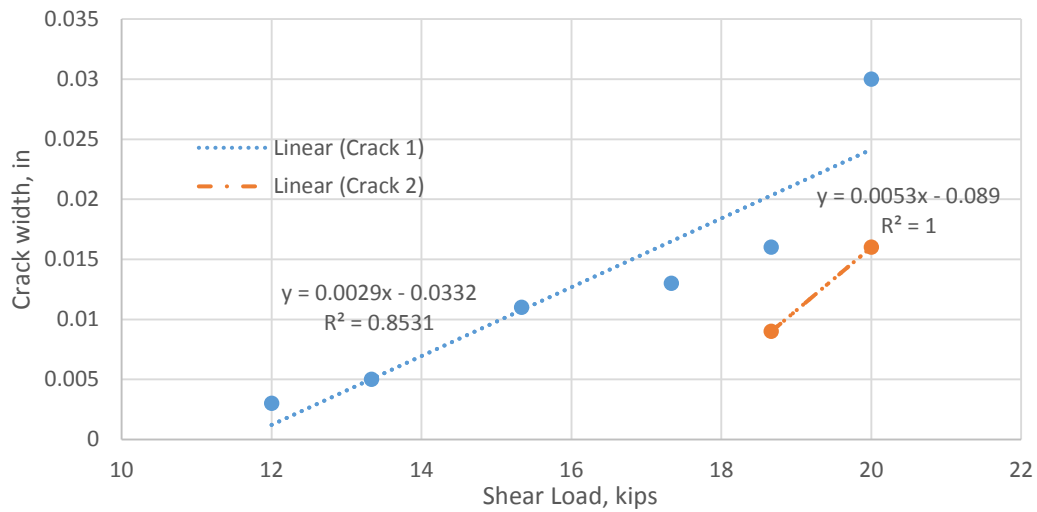
Figure 72. Crack Propagation of Specimen 5 with Typical NEFMAC Reinforcement
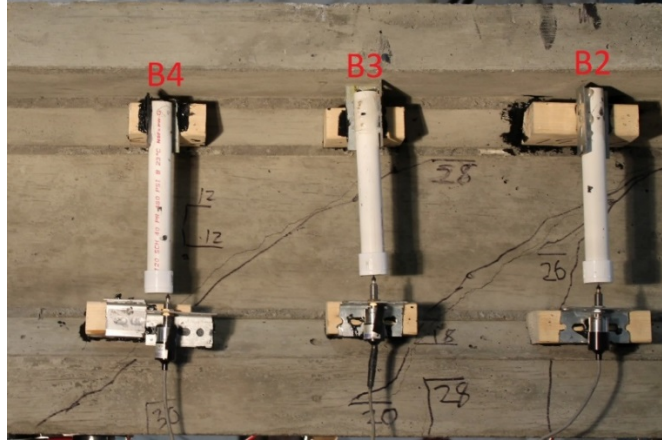
Figure 73. Crack Propagation through LVDTs for Specimen 5 with Typical NEFMAC Reinforcement
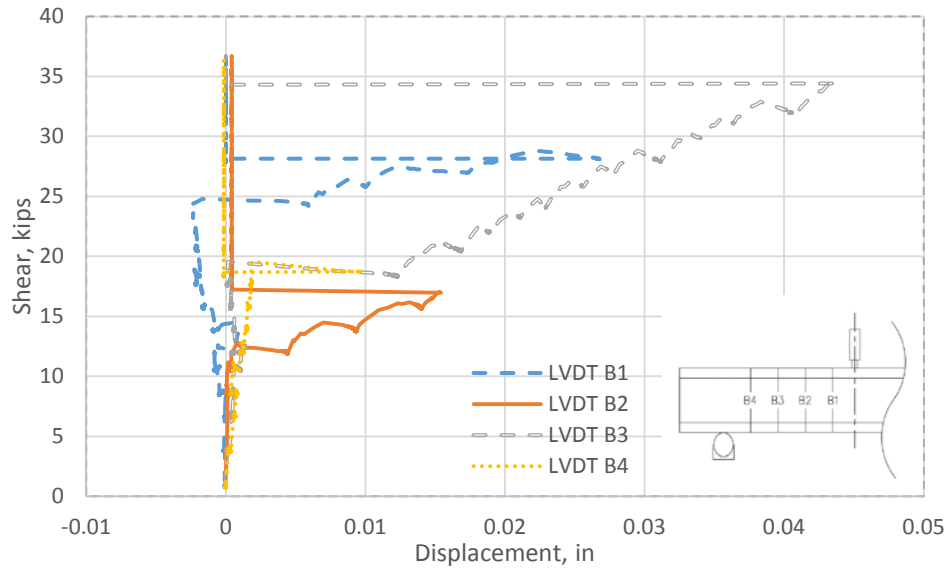
Figure 74. LVDT Displacement Measurements of Specimen 5 with Typical NEFMAC Reinforcement

Results of the End Zone Design Parametric Study

Determination of Allowable Stress

The first step in this study was to determine the working stress in the C-Grid and NEFMAC grid that would result in cracks of comparable widths as steel reinforcing, which was required to have a working stress of 18 ksi in the end zone. The most straight forward approach was to calculate the stress that corresponded to the same strain as steel at 18 ksi, or

$$\varepsilon_s = \frac{f_s}{E_s} = \frac{18\ ksi}{29,000\ ksi} = 620\ \mu\varepsilon$$

Eq. 19

53

Based on the respective moduli of 32,600 ksi and 14,500 ksi provided by the manufacturers, the stresses in the C-Grid and NEFMAC grid that corresponded to 620με were 20 ksi and 13.5 ksi, respectively. However, crack widths are influenced by factors other than modulus, including the bond properties of the material and the spacing of the bars or tows.

To evaluate these factors, crack widths were investigated, based on the best linear fit lines of data in the shear specimens with typical reinforcement ratios, as analyzed earlier in this report. Comparisons were made between the steel and NEFMAC grid as well as the steel and C-grid. The ratio of the crack width in the steel reinforced specimen to the crack width in each CFRP grid-reinforced specimen is presented in Table 10. For the C-Grid, all ratios are larger than 1.0, indicating that at the same level of shear, the cracks in the steel reinforced beam were larger than those in the C-Grid reinforced beam. So, C-Grid controlled cracking better. On the other hand, the ratios for the NEFMAC grid were all less than 1.0, indicating that this material was less effective at controlling cracks compared to steel. Given these results, the average crack width ratios was multiplied by the strain-based working stresses calculated above to arrive at the modified working stress limits, which were 41.5 ksi and 8.7 ksi for C-grid and NEFMAC grid, respectively.

Table 10. Comparisons of Crack Control at Equal Shear Loads

Shear Load, kips	Crack Width, in			Ratio of crack widths	
	Steel	C-Grid	NEFMAC	Steel /C-Grid	Steel / NEFMAC
13	0.0042	0.0014	0.0045	3.00	0.93
15	0.0064	0.0032	0.0103	2.00	0.62
17	0.0086	0.0050	0.0161	1.72	0.53
19	0.0108	0.0068	0.0219	1.59	0.49
			Average	**2.08**	**0.65**

Although simple, the above analysis is does not address the fact that at a given level of shear, the stresses in the steel, C-Grid and NEFMAC grid are not necessarily the same. So, there was one additional analysis to assess the concrete contribution to total shear resistance using the ACI expression for V_c (Eq. 8) along with the measured concrete compressive strength. This contribution was then subtracted from the total applied shear at each load step to determine the contribution from the reinforcement. Based on the angle of the failure crack, the number of bars or tows of grid crossing each crack was determined, and subsequently, the area of reinforcement across the crack was found. Finally, a rough estimate of the stress in the reinforcement was found by dividing the shear resistance contribution from the reinforcement by the gross area of reinforcement crossing the crack. Figure 75 shows a plot of the calculated reinforcement stress versus the measured crack width at each load step. Also included in the plot is the reading from the vertical LVDT that crossed the measured crack; the LVDT and crack width readings were similar, but not exactly the same, due to the fact that some LVDTs crossed multiple cracks.

According to Crispino, an acceptable crack width in anchorage zones is 0.005 in. Table 11 presents the calculated stress for each reinforcement type and measurement method at a crack width of 0.005 in. For a given reinforcement type, the average of the stresses from the two measurement methods was calculated. As can be seen in the table, all stresses were above the recommended stress in steel reinforcement for anchorage zones, which is 18 ksi. Thus, the right-most column in the table presents a modified working stress, which is simply the ratio of the average reinforcement stress versus the average steel reinforcement stress multiplied by the 18

54

ksi working stress recommended for steel. This modified working stress for CFRP based on the ratio with steel reinforcement stress should provide a similar level of crack control as steel at 18 ksi.
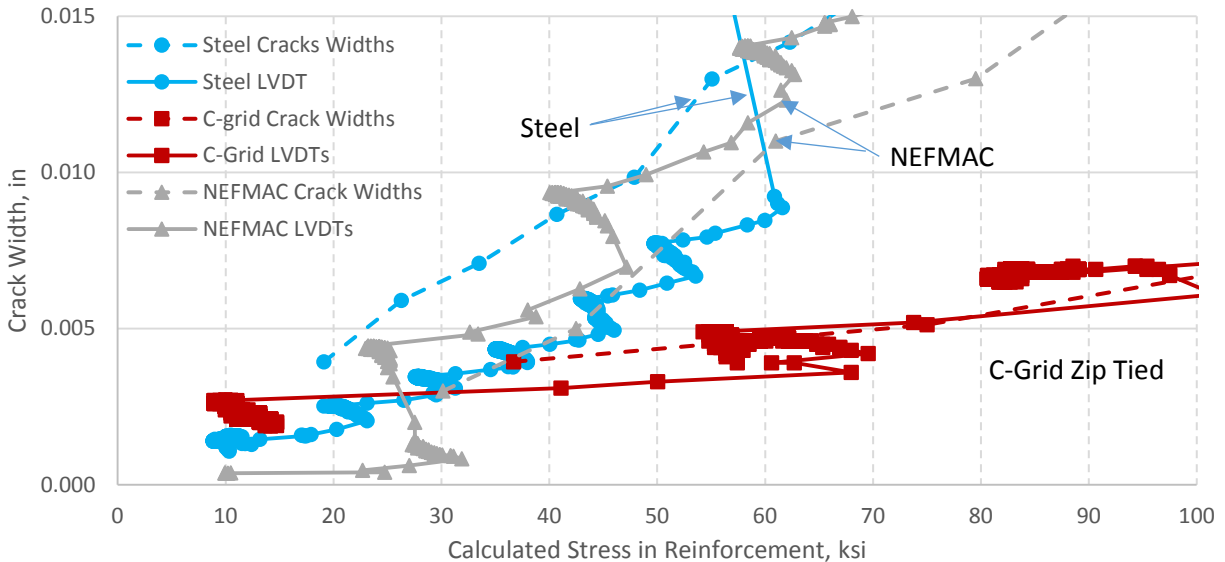
Figure 75. Calculated Reinforcement Stress versus Crack Width and LVDT Web Deformation

Table 11. Calculated Stress in in Reinforcement at Equivalent Crack Width (0.005 in)

Material	Stress at crack width of 0.005 in, ksi	Stress at web deformation (LVDT) of 0.005 in, ksi	Average, ksi	Average Stress/ Average Steel Stress	Modified Working Stress, ksi
Steel	23	44	33.5	1.0	18
C-Grid	72	62	67	2.0	36
NEFMAC	42	35	38.5	1.15	21

Table 12 provides a summary of the three methods used to arrive at a working stress for CFRP grids in anchorage zones. The selected stress for use in the analysis of anchorage zone was the average of the stress at equivalent strain and the reinforcement stress ratio method. Despite the many assumptions made in the reinforcement stress ratio method, the average of the two methods gives what should still be a conservative allowable stress. The reinforcement stress ratio method results in a larger working stress than the equivalent strain method, because it accounts for the shorter development length of the grids and the cross-tows that help in controlling cracks. This analysis is very approximate, and further testing is required to better determine the working stress in the grids to result in equivalent crack control compared to steel at a working stress of 18 ksi.

Table 12. Working Stress and Working Force per Tow for CFRP Grids

Material	Method for Stress Determination				Area per Tow, in^2	Working Force per Tow, kips
	Stress at Equivalent Strain, ksi	Stress From Crack Width Ratio, ksi	Stress at 0.005 in Crack, ksi	Stress for Anchorage Zone Analysis, ksi		
Steel	18	18	18	18	Varies	Varies
C-Grid	20	41.5	36	28	0.00286	0.080
NEFMAC	13.5	8.7	21	17	0.027	0.466

CFRP Grid End Zone Design Procedure

This section presents the parametric study calculations for the PCBT-45A girder section provided in Table 3. The values for the strut-and-tie model have been calculated based on the process shown in Crispino (2007) and Magee (2016). The strut-and-tie model for this specific beam case is shown in Figure 76.

Using this model and Equation 18, the resulting values for tension ties, *T1* and *T2*, are both 28.9 kips, as shown below:

$$T1 = T2 = \frac{8P_1y}{7h} = \frac{8(357.06 \text{ kip}) (5.77 \text{ in} - 2.58 \text{ in})}{7(45 \text{ in})} = 28.9 \text{ kip}$$

Eq. 20
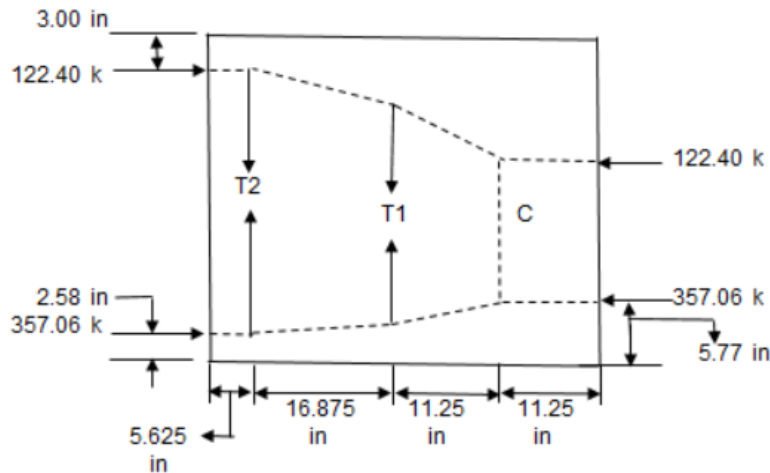
Figure 76. Strut-and-Tie Model for PCBT-45A

Because the overall height, *h*, of a PBCT-45 is 45 in, the length of *h*/4 and the distance between *h*/4 and 3*h*/4 are 11.25 in and 22.5 in, respectively. With the known area and spacing for the vertical tows in the CFRP grids, the total number of vertical tows per layer needed within each sub-region in the end zone can be calculated. With the number of vertical tows per layer, one can calculate the strength per layer of CFRP grid using the allowable strength per tow. From there, the designer can determine the total number of layers of CFRP grid that will be needed for

each sub-region. Detailed calculations for the above steps are given below for the *T2* region, using C-Grid with 1.6 in tow spacing and additional values for the PCBT-45A case given in Table 13.

$$\frac{h}{4} = \frac{45 \text{ in}}{4} = 11.25 \text{ in} \tag{Eq. 21}$$

$$\frac{Vertical\ tows}{Layer} = 1 + \frac{stirrup\ area}{tow\ spacing} = 1 + \frac{11.25 \text{ in}}{1.6 \text{ in}} = 8.03 \rightarrow 8 \text{ vertical tows per layer} \tag{Eq. 22}$$

$$\frac{Strength}{Layer} = \frac{Vertical\ tows}{Layer} \times Allowable\ Tow\ Strength = 8(0.08008 \text{ kip}) = 0.641 \text{ kip per layer} \tag{Eq. 23}$$

$$Min.\ \#\ of\ Layers\ CFRP\ Grid\ Needed = \frac{T2}{Strength/Layer} = \frac{28.9 \text{ kip}}{0.641 \text{ kip}} = 45.1 \text{ layers} \rightarrow 46 \text{ layers} \tag{Eq. 24}$$

Table 13. PCBT-45A – CFRP Grid End Zone Design

Tie	Required Strength, kips	Distribution Length, in	Maximum Vertical Tows in Distribution Length, per Layer of Grid		Strength per Layer of Grid, kips		Minimum Layers of Grid Required	
			NEFMAC	C-Grid	NEFMAC	C-Grid	NEFMAC	C-Grid
T1	28.9	22.5	3	15	1.398	1.201	21	25
T2	28.9	11.25	2	8	0.932	0.641	31	46

Thus, 46 layers of C-Grid would be needed in the region *h*/4 (measured from the beam end) for the tie *T2* in the parametric case PBCT-45A. Similarly, the number of layers needed for each case in the PCBT-45A example is also large in order to meet strength requirements, regardless of the design region or type of CFRP reinforcement. The two far right columns in Table 13 summarize the number of required grid layers.

Steel with CFRP Grid End-Zone Design

This section presents a second end zone design case using single-legged steel stirrups in combination with CFRP grid. The design process is identical to the previous example up to the point of calculating the strength per layer of CFRP. For simplicity, these example calculations use the same *T2* region with C-Grid reinforcing as in the previous section.

The first step in this process is to determine the steel stirrup layout that would help reduce congestion in the beam while providing the necessary reinforcing when combined with CFRP grid. The selected bars for the *T2* region were three No. 5 bars spaced at 5 in, center-to-center. Assuming this layout, the engineer can calculate the total bar area and then determine how much resistance the steel provided in the *T2* region by multiplying the allowable working stress for steel by the total bar area. The remaining resistance that needs to be provided by CFRP is calculated by subtracting the steel contribution from the force *T2*. Knowing the CFRP contribution, the total number of CFRP layers can be determined. Detailed calculations for the

above steps are given below for the *T2* region, again using C-Grid with 1.6 in tow spacing and additional values for the PCBT-45A case given in Table 14.

$$A_v = \text{\# of bars} \times \text{bar area} = 3(0.31\,in^2) = 0.93\,in^2 \qquad \text{Eq. 25}$$

$$T2_{steel} = \sigma_{working} A_v = (18\,ksi)(0.93\,in^2) = 16.74\,kip \qquad \text{Eq. 26}$$

$$T2_{CFRP} = T2 - T2_{steel} = 28.9\,kip - 16.74\,kip) = 12.16\,kip \qquad \text{Eq. 27}$$

$$\textit{Minimum \# of Layers CFRP Grid Needed} = \frac{T2_{CFRP}}{Strength/Layer} = \frac{12.16\text{ kip}}{0.641\text{ kip/layer}} = 18.97\text{ layers} \rightarrow 19\text{ layers}$$

Eq. 28

Table 14. PCBT-45A – Steel and CFRP Grid End Zone Design

Tie	Required Strength, kips	Distribution Length, in	Steel Bar Size and Spacing	Total Steel Reinforcing Area, in²	Strength from Steel, kips	Minimum Layers of CFRP Required	
						NEFMAC	C-Grid
T1	28.9	22.5	4 ea. No. 5 bars @ 8 in	1.24	22.32	5	6
T2	28.9	11.25	3 ea. No 5 bars @ 5 in	0.93	16.74	13	19

So, with three No.5 bars at 5 in spacing, the region *h*/4 (measured from the beam end) for the tie *T2* in the parametric case PBCT-45A would still need 19 layers of C-Grid to meet crack control requirements. As shown in Table 14, 13 layers of NEFMAC grid would be required for the same scenario. For the *T1* region between *h*/4 and 3*h*/4 (measured from the end of the beam), five layers of NEFMAC grid and six layers of C-Grid would be needed, provided that there were four No. 5 steel bars at 8 in spacing.

Results from Parametric Calculations

For this study, there were 18 different cases for end zone design. Nine used CFRP grid as the only type of transverse reinforcing, and the other nine used CFRP grid in combination with steel stirrup reinforcing. Table 15 shows a summary of all 18 designs. The table is split into two portions for design of the end zones, using only CFRP grid as reinforcement and using a combination CFRP grid and steel reinforcement. More detailed tables can be found in Magee (2016) for all of the design cases.

As shown in Table 15, the number of CFRP grid layers needed for design was very high, regardless of reinforcement scenario. For the design utilizing only CFRP grid, the required number of NEFMAC layers ranged from 19 to 53 layers. Even the smallest number of layers needed was far greater than would be feasible. Similarly for C-Grid, 25 to 61 layers were needed for design. As expected, utilizing steel in combination with CFRP grid helped to decrease the amount of CFRP grid layers needed for each design case. However, total amount of reinforcement would not be practical for construction.

Based on these findings, CFRP grid is not a viable reinforcing material to be used in design for end zone regions of prestressed beams. The stress limits placed on the CFRP grid for

use in end zones reduce the usable strengths too much for efficient design. If VDOT wants to implement CFRP grids in design standards, then the current limits on working stresses for the CFRP grids need to be increased.

Table 15. End Zone Design Summary for CFRP only and for Steel and CFRP Grid Combined

| Beam | Tie Region | CFRP Grids Only | | Steel and CFRF Grid Combined | | |
| | | Minimum Layers of CFRP Grid | | Bar Size and Spacing | Minimum layers of CFRP Grid | |
		NEFMAC	C-Grid		NEFMAC	C-Grid
PCBT-45A	T1	21	25	4 ea. No. 5 bars @ 8 in	5	6
	T2	32	46	3 ea. No. 5 bars @ 5 in	13	19
PCBT-45B	T1	26	30	4 ea. No. 5 bars @ 8 in	10	11
	T2	39	55	3 ea. No. 5 bars @ 8 in	20	29
PCBT-45C	T1	24	28	4 ea. No. 5 bars @ 5 in	8	9
	T2	36	52	3 ea. No. 5 bars @ 8 in	18	26
PCBT-61A	T1	23	27	5 ea. No. 5 bars @ 7 in	8	10
	T2	47	53	3 ea. No. 5 bars @ 7 in	28	33
PCBT-61B	T1	23	27	5 ea. No. 5 bars @ 7 in	8	10
	T2	47	53	3 ea. No. 5 bars @ 7 in	3	33
PCBT-61C	T1	27	31	5 ea. No. 5 bars @ 7 in	11	13
	T2	53	61	3 ea. No. 5 bars @ 7 in	34	40
PCBT-77A	T1	19	22	5 ea. No. 5 bars @ 10 in	7	8
	T2	32	42	5 ea. No. 5 bars @ 5 in	12	16
PCBT-77B	T1	24	28	5 ea. No. 5 bars @ 10 in	12	14
	T2	40	53	5 ea. No. 5 bars @ 5 in	14	26
PCBT-77C	T1	22	26	5 ea. No. 5 bars @ 10 in	10	12
	T2	37	49	5 ea. No. 5 bars @ 5 in	17	22

DISCUSSION

Discussion of Shear Design Methods

As previously discussed in the *Methods* section of this report, several different design methods were investigated to predict the shear strength of concrete beams with different shear reinforcing materials and ratios. For each design method discussed in this section, tables are presented which present the ratio of the experimental shear strength versus the calculated shear strength. Calculated strengths are presented based on design material properties and actual measured material properties. The design material properties for the CFCC, C-Grid and NEFMAC were taken as those specified by the manufacturer, which for the guaranteed tensile strength ($f*_{fu}$) of the material, is the average rupture strength reduced by three standard deviations. No environmental degradation factor was applied since the beams were not exposed to the environment. The actual properties for the C-Grid were from the material tests discussed in this report, and are also the mean minus three standard deviations. The actual CFCC values were from the quality control testing documents provided with the stirrup shipment from Tokyo Rope. The actual steel properties were based on tests performed in this research. The NEFMAC design and actual values were provided by the manufacturer. Table 16 summarizes all of these material property values.

Table 16. Design and Actual Tested Material Properties

Material and Property	Design Value	Actual Value
Concrete f'$_c$ Specimens 1 and 2	7.00 ksi	7.99 ksi
Concrete f'$_c$ Specimens 3 and 4	7.00 ksi	7.35 ksi
Concrete f'$_c$ Specimen 5	7.00 ksi	6.34 ksi
Steel Yield Stress	60 ksi	59 ksi
Steel Modulus of Elasticity	29,000 ksi	29,900 ksi
CFCC Guaranteed Tensile Stress, f*$_{fu}$	352 ksi	437 ksi
CFCC Modulus of Elasticity	22,500 ksi	21,750 ksi
C-Grid Tow Guaranteed Tensile Stress, f*$_{fu}$	290 ksi	339 ksi
C-Grid Modulus of Elasticity	34,000 ksi	32,600 ksi
NEFMAC Tow Guaranteed Tensile Stress, f*$_{fu}$	173 ksi	173 ksi
NEFMAC Modulus of Elasticity	14,500 ksi	14,500 ksi

Note: CFCC, C-Grid and NEFMAC guaranteed tensile stress reported is the average reduced by three standard deviations

Because not every test resulted in failure, the tables also have a column indicating whether or not a failure occurred, and if so, what the failure mode was. Thus, the test-to-calculated shear strength ratio may be higher if the specimen had a shear capacity that was actually greater than the maximum shear load observed during testing.

AASHTO Modified Compression Theory

Recall that AASHTO specifies a stress limit on reinforcing of 0.0035 times the modulus of elasticity or a maximum of 75 ksi. For the CFCC stirrups, the maximum stress was limited to 75 ksi due to the large modulus of elasticity. There was no additional strength reduction for the bend zones, as the AASHTO specifications do not cover bend reductions with CFRP products. The maximum stress for the C-Grid was also limited to 75 ksi, again due to a high modulus of elasticity. On the other hand, the stress for NEFMAC was limited to 50.8 ksi, due to a low modulus of elasticity. Values for maximum stress are summarized in Table 17.

Table 17. AASHTO Maximum Stirrup Stresses

Design Values, ksi			
Material	f$_y$ or f*$_{fu}$	0.0035 E	f$_{max}$
Steel	60	102	60
CFCC	352	79	75
C-Grid	290	119	75
NEFMAC	173	50.8	50.8
Actual Values, ksi			
Material	f$_y$ or f*$_{fu}$	0.0035 E	f$_{max}$
Steel	59	105	59
CFCC	437	76	75
C-Grid	339	114	75
NEFMAC	173	50.8	50.8

Table 18 provides comparisons between the experimental shear strengths the calculations using the AASHTO method. Clearly, the AASHTO method was conservative for all specimens. The specimen with the best fit was the CFCC stirrups with Typical Reinforcement Ratio, which had an experimental versus calculated ratio of 1.08. The AASHTO method did provide a good fit for the specimens containing steel stirrups, even though none of the specimens failed in shear.

The reduction of strength due to strain limitations in the C-Grid and NEFMAC provided a very conservative estimate of shear strength.

Table 18. AASHTO MCFT Comparisons with Transverse Reinforcement Stress Limitations

Shear Reinforcing	V_n – Design, kips	V_n – Actual, kips	Max Applied Shear, V_{test} kips	Failure Mode	V_{test}/V_n - Design	V_{test}/V_n- Actual
Typ Steel	28.5	28.6	43.6	Yes, Compression	1.53	1.52
Min Steel	18.4	18.6	23.0	No	1.25	1.24
Min C-Grid	12.3	12.7	28.9	Yes, Shear	2.35	2.27
Typ CFCC	39.3	39.5	42.6	Yes, Shear	1.08	1.08
Min CFCC	25.0	25.2	33.2	No	1.33	1.32
C-Grid Zip Tied	16.6	16.9	36.3	Yes, Shear	2.18	2.15
C-Grid Spaced	16.6	16.9	38.2	Yes, Shear	2.30	2.27
Typ NEFMAC	13.5	16.5	36.7	Yes. Shear	2.71	2.23
Min NEFMAC	12.3	13.9	34.2	Yes, Shear	2.77	2.45

AASHTO Modified Compression Theory without Stress Limitations

Due to the overly conservative nominal shear calculations for the C-Grid and NEFMAC discussed above, a separate analysis of the AASHTO method was performed, which used the full guaranteed tensile strength of the CFRP material and did not apply the AASHTO limits. Again, note that the design and actual tested guaranteed tensile strengths for the CFRP reinforcing were the mean reduced by three standard deviations, as given in Table 16.

Table 19 shows that assuming the full guaranteed tensile strength of the CFCC stirrups resulted in a very unconservative nominal shear capacity. However, assuming the full guaranteed tensile strength in the AASHTO method does provide a good fit for the C-Grid, especially when using two layers. Note that this approach also led to less conservative, but still reasonable, estimates for the NEFMAC grid.

Table 19. AASHTO MCFT Comparisons without Transverse Reinforcement Stress Limitations

Shear Reinforcing	V_n – Design, kips	V_n – Actual, kips	Max Applied Shear, V_{test} kips	Failure	V_{test}/V_n - Design	V_{test}/V_n- Actual
Typ Steel	28.5	28.6	43.6	Yes, Compression	1.53	1.52
Min Steel	18.4	18.6	23.0	No	1.25	1.24
Min C-Grid	18.4	20.1	28.9	Yes, Shear	1.57	1.44
Typ CFCC	95.4	106.2	42.6	Yes, Shear	0.45	0.40
Min CFCC	61.0	69.4	33.2	No	0.54	0.48
C-Grid Zip Tied	29.7	32.6	36.3	Yes, Shear	1.22	1.11
C-Grid Spaced	29.7	32.6	38.2	Yes, Shear	1.29	1.17
Typ NEFMAC	28.1	27.8	36.7	Yes. Shear	1.31	1.72
Min NEFMAC	20.2	19.8	34.2	Yes, Shear	1.69	1.72

ACI 318 Shear Design Method

Because ACI 318 was developed for use with steel reinforcing bars, the maximum allowable stress for the transverse reinforcing in shear is the yield strength of the bar, not greater than 80 ksi. This is much lower than the guaranteed tensile strength according to the

manufacturers of CFCC, C-Grid, and NEFMAC. Maximum stresses for the shear design of stirrups are presented in Table 20.

As would be expected, Table 21 shows that the ACI method is a good fit when designing beams with steel transverse reinforcement. Also, the predictions for CFCC stirrups with Typical Reinforcement Ratio matched very well, being only 10% less than the experimental values. The predicted strengths for C-Grid and NEFMAC specimens did not compare well with the tested strengths. Instead, the ACI method proved to be conservative with the experimental-to-calculated ratios all being over 2.3.

Table 20. ACI 318 Maximum Stirrup Stresses

Design Values, ksi		
Material	f_y or f^*_{fu}	f_{max}
Steel	60	60
CFCC	352	80
C-Grid	290	80
NEFMAC	173	80
Actual Values, ksi		
Material	f_y or f^*_{fu}	f_{max}
Steel	59	59
CFCC	437	80
C-Grid	339	80
NEFMAC	173	80

Table 21. ACI 318 Method Comparisons with Transverse Reinforcement Stress Limitations

Shear Reinforcing	V_n – Design, kips	V_n – Actual, kips	Max Applied Shear, V_{test} kips	Failure	V_{test}/V_n - Design	V_{test}/V_n- Actual
Typ Steel	27.2	27.5	43.6	Yes, Compression	1.60	1.58
Min Steel	17.9	18.3	23.0	No	1.29	1.26
Min C-Grid	11.0	11.6	28.9	Yes, Shear	2.63	2.50
Typ CFCC	38.7	38.9	42.6	Yes, Shear	1.10	1.09
Min CFCC	21.9	22.1	33.2	No	1.52	1.50
C-Grid Zip Tied	13.3	13.5	36.3	Yes, Shear	2.74	2.69
C-Grid Spaced	13.3	13.5	38.2	Yes, Shear	2.89	2.83
Typ NEFMAC	15.7	15.5	36.7	Yes. Shear	2.34	2.37
Min NEFMAC	12.1	11.8	34.2	Yes, Shear	2.83	2.90

ACI 318 Shear Design Method without Stress Limitations

Like the AASHTO calculations, the conservative nature of ACI's allowable stress limitations resulted in a second analysis the ACI method using the guaranteed tensile strength of the CFRP material without the imposed maximum stress limitation (80 ksi). Again, note that the design and actual tested guaranteed tensile strengths were the mean reduced by three standard deviations. Table 22 presents the results of this separate analysis. Using the guaranteed tensile strength for the CFCC stirrups resulted in an unconservative estimate of the shear strength of the section. On the other hand, the guaranteed tensile strength of the C-Grid and NEFMAC grid resulted in better estimates of the shear strength of beams designed with CFRP reinforcement. This method could be used for design with C-Grid or NEFMAC grid, but the stress limitation should be used for the CFCC stirrups.

Table 22. ACI 318 without Transverse Reinforcement Stress Limitations and Results

Shear Reinforcing	V_n – Design, kips	V_n – Actual, kips	Max Applied Shear, V_{test} kips	Failure	V_{test}/V_n - Design	V_{test}/V_n- Actual
Typ Steel	27.23	27.51	43.6	Yes, Compression	1.60	1.58
Min Steel	17.88	18.32	23.0	No	1.29	1.26
Min C-Grid	17.35	19.43	28.9	Yes, Shear	1.67	1.49
Typ CFCC	141.57	173.96	42.6	Yes, Shear	0.30	0.24
Min CFCC	67.61	82.14	33.2	No	0.49	0.40
C-Grid Zip Tied	25.88	29.06	36.3	Yes, Shear	1.40	1.25
C-Grid Spaced	25.88	29.06	38.2	Yes, Shear	1.48	1.32
Typ NEFMAC	24.2	23.8	36.7	Yes. Shear	1.51	1.54
Min NEFMAC	16.3	15.9	34.2	Yes, Shear	2.09	2.15

ACI 440.4R Shear Design Method

ACI 440.4R limits the maximum stress of the material to the minimum of 0.002 times the elastic modulus, the design tensile strength, or the bend radius reduction strength. In this study, all materials were controlled by 0.002 times the elastic modulus of the materials, resulting in maximum stresses allowed for the CFRP materials that were considerably less than their breaking strengths. The steel was limited to 58 ksi, which is less than, but close to, the typical 60-ksi yield stress. The maximum stirrup stresses are shown in Table 23.

Table 23. ACI 440.4R Maximum Stirrup Stresses

Design Values, ksi		
Material	f_y or f^*_{fu}	0.002 E	f_{max}
Steel	60	58	58
CFCC	352	45	45
C-Grid	290	68	68
NEFMAC	173	29	29
Actual Values, ksi		
Material	f_y or f^*_{fu}	0.002 E	f_{max}
Steel	59	60	60
CFCC	437	43	43
C-Grid	339	65	65
NEFMAC	173	29	29

The results of the shear capacity calculations are presented in Table 24. Like ACI 318, the ACI 440.4R method was very conservative when designing with the C-Grid and the NEFMAC grid, as the ratios were above 2.6 when calculating with actual material properties. The method was also conservative for the CFCC stirrups. Despite being written for FRP beams with prestressed reinforcement, the only material the ACI 440.4R code predicted reasonably well was the steel stirrups, probably because 0.002 times the modulus is nearly identical to the yield strength. Although a very safe method, the ACI 440.4R method would likely result in much more reinforcing than needed in a section.

Table 24. ACI 440.4R Comparisons with Transverse Reinforcement Stress Limitations

Shear Reinforcing	V_n – Design, kips	V_n – Actual, kips	Max Applied Shear, V_{test} kips	Failure	V_{test}/V_n - Design	V_{test}/V_n- Actual
Typ Steel	26.6	27.5	43.6	Yes, Compression	1.64	1.58
Min Steel	17.6	18.3	23.0	No	1.31	1.26
Min C-Grid	10.6	11.1	28.9	Yes, Shear	2.73	2.60
Typ CFCC	25.5	25.1	42.6	Yes, Shear	1.67	1.70
Min CFCC	16.0	16.0	33.2	No	2.08	2.08
C-Grid Zip Tied	12.5	12.6	36.3	Yes, Shear	2.89	2.88
C-Grid Spaced	12.5	12.6	38.2	Yes, Shear	3.05	3.04
Typ NEFMAC	11.1	10.8	36.7	Yes. Shear	3.31	3.40
Min NEFMAC	9.8	9.5	34.2	Yes, Shear	3.50	3.62

ACI 440.4R Shear Design Method without Stress Limitations

As before, the reductions in strength of the CFRP materials as required by ACI 440.4R provided very conservative estimates of the shear strength of a concrete section. For this reason, the predicted strengths were recalculated using the ACI 440.4R method along with the guaranteed tensile strength of the stirrups without imposing any stress limitations. Again, this guaranteed tensile strength was the average minus three standard deviations for the CFRP materials, as found in Table 16. Table 25 presents the results of these calculations. As could be expected, the predicted shear strength of the specimens with steel stirrups barely increased from the previous analysis because the previously limited working stress was nearly the same as the yield strength of steel reinforcing, which was used in this second set of calculations. The predicted strengths for the specimens with CFCC stirrups were very unconservative. On the other hand, the ratio of predicted-to-tested values were much smaller for the C-Grid and NEFMAC, compared to the previously discussed ACI 440.4R calculations. However, these ratios were not as close to 1.0 as they were for the ACI 318 and AASHTO methods without stress limitations, thus having a slightly larger degree of inherent safety.

Table 25. ACI 440.4R Comparisons without Transverse Reinforcement Stress Limitations

Shear Reinforcing	V_n – Design, kips	V_n – Actual, kips	Max Applied Shear, V_{test} kips	Failure	V_{test}/V_n - Design	V_{test}/V_n- Actual
Typ Steel	27.2	27.5	43.6	Yes, Compression	1.60	1.58
Min Steel	17.9	18.3	23.0	No	1.29	1.26
Min C-Grid	17.4	19.4	28.9	Yes, Shear	1.67	1.49
Typ CFCC	141.6	174.0	42.6	Yes, Shear	0.30	0.24
Min CFCC	67.6	82.1	33.2	No	0.49	0.40
C-Grid Zip Tied	25.9	29.1	36.3	Yes, Shear	1.40	1.25
C-Grid Spaced	25.9	29.1	38.2	Yes, Shear	1.48	1.32
Typ NEFMAC	24.2	23.8	36.7	Yes. Shear	1.51	1.54
Min NEFMAC	16.3	15.9	34.2	Yes, Shear	2.09	2.15

ACI 440.1R Shear Design Method

The ACI 440.1R method limits the maximum stress of the material to the minimum of 0.004 times the elastic modulus, the design tensile strength, or the bend radius reduction strength. For this study, the 60-ksi yield stress controlled for the steel. The CFCC stirrups were limited by

0.004 times the modulus of the strand, or 90 ksi, which was much larger than what had been used in previous calculations. The NEFMAC grid and C-Grid were also limited by the 0.004 strain. The maximum stirrup stresses are shown in Table 26.

Table 27 presents the ACI 440.1R calculations for the calculated shear capacity and measured shear capacity of the sections. The method was not always conservative, as shown by the experimental versus predicted ratio of less than 1.0 for the Typical CFCC transverse reinforcement. The CFCC shear strengths for both the minimum and typical reinforcing were also much higher than the shear strengths with the other materials due to the large stress in the stirrups allowed by the design recommendations. The method does a reasonable job of predicting the shear strength of the CFRP grids without being overly conservative like ACI 440.4R. However, the additional calculations needed to determine the area of the shear funnel in unusual shapes make the 440.1R method more cumbersome than others.

Table 26. ACI 440.1R Maximum Stirrup Stresses

Design Values, ksi				
Material	f_y or f^*_{fu}	f_{fb}	**0.004 E**	f_{fv}
Steel	60	-	116	60
CFCC	352	170	90	90
C-Grid	290	-	136	136
NEFMAC	173	-	58	58
Actual Values, ksi				
Material	f_y or f^*_{fu}	f_{fb}	**0.004 E**	f_{fv}
Steel	59	-	120	59
CFCC	437	211	87	87
C-Grid	339	-	130	130
NEFMAC	173	-	58	58

Table 27. ACI 440.1R Comparisons with Transverse Reinforcement Stress Limitations

Shear Reinforcing	V_n – Design, kips	V_n – Actual, kips	Max Applied Shear, V_{test} kips	Failure	V_{test}/V_n - Design	V_{test}/V_n - Actual
Typ Steel	31.8	31.2	43.6	Yes, Compression	1.37	1.35
Min Steel	22.4	23.0	23.0	No	1.03	1.00
Min C-Grid	17.2	17.8	28.9	Yes, Shear	1.68	1.63
Typ CFCC	49.9	49.3	42.6	Yes, Shear	0.85	0.86
Min CFCC	31.0	31.0	33.2	No	1.07	1.07
C-Grid Zip Tied	24.1	24.2	36.3	Yes, Shear	1.51	1.50
C-Grid Spaced	24.0	24.2	38.2	Yes, Shear	1.59	1.58
Typ NEFMAC	21.2	20.5	36.7	Yes. Shear	1.73	1.79
Min NEFMAC	18.5	17.8	34.2	Yes, Shear	1.85	1.92

ACI 440.1R Shear Design Method without Stress Limitations

Even though the ACI 440.1R method provided slightly less conservative estimates of strength relative to the other calculation methods, the shear strengths were also calculated using the guaranteed tensile strength of the stirrups, without stress limitations. As seen in Table 28, the predicted shear capacity assuming guaranteed tensile strength of the CFCC stirrups is extremely unconservative. However, the values for the C-Grid and NEFMAC correlated well with the measured values.

Table 28. ACI 440.1 Comparisons without Transverse Reinforcement Stress Limitations

Shear Reinforcing	V_n – Design, kips	V_n – Actual, kips	Max Applied Shear, V_{test} kips	Failure	V_{test}/V_n - Design	V_{test}/V_n - Actual
Typ Steel	31.8	32.2	43.6	Yes, Compression	1.37	1.35
Min Steel	22.4	23.0	23.0	No	1.03	1.00
Min C-Grid	21.9	24.1	28.9	Yes, Shear	1.32	1.20
Typ CFCC	149.0	181.7	42.6	Yes, Shear	0.29	0.23
Min CFCC	75.1	89.8	33.2	No	0.44	0.37
C-Grid Zip Tied	33.3	36.8	36.3	Yes, Shear	1.09	0.99
C-Grid Spaced	33.3	36.8	38.2	Yes, Shear	1.15	1.04
Typ NEFMAC	31.7	30.9	36.7	Yes. Shear	1.16	1.19
Min NEFMAC	23.8	23.0	34.2	Yes, Shear	1.44	1.49

Summary of Design Methodologies

Because there were several specimens that did not fail in shear, one important note is that some of the capacity-to-design ratios were not as relevant as they could have been. Nevertheless, comparing the values for the specimens that did fail in shear can provide insight into which methods better predict capacity for which materials. Table 29 aggregates the ratios of the experimental versus predicted shear capacities for all of the design methods, both with and without stress limitations, but based on design material properties. Note that the three specimens that did not have a shear failure have been shaded in the table. The AASHTO MCFT method with stress limitations performed the best in terms of calculating the shear capacity of the beam with CFCC stirrups at a typical reinforcement ratio. The ACI 440.1R method without stress limitations was the best fit for the beams with both C-Grid and NEFMAC transverse reinforcement. The AASHTO method without stress limitations also provided reasonable estimates of shear strength for beams with grid, but was slightly more conservative than ACI 440.1R. While somewhat more conservative than the two aforementioned methods, the ACI 318 method without stress limitations provided a good prediction for shear strengths with CFRP grids and could be used for a relatively quick initial calculation or check of the section.

Table 29 also shows that the ACI 440.4R method is very conservative when keeping the transverse reinforcement stress limitations in place, due to the 0.002E requirement for CFRP products. The resulting designs may be more conservative than needed to ensure a safe and predictable design. Grace et al. (2015) noted that this method needed revision due to its conservative nature; the findings of this study support that conclusion. Note that the ACI 318 and ACI 440.4R shear strength calculations with no stress limitations result in the same estimates of strength. This is because, except for differences in stress limitations, they are identical methods.

Table 30 presents the same comparison of the shear calculation methods as Table 29, but considers the actual tested material values instead, giving a better picture of the performance of the shear strength calculation methods when the materials used in construction are known. Again, the AASHTO method provided the ratios that were closest to 1.0 for the specimen containing the typical reinforcement ratio of CFCC stirrups. As found in Table 29, ACI 440.1R proved to be the best at estimating the strength of the CFRP grid materials when using the as-

tested material properties with no stress limitations. The AASHTO method was approximately 10% more conservative than the ACI 440.1 method.

Table 29. Comparison of All Calculation Methods Using Design Material Values

Shear Reinforcing	With Transverse Reinforcement Stress Limitations				Without Transverse Reinforcement Stress Limitations			
	AASHTO MCFT	ACI 318	ACI 440.4	ACI 440.1	AASHTO MCFT	ACI 318	ACI 440.4	ACI 440.1
Typ Steel	1.53	1.60	1.64	1.37	1.53	1.60	1.60	1.37
Min Steel	1.25	1.29	1.31	1.03	1.25	1.29	1.29	1.03
Min C-Grid	2.35	2.63	2.73	1.68	1.57	1.67	1.67	1.32
Typ CFCC	1.08	1.10	1.67	0.85	0.45	0.30	0.30	0.29
Min CFCC	1.33	1.52	2.08	1.07	0.54	0.49	0.49	0.44
C-Grid Zip Tied	2.18	2.74	2.89	1.51	1.22	1.40	1.40	1.09
C-Grid Spaced	2.30	2.89	3.05	1.59	1.29	1.48	1.48	1.15
Typ NEFMAC	2.71	2.34	3.31	1.73	1.51	1.51	1.51	1.16
Min NEFMAC	2.77	2.83	3.50	1.85	1.69	2.09	2.09	1.44

Table 30. Comparison of All Calculation Methods Using Actual Material Properties

Shear Reinforcing	With Transverse Reinforcement Stress Limitations				Without Transverse Reinforcement Stress Limitations			
	AASHTO MCFT	ACI 318	ACI 440.4	ACI 440.1	AASHTO MCFT	ACI 318	ACI 440.4	ACI 440.1
Typ Steel	1.52	1.58	1.58	1.35	1.52	1.58	1.58	1.35
Min Steel	1.24	1.26	1.26	1.00	1.24	1.26	1.26	1.00
Min C-Grid	2.27	2.50	2.60	1.63	1.44	1.49	1.49	1.20
Typ CFCC	1.08	1.09	1.70	0.86	0.40	0.24	0.24	0.23
Min CFCC	1.32	1.50	2.08	1.07	0.48	0.40	0.40	0.37
C-Grid Zip Tied	2.15	2.69	2.88	1.50	1.11	1.25	1.25	0.99
C-Grid Spaced	2.27	2.83	3.04	1.58	1.17	1.32	1.32	1.04
Typ NEFMAC	2.23	2.37	3.40	1.79	1.32	1.54	1.54	1.19
Min NEFMAC	2.45	2.90	3.62	1.92	1.72	2.15	2.15	1.49

The ACI 440.4R method with stress limitations provides very conservative estimates of strength for all shear reinforcement material except steel. Without the stress limitations, the method vastly overestimated the shear capacity of the specimens with CFCC stirrups, but provide a closer approximation of shear capacity for C-Grid and NEFMAC. The ACI 318 method appears to provide simple and conservative calculation of the section capacity. For calculation of shear strength using ACI 318, the method should be followed including the stress limitations when designing beams containing CFCC shear stirrups. However, if calculating shear strength for beams reinforced for shear with CFRP grid, the limitations are not needed.

The AASHTO method presents a straightforward method for the calculation of shear capacity of beams using C-Grid and NEFMAC transverse reinforcement. However, the AASHTO strength reduction factor for shear, ϕ_v, is 0.9. Because failure of the C-Grid and NEFMAC results in a complete loss of load carrying capacity of the section, this value should be reduced to provide more room for errors in calculation. Because there has been only a limited amount of testing completed to date and without any statistical analysis, a smaller and more appropriate value for ϕ_v would be 0.75, which is the recommended factor for shear design in all

three ACI design methods discussed in this study. Recall that both 440.1R and 440.4R were developed specifically for CFRP materials.

Design Examples

Based on the outcome of the shear tests, the AASHTO shear design method using the manufacturers' reported guaranteed tensile strength without stress limitations was deemed to provide the best estimate of shear capacity for those beams containing CFRP grid shear reinforcement. No environmental degradation factor was applied in these examples. If CFRP is in a harsh environment a factor of 0.9 (ACI 440.1R, 2006) should be applied to reflect a gradual loss of strength over time. To determine if the CFRP grids would result in reasonable, practical solutions, two separate designs were developed for a realistic bridge, one design with C-Grid and the other with NEFMAC.

C-Grid Design Example

The design is for the Bulb-Tee (BT-72) Single Span, Composite Deck, LRFD Specifications example given in the PCI Bridge Design Manual Chapter 9, Section 9.4 (PCI Bridge Design Manual Steering Committee, 2003). The following calculations provide guidance for the use of C-Grid transverse reinforcement to ensure adequate shear capacity of the girders in this example.

The bridge has a 120-ft span with no skew, supported by BT-72 prestressed girders that are spaced at 9 ft on center with an 8-in uniform thickness composite deck above (including the ½-in wearing surface). Therefore, the composite structural deck is 7½ in thick. The design live load is specified as AASHTO HL-93, resulting in 48 ½-in prestressing strands distributed in ten layers for flexural strength. The top 12 strands were harped, starting at 48 ft-6 in from the end of the beam.

Section 9.4.11 of the example provides the necessary information to perform the shear design. The critical shear depth, d_v, is 73.14 in and the ultimate shear load, V_u, is 316.2 kips at the critical section. The values of θ and β are 22.8° and 2.94, respectively. The shear resistance of the concrete, V_c, is 103.9 kips and the contribution to shear resistance from the prestressing steel, V_p, is 23.4 kips. Using the design equations (Equations 2, 3, 4, 6 and 7) and a ϕ factor of shear resistance of the reinforcing 0.75, as suggested in the *Discussion* section, the required shear resistance of the reinforcing, V_s, becomes 294.3 kips.

For this example, C50 1.6 x 1.8 grid is the reinforcement used to provide V_s. C50 1.6 x 1.8 is the largest and tightest spacing of the C-Grid available from Chomarat. Recall that AASHTO calculates V_s using the formula given as Equation 7 in this report. However, to the designer can easily modify Equation 7 to find the number of grids required, as shown below:

$$n = \frac{V_s s}{F_{frp} d_v \cot \theta} \qquad \text{Eq. 29}$$

where:

n = the number of layers of grid needed
F_{frp} = the strength of one tow of the grid given by the manufacturer.

Note that F_{frp} must be the result of reducing the mean tensile strength determined from testing by three standard deviations. The other terms in Equation 19 are the same as those indicated in Equation 7.

The vertical tows in the C50 grid have 1.6-in spacing. Therefore, s in Equation 29 is 1.6 in and F_{frp} is 0.83 kips/tow with no stress limitations imposed. The PCI example provides all of the other relevant variables for this example. Thus, the required number of layers of C50 1.6 x 1.8 grid equates to:

$$n = \frac{V_s s}{F_{frp} d_v \cot \theta} = \frac{(294.3 \text{ kip}) (1.6 \text{ in})}{(0.83 \text{ kip})(73.14 \text{ in}) \cot(22.8°)} = 3.26 \rightarrow 4 \text{ layers}$$

Eq. 30

The next important step is to ensure the grid has enough embedment in the beam flange and bulb in order to fully develop strength. The top flange of the beam provides 7½ in and the bulb provides 10½ in for development, as shown in Figure 77. Because the C-Grid can become fully developed in 4 in, the beam provides adequate embedment for full development, including room for clear cover. The four layers of C-Grid will fit easily into the 6-in thick web, provided that two layers of grid are zip tied together and placed on each side of the web with 1 in of minimum cover.
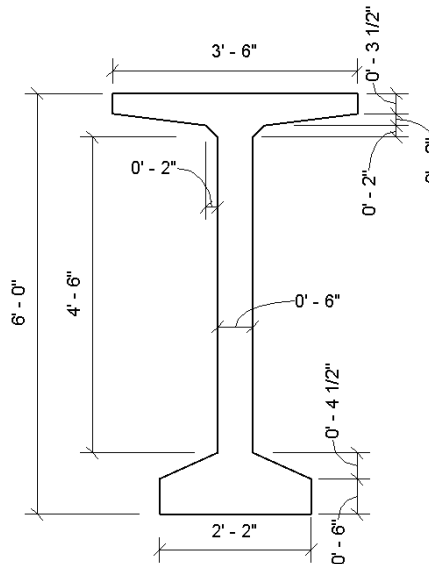

Figure 77. BT-72 Beam from PCI Bridge Design Manual

To implement this design:
- Use four layers of C-Grid C50 1.6 x 1.8 with the 1.6 in direction acting as the stirrups.
- Provide 1 in minimum cover over the grid, and zip tie two layers together on each side of the web.
- Laterally support the grid vertically every 18 in to ensure grid does not buckle during concrete placement.

- Extend the grid as high and as low in the cross-section as possible, leaving at least 1 in of clear cover at the bottom, to ensure proper development of grid in top and bottom flange.
- The top flange will be covered with deck, so cover is not mandatory.

NEFMAC Design Example

The design example for C-Grid is repeated here, but using NEFMAC C6 Grid instead. The calculations are the same up to and including the point where the required V_s has been determined to be 294.3 kips.

Although the NEFMAC C6 ordinarily has 8 in by 10 in spacing, the grid layers will be oriented and staggered such that the spacing of the vertical tows will be 5 in. F_{frp} is 4.69 kips/tow. PCI provided all other relevant variables that are needed to solve Equation 29. Plugging in and solving that equation provides a value for n as shown below in Equation 31.

$$n = \frac{(294.3 \text{ kip})(5 \text{ in})}{(4.69 \text{ kip})(73.14 \text{ in})\cot(22.8°)} = 1.8 \qquad \text{Eq. 31}$$

The design requires 1.8 NEFMAC layers if the tows are spaced at 5 in, which is the equivalent of 3.6 layers if the tows are spaced at 10 in, and offset to create a 5 in spacing. This means a total of four NEFMAC C6 layers are needed for the beam. The next important step is to ensure that the grid has enough embedment in the bulb flange and bulb to develop full strength. The top flange of the beam provides 7½ in for development and the bulb provides 10½ in. Because the NEFMAC grid can fully develop strength in 4 inches, the beam provides adequate embedment with room for clear cover. The four layers of NEFMAC grid will also fit easily into the 6-in thick web with clear cover.

To implement this design:
- Use four layers of NEFMAC C6 with the grids oriented and staggered to create 5-in spacing of vertical tows.
- Provide 1 in minimum cover over the grid, and zip tie two layers together on each side of the web.
- Extend the grid as high and as low in the cross-section as possible to ensure proper development of grid in top and bottom flange, but leave at least 1 in of clear cover at the bottom.
- The top flange will be covered with a deck so cover is not mandatory.

CONCLUSIONS

Comparison of the observed experimental results to current codes, specifications, and design recommendations has led to the following conclusions for CFRP shear reinforcing:

- *C-Grid and NEFMAC are both viable shear reinforcement options for concrete bridge girders.*

- *C-Grid C50 1.6 x 1.8 and NEFMAC C6 have a development length that is as short as 4 in.* This conclusion for the NEFMAC C6 grid assumes that at least one transverse tow is embedded at least 2 ½ in into the concrete.

- *The manufacturer's reported guaranteed tensile strength and modulus of elasticity for C-Grid and NEFMAC can be used for the design of shear reinforcement as long as the value is the mean tested strength reduced by three standard deviations.* Note that the design strength should also include the appropriate environmental degradation factor.

- *Regardless of the design code used, applying code-prescribed stress limitations results in overly conservative designs for C-Grid and NEFMAC reinforcement.* The AASHTO Modified Compression Field Theory equations provide the best prediction of shear strength for C-Grid and NEFMAC grid when using the manufacturers' reported strength without stress limitations.

- *The AASHTO Modified Compression Field Theory with equations and stress limitations most accurately predicts the shear capacity of a section with CFCC stirrups.*

- *A shear design ϕ-factor of 0.75 is prudent for the time being.* The fact that the brittle nature of C-Grid and NEFMAC materials tends to result in sudden and complete loss of load carrying capacity of section reinforces this conclusion.

- *C-Grid and NEFMAC grid materials need to be supported vertically at a minimum of 18 in on-center (in the lateral direction) to keep them in the correct position during concrete placement.*

- *CFRP grid is not a viable reinforcing material for reinforcing end zone regions of prestressed beams.* The stress limits placed on the CFRP grid used to control cracking in these regions reduce the usable strengths too much for efficient design.

RECOMMENDATIONS

The research presented in this report was an exploratory effort to determine the viability of CFRP grids as shear reinforcement. Based on the findings of this study, tentative design and handling methods are recommended below:

1. *VTRC and VDOT's Structure and Bridge Division should support additional small-scale tests of C-Grid and NEFMAC as shear reinforcement.* Furthermore, other commercially-available CFRP grid materials should be included in order to determine their mechanical properties, development lengths, and design recommendations. The results from these tests will augment the existing database, which improve the knowledge necessary for designing full-scale prestressed concrete beams with CFRP grid as shear reinforcement. These additional small-scale tests should include:

71

- beam shear tests that will help to properly calibrate the ϕ-factor, assess the reliability of the design, and determine if a maximum allowable strain needs to be set for CFRP grids in order to ensure a safe shear design
- panel tests to help determine the allowable stress in CFRP grid materials for end zone crack control
- horizontal push-off tests to determine the viability of C-Grid or NEFMAC grid as horizontal shear reinforcement to provide adequate composite interaction between bridge deck and girders
- bond tests using multiple layers of C-Grid or NEFMAC grid that are tied together with zip ties to ensure that the development length does not change compared to a single layer of grid. These tests will also help to determine the clear cover required to fully develop C-Grid or NEFMAC Grid such that a splitting failure does not occur at the concrete face.

2. *VTRC and VDOT's Structure and Bridge Division should support the testing of C-Grid and NEFMAC grid in full-scale, pretensioned bridge beams before implementing these materials as standard practice.* This additional research will help to ensure that actual designs scale up properly from the small-scale results in this study.

BENEFITS AND IMPLEMENTATION

Benefits

As design methodologies move closer toward corrosion-resistant and corrosion-free reinforcement, CFRP grids have the potential to have a large impact on the fabrication of prestressed concrete members. CFCC used as the primary flexural reinforcement require nonmetallic shear reinforcement (or at the very least, protection from metallic shear reinforcement) in order to avoid galvanic corrosion. Although shear stirrups manufactured from CFCC fulfill that requirement, CFRP grids are a relatively cheap alternative. Furthermore, unlike CFCC stirrups, CFRP grids do not need to be specially produced in the event of a shortage of stirrups for a particular project, thus reducing any delays in production and the accompanying cost increases. In addition, grids such as NEFMAC grid can be set in the forms quickly compared to conventional stirrups because such materials need fewer connections to be held in place. These grids are also lighter compared to welded wire mesh.

The pay off in following *Recommendation 1* will be improved knowledge about some of the design properties for this type of material, which could result in greater efficiency in terms of material and construction. Even more importantly, additional testing will lead to greater certainty in the safety of the shear design of structures reinforced with CFRP grid. Combined with *Recommendation 1*, *Recommendation 2* will be critical to deploying this type of reinforcement in prestressed concrete beams for actual bridges because, to date, there's only been testing on small-scale specimens in an exploratory manner. So, there will need to be confirmation that the structural performance observed in those tests will be replicated in full-sized members.

The issue does have a small amount of urgency because of two bridge replacements that will potentially take place in 5 to 10 years: the northern approaches to the Hampton Roads Bridge-Tunnel (HRBT) and the Norris Bridge (Route 3 over the Rappahanock River). The pile bents for both structures and the beams in the HRBT exhibit severe signs of corrosion damage after years of saltwater exposure. There are many other structures in the commonwealth that are subjected to similar environments. Thus, there will be a need for corrosion-free / corrosion-resistant materials to ensure a longer life span for new bridges. Having CFRP grid as an alternative reinforcement will allow for greater competition of various bridge designs, which could potentially limit the "first-time" costs of these projects.

Implementation

VTRC and VDOT's *Structure and Bridge Division* will implement *Recommendations 1* and *2* by funding and supporting research that builds on what has been done recently with CFRP grid and validating all results through full-scale testing. Implementation will be in place by the end of January 2018.

ACKNOWLEDGEMENTS

REFERENCES

American Association of State Highway and Transportation Officials (AASHTO), *AASHTO LRFD Bridge Design Specifications*, 7th Ed., Washington, DC, 2014.

American Concrete Institute Committee 440 (ACI 440), *Prestressing Concrete Structures with FRP Tendons, ACI 440.4R-04*, American Concrete Institute, Farmington Hills, MI, 2004.

American Concrete Institute Committee 440 (ACI 440), *Guide for the Design and Construction of Structural Concrete Reinforced with FRP Bars, ACI 440.1R-06*, American Concrete Institute, Farmington Hills, MI, 2006.

American Concrete Institute Committee 318 (ACI 318), *Building Code Requirements for Structural Concrete, ACI 318-14*, American Concrete Institute, Farmington Hills, MI, 2014.

ASTM A370-14, *Standard Test Methods and Definitions for Mechanical Testing of Steel Products,* ASTM International, West Conshohocken, PA, 2014.

ASTM C39/C39M-14a.), *Standard Test Method for Compressive Strength of Cylindrical Concrete Specimens,* ASTM International, West Conshohocken, PA, 2014.

ASTM C469/C469M-14, *Standard Test Method for Static Modulus of Elasticity and Poisson's Ratio of Concrete in Compression*, ASTM International, West Conshohocken, PA, 2014.

ASTM C496/C496M-11, *Standard Test Method for Splitting Tensile Strength of Cylindrical Concrete Specimens,* ASTM International, West Conshohocken, PA, 2011.

Chomarat North America, Technical Data Sheet C50 1.8 x 1.6. Chomarat North America, Anderson, SC, 2010.

Chomarat North America, *Test Method for Individual Strand Tensile Strength of C-Grid Products,* Chomarat North America, Anderson, SC, 2011.

Cousins, T., Roberts-Wollmann, C., and Brown, M, *NCHRP 733: High-Performance/High-Strength Lightweight Concrete for Bridge Girders and Decks*, Transportation Research Board, Washington, DC, 2013.

Crispino, E.D., *Anchorage Zone Design for Pretensioned Bulb-Tee Bridge Girders in Virginia*, Master's Thesis, Virginia Tech, 2007, available online at www.lib.vt.edu.

Ding, L., Rizkalla, S., Wu, G., and Wu, Z.S., "Bond Mechanism of Carbon Fiber Reinforced Polymer Grid to Concrete", *Advances in FRP Composites in Civil Engineering*, Springer, Berlin, Heidelberg, 2011, pp. 589-592.

Grace, N. F., "Response of Continuous CFRP Prestressed Concrete Bridges under Static and Repeated Loadings, *PCI Journal*, Vol. 45, No. 6, Nov-Dec 2000, pp. 84-102.

Grace, N. F., Enomoto, T., Sachidanandan, S., and Puravankara, S., "Use of CFRP/CFCC Reinforcement in Prestressed Concrete Box-Beam Bridges", *ACI Structural Journal*, Vol. 103, No. 1, Jan-Feb 2006, pp. 123-132.

Grace, N. F., Jensen, E. A., Eamon, C. D., and Shi, X. W., "Life-Cycle Cost Analysis of Carbon Fiber-Reinforced Polymer Reinforced Concrete Bridges", *ACI Structural Journal*, Vol. 109, No. 5, Sept-Oct 2012, pp. 697-704.

Grace, N., Ushijima, K., Baah, P., and Bebawy, M., "Flexural Behavior of a Carbon Fiber–Reinforced Polymer Prestressed Decked Bulb T-Beam Bridge System", *ASCE Journal of Composites for Construction*, Vol. 17, No. 4, July-Aug 2013, pp. 497-506.

Magee, M., *CFRP as Shear and End-Zone Reinforcement in Concrete Bridge Girders*, Master's Thesis, Virginia Tech, 2016, available online at www.lib.vt.edu.

Morphy, R., Shehata, E., and Rizkalla, S., "Bend Effect on Strength of CFRP Stirrups", *Proceedings of the Third International Symposium on Non-Metallic (FRP) Reinforcement for Concrete Structures*, 1997, pp 589-592.

Nilson, A.H., *Design of Prestressed Concrete*, Second Edition, John Wiley and Sons, NewYork, 1987.

PCI Bridge Design Manual Steering Committee, *Precast Prestressed Concrete Bridge Design Manual*, Precast/Prestressed Concrete Institute, Chicago, IL, 2003.

Steffen, R., Scott, D., Goodspeed, C., Bowman, M. D., and Trunfio, J., "Design Issues and Constructibility af a CFRP Grid Reinforced Bridge Deck", *Proceeding of the International Conference in High Performance Materials in Bridges*, 2011.

Tokyo Rope Mfg Co. Ltd., Characteristics of CFCC: Carbon Fiber Composite Cable. http://www.tokyorope.co.jp/english/products/cfcc/feature/index.html

Tureyen, A. K., and Frosch, R. J., "Concrete Shear Strength: Another Perspective", *ACI Structural Journal*, Vol. 100, No. 5, Sept-Oct 2003, pp. 609-615.

Tureyen, A. K., Wolf, T. S., and Frosch, R. J., "Shear Strength of Reinforced Concrete T-Beams without Transverse Reinforcement", ACI Sructural Journal, Vol. 103, No. 5, Sept-Oct 2006, pp. 656-663.

Collins, M.P, Mitchell, D., Adebar, P, and Vecchio, F. J., "A General Shear Design Method", *ACI Structural Journal,* Vol. 83, No. 1, Jan-Feb 1996, pp. 36-45.

Ward, J., *C-Grid as Shear Reinforcement in Concrete Bridge Girders*, Master's Thesis, Virginia Tech, 2016, available online at www.lib.vt.edu.